8-13-2014 12:00 AM

Synaptic architecture of the acoustic startle response pathway

Mahabba Smoka, *The University of Western Ontario*

Supervisor: Dr. Susanne Schmid, *The University of Western Ontario*
Joint Supervisor: Dr. Raj Rajakumar, *The University of Western Ontario*
A thesis submitted in partial fulfillment of the requirements for the Master of Science degree in Anatomy and Cell Biology
© Mahabba Smoka 2014

Recommended Citation

SYNAPTIC ARCHITECTURE OF THE ACOUSTIC STARTLE RESPONSE PATHWAY

(Thesis format: Monograph)

by

Mahabba Smoka

Graduate Program in Anatomy and Cell Biology

A thesis submitted in partial fulfillment
of the requirements for the degree of
Master of Science

The School of Graduate and Postdoctoral Studies
The University of Western Ontario
London, Ontario, Canada

Abstract

The acoustic startle response (ASR) is mediated by a simple pathway which includes the giant neurons of the caudal pontine reticular nucleus (PnC). Habituation is theorized to occur via hyperpolarizing big potassium (BK) channels localized at glutamatergic terminals of auditory afferents in the PnC. Prepulse inhibition is suggested to be mediated by cholinergic innervation of PnC giant neurons, with possible glutamate and/or GABA co-release. Animals were injected with Fluorogold at C3/C4 to label a subpopulation of PnC giant neurons, and following a startle experiment, brainstems were processed for pCREB expression. Using their respective markers, BK channels, glutamatergic, GABAergic, and cholinergic terminals were also stained. pCREB expression overlapped with retrogradely-labeled PnC giant neurons of startled animals but not controls, supporting their startle-mediating role. Dual-staining shows some BK channel expression on glutamatergic terminals and glutamate/GABA co-expression in a subpopulation of cholinergic terminals which validate their respective implications in habituation or prepulse inhibition of startle.

Keywords

Acknowledgments

Table of Contents

List of Abbreviations

ABC – Avidin-Biotin complex

Ach – acetylcholine

AF – Alexa Fluor

AMPA(R) – α-amino-3-hydroxy-5-methyl-4-isoxazolepropionic acid (receptor)

AP-1 – activating protein 1

ASR – acoustic startle response

BK – big K^+ (potassium)

BT – Biotinylated Tyramide

CaM – Ca^{2+}-calmodulin complex

CaMKII - Ca^{2+}-calmodulin dependent kinase II

CBP – CREB binding protein

ChAT – acetylcholine transporter

CHT1 – high-affinity choline transporter 1

CaRE/CRE – Ca^{2+}/cAMP response element

(p)CREB – (phosphorylated) cAMP response element binding protein

CRN(s) – cochlear root nucleus (neurons)

DCN – dorsal cochlear nucleus

EGR-1 – early growth response protein 1

FG – Fluoro-Gold

GABA – gamma-amino-butyric acid

GAD67 – glutamate decarboxylase 67

HRP – horseradish peroxidase

IC – inferior colliculus

IEG(s) – immediate early gene(s)

LL – lateral lemniscus

LSO – lateral superior olivary nucleus

LTDg – laterodorsal tegmental nucleus

LTH – long-term habituation

Mo5 – motor trigeminal nucleus

MVeMC/MVePC – medial vestibular nucleus magnocellular/parvicellular

NeuN – neuronal nuclei

NMDA(R) – N-methyl-D-aspartate (receptor)

PBS – phosphate buffered saline

PFA – paraformaldehyde

PnC – pontine caudal reticular nucleus

PPTg – pedunculopontine tegmental nucleus

RCK1 – regulatory K+ response domain

SC – superior colliculus

SD – standard deviation

SEM – standard error of the mean

SNC – substansia nigra pars compacta

SNR – substansia nigra pars reticulate

STH – short-term habituation

SRE – serum response element

SRF – serum response factor

VaChT – vesicular acetylcholine transporter

VCN – ventral cochlear nucleus

VGLUT1 – vesicular glutamate transporter 1

VTA – ventral tegmental area

Zif268 – zinc finger protein 268

List of Figures

1 Introduction

The human brain is an intricate structure that is continuously being bombarded with sensory information from a variety of modalities. Sensorimotor gating is a process within the brain that regulates the transmission of sensory information to a motor system; it provides a mechanism for the prevention of excessive behavioral responses. One of the best tools we can use to study sensorimotor gating in a lab setting is the acoustic startle response (ASR). The ASR is mediated by a simple synaptic pathway within the brainstem that results in an activation of spinal and cranial motor neurons in response to an intense acoustic stimulus. The behavioral patterns observed in the ASR seem to be a protective reaction to the unexpected acoustic stimulus and consists of muscle flexion, eyelid closure, and heart rate acceleration (Koch and Schnitzler, 1997; Koch, 1999). The primary startle pathway in rodents consists of auditory hair cells, spiral ganglion cells, and secondary auditory neurons in the cochlear root nucleus. The latter synapse onto giant neurons of the caudal pontine reticular nucleus (PnC), which is believed to be the sensorimotor interface of this oligosynaptic pathway (Lingenhöhl and Friauf, 1994) since giant neurons directly project their axons to the spinal cord and most likely synapse onto motor and/or spinal interneurons.

Interestingly, the ASR can also be modulated intrinsically, within the pathway itself, or extrinsically, via higher order brain nuclei, to exhibit plasticity such as enhancement or decrement, depending on environmental conditions. Some of the modulations observed are fear-potentiation, sensitization, habituation, prepulse inhibition and pleasure-attenuation. Prepulse inhibition and habituation are of particular interest because of the role they play in sensory gating mechanisms. Prepulse Inhibition (PPI) occurs when a weak, non-startling prepulse strongly attenuates the ASR to the following startling stimulus. Theory suggests that the processing of the prepulse disrupts processing of the pulse, resulting in decreased startle (Koch and Schnitzler, 1997). PPI is processed by a feed-forward inhibitory pathway whereby cochlear root neurons project onto the superior and inferior colliculi, which synapse onto the pedunculopontine tegmental nucleus (PPT). This structure presumably sends cholinergic projections to the PnC (Fendt et al., 2001). These cholinergic projections are believed to be inhibitory and thereby responsible for the attenuation of the startle response following a

prepulse. It is important to keep in mind however that the PPT has also been shown to be a heterogeneous structure containing distinct populations of cholinergic, GABAergic (Gamma-Aminobutyric acid), and glutamatergic neurons (Wang and Morales, 2009), thus any one or a combination of these neurotransmitters may play a role in PPI.

Habituation is the reduction in amplitude of the startle response after repeated presentation of the startling stimulus (Koch and Schnitzler, 1997). In this way, habituation allows for the filtering out of irrelevant stimuli in favor of more pertinent ones, and is known as the simplest form of learning. Habituation is thought to occur because of presynaptic depression in terminals of the cochlear root neurons synapsing onto the PnC. These terminals are hypothesized to express big potassium (BK) channels, which are activated both by a strong depolarization and calcium influx (Sausbier et al., 2006; Sailer et al., 2006). BK channel activation truncates synaptic transmission via hyperpolarization, which is believed to be responsible for short-term habituation.

Although the hypothetical primary ASR pathway has been established, its synaptic architecture has not been mapped out. The present study aims to describe the synaptic organization of the ASR pathway and its modulatory afferents using histological and immunohistochemical tools in order to better understand the neurotransmitters involved and the effect of drugs on sensory gating. The giant neurons within the PnC, hypothesized to form the sensorimotor interface of this oligosynaptic pathway, were visualized using Fluorogold retrograde tracer and their response to activation by startle stimuli validated by testing expression of immediate early genes and transcription factors. We hypothesized that PnC giant neurons would express activity dependent markers only in animals receiving startle stimuli as opposed to control animals. We further employed dual and triple labeling immunofluorescence to stain for BK channels as well as glutamatergic, GABAergic, and cholinergic terminals that synapse on PnC giant neurons, to gain a better insight into the synaptic input(s) modulating startle. We hypothesized that a subpopulation of cholinergic terminals in the PnC would co-express glutamatergic and/or GABAergic markers, and that markers for BK channels would be expressed on glutamatergic presynaptic afferents.

2 Literature Review

2.1 The various modalities and universality of the startle response

The characteristics of the startle response were first introduced to the scientific community through a pioneering study undertaken by Landis and Hunt (1939). They tested the effect of a loud acoustic stimulus on human subjects who varied in age, race, drug-use, and psychosis, documenting the response with a high-speed camera. Landis and Hunt discovered that an involuntary pattern of movement consisting of eye blinks and contraction/jerking of the head, arms, trunk, and knees was generated uniformly across the subjects tested. Previous emotion theorists held that this reaction was an emotion, an extreme extension of surprise (Bull, 1951). Using a pistol, Ekman et al. (1985) were able to show that visible reactions to startle could not be suppressed upon anticipation of the gunshot nor properly simulated when no firing occurred. They concluded that startle must be a reflex, not an emotion, because cognition did not play a causal role in eliciting it. Thus, this rapid reaction to sudden and intense stimuli became known as the startle reflex and has since been replicated using various stimuli modalities across a diversity of test subjects (Prosser and Hunter, 1936; Pfeiffer, 1962; Fleshler, 1965; Davis, 1974a; Russell, 1974; Currie and Carlsen, 1985; Wu et al., 1988; Baird et al., 1993; Wicks et al., 1996; Koch, 1999; Yeomans et al., 2002).

Both albino Wistar (Prosser and Hunter, 1936; Fleshler, 1965) and Sprague-Dawley (Davis, 1974a) rats exhibit top-down, abrupt crouch-like movements when a strong acoustic stimulus, in the form of a telegraph click (Prosser and Hunter, 1936) or pure tone (Fleshler, 1965; Davis, 1974a) is introduced. A similar phasic contraction of skeletal muscle was observed in cats presented with clicks or white noise bursts between 70–120dB (Wu et al., 1988). Both of these species can also evoke motor responses that mimic the startle pattern upon presentation with intense free-fall stimuli that excite the vestibular nerve (Yeomans et al., 2002). Vestibular stimuli in the form of water vibrations and mechanical taps delivered to the side of a substrate on which an animal moves, respectively induce C-type responses in *Petromyzon marinus* larval sea lampreys (Currie and Carlsen, 1985) and withdrawal reflexes in *Caenorhabditis elegans*

(*C.elegans*) nematodes (Wicks et al.,1996), both of which exhibit startle-like characteristics. In addition to acoustic and vestibular stimuli, powerful tactile stimuli in the form of airpuffs were shown by Simons-Weidenmaier et al. (2006) to elicit startle responses in both rats and C57BL/6 mice, through the activation of the trigeminal pathway and the principal nucleus of the 5th nerve. Furthermore, Yeomans and colleagues (2002) described how cross modal summation between tactile, acoustic, and vestibular stimuli in rats, cats, and humans can produce a startle response stronger than single-modality stimulations, using an intensity threshold far below the intensity required for startle when the stimuli are individually presented.

Despite their extensive startle responses to the above mentioned stimuli modalities, mammals are not as reactive to visual and olfactory stimuli as are flies and fish, respectively. For instance, *Drosophila Melanogaster* jump or initiate flight in response to a light-off stimulus (Baird et al., 1993) and European minnows (*Phoxinus laevis*) undergo a fright reaction in which they swim to the opposite side of the alarm substance, when they smell the injured skin of fellow school members (Pfeiffer, 1962).

It is well understood that across the animal kingdom and regardless of stimulus modality, the purpose of the startle reflex is to protect against life threatening blows or predatory attacks (Pfeiffer, 1962; Russell, 1974; Currie and Carlsen, 1985; Baird et al., 1993; Wicks et al., 1996; Koch and Schnitzler, 1997; Koch, 1999; Yeomans et al., 2002). This is especially noted in studies by Koch (1999) and Yeomans et. al. (2002) both of whom report that in addition to the abrupt movements generated by startle, test subjects showed increased heart rates and arrests of ongoing behaviours, indicative of a fight/flight sympathetic response.

In spite of the many startle models that exist, the acoustic startle response (ASR) in mammals (rats, mice, cats, and humans) has the greatest amount of neurobiological data gathered and can be used to study behavioural plasticity due to its non-zero baseline (i.e., the response magnitude can be enhanced or diminished based on environmental conditions or experimental manipulations; Koch, 1999). Additionally, the ASR neuronal circuitry in rats is well characterized and can be generalized to humans since equal response paradigms in both mammals are observed when identical stimulus parameters are used (Koch, 1999).

2.2 The acoustic startle response circuitry

One of the principal reasons why the ASR is a preferable study model is due to the ease in measuring the response in a laboratory setting: animals are placed on a transducer platform inside startle boxes, which converts their vertical movements into voltage signals (Koch, 1999; Valsamis and Schmid, 2011). Studies conducted in both rats (Davis et al., 1982a; Lingenhöhl and Friauf, 1994; Lee et al., 1996; Koch and Schnitzler, 1997; Koch, 1999; Yeomans et al., 2002) and cats (Wu et al., 1988; Yeomans and Frankland, 1996) reveal that the startle response occurs when the acoustic stimulus is > 80dB, and that the latency of this reflex is very short – about 10ms in duration. It is this short latency that formed the basis of the assumption that the primary startle pathway is composed of a simple circuit with a small number of synapses (Davis et al., 1982a, Pilz et al., 1988).

The involvement of the cerebral cortex was ruled out by Forbes and Sherrington (1914) who were able to show that decerebrated cats still startled, and by Prosser and Hunter (1936) who proposed that cerebral involvement was not likely due to its minimum latency of 8ms to auditory stimulation. Furthermore, based on latency data alone, Prosser and Hunter (1936) hypothesized that the startle circuit included the cochlea, eighth cranial nerve, cochlear nuclei, inferior colliculus, midbrain reticular nucleus, reticulo-spinal tract, anterior horn cells, and motor neurons. In 1982, Davis and his colleagues conducted the first systematic study of the primary startle pathway using a combination of horseradish peroxidase (HRP) tracing techniques, electrical stimulations, and electrolytic lesions. The startle response was abolished following bilateral lesions in the ventral cochlear nucleus (VCN), nuclei of the lateral lemniscus (LL), and nucleus reticularis pontis caudalis (PnC), and elicited with electrical stimulation to these same regions. Davis et al. (1982a) thus concluded that the startle circuit involved five synapses which connect neurons of the following structures: VCN, LL, PnC, spinal interneurons, and spinal motor neurons. The circuit was further modified and shortened as a result of more modern and sensitive analytical methodologies which included using dual retrograde and anterograde tracing techniques to identify sources of input and efferent targets of the PnC (Lingenhöhl and Friauf, 1994). Retrograde tracing observations demonstrated the bilateral input of cochlear root neurons (CRNs) to the PnC with no afferents coming from the nuclei of the LL, and anterograde tracing showed that PnC neurons are reticulospinal cells with

similar axonal trajectories. This neuronal pathway implies that the primary startle circuit is composed of three central relay stations consisting of the CRNs, PnC, and cranial/spinal motor neurons (Figure 2.1). Further evidence for the obligatory role of cochlear root neurons in the elementary startle circuit was provided when bilateral kainic acid lesions of CRNs abolished startle without causing damage to the auditory nerve (Lee et al., 1996), and biotinylated dextran amine injections in CRNs were shown, using electron microscopy, to form synapses with PnC reticulospinal neurons (Nodal and López, 2003).
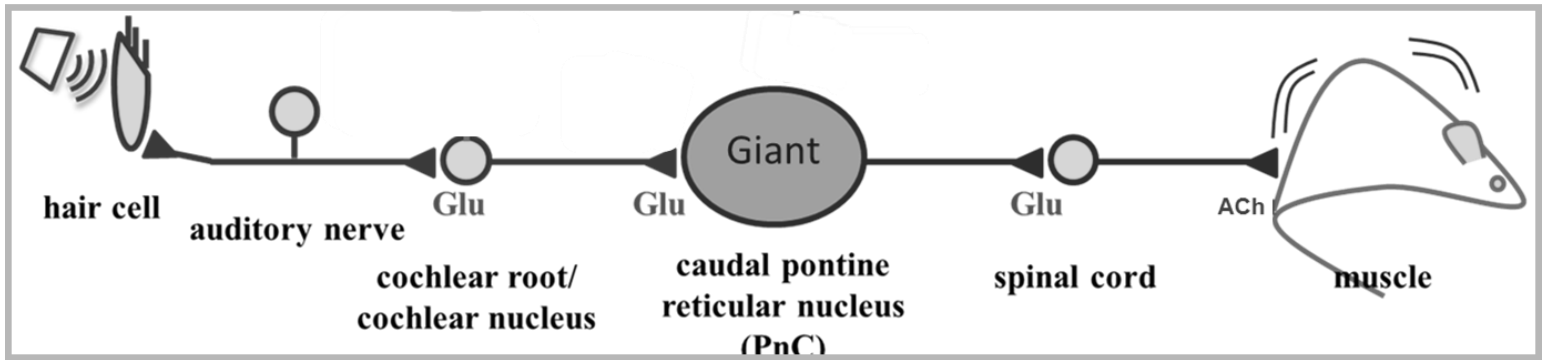
Figure 2.1 A schematic representation of the neural circuitry mediating the acoustic startle response.

In addition to their tracing experiments, Lingenhöhl and Friauf (1994) combined HRP morphological identification with electrophysiology to characterize the giant neurons within the PnC (named so because of their large soma diameter, >40µm) which they believed to be good candidate mediators of startle and the location of sensorimotor integration. These 20-60 giant neurons, polygonal in soma shape and consisting of multiple proximal dendrites (Koch et al., 1992; Nodal and López, 2003) make up about 1% of the PnC (Koch et al., 1992), and are sufficient to relay the acoustic stimuli to the many hundreds of motor neurons in the spinal cord and brainstem (Yeomans and Frankland, 1996). Targeted lesions of the PnC giant neurons were executed using the excitotoxin quinolinic acid, an *N*-methyl-D-aspartate (NMDA) receptor agonist, which selectively destroys giant neurons due to their relative sensitivity to glutamate (Koch et al., 1992). Loss of giant neurons significantly reduced the startle amplitude and a positive correlation was observed between the number of neurons lost and the reduction of the amplitude (Koch et al., 1992). Giant PnC neurons show a remarkable number of physiological features such as short-latency auditory input, high firing threshold, sensitivity to pre-pulse stimulation, habituation to repetitive acoustic stimulation, and response enhancement following amygdaloid activity, all supporting their pivotal role as the sensorimotor interface between CRNs and motor neurons (Lingenhöhl and Friauf, 1994). Giant neurons within the pontine caudal reticular nucleus of cat (Wu et al., 1988; Yeomans and Frankland, 1996) and human (Martin et al., 1990) brains with similar characteristics to those described in the above mentioned rodent models, were likewise revealed to play an important role in the mediation of startle. Similarly, large neurons known as Mauthner cells, in goldfish (Russell, 1974) and larval lampreys (Currie and Carlsen, 1985), have been shown to actively initiate the motor response following startling stimuli. Furthermore, PnC giant neurons are important relay centers of multiple sensory stimuli, including vestibular stimuli from the lateral vestibular nucleus and tactile stimuli from the trigeminal neurons, into motor activity (Koch et al., 1992; Yeomans et al., 2002). Taken together, these studies provide adequate evidence for PnC giant neurons as the sensorimotor interface of the acoustic startle response pathway.

2.3 Modulation of the acoustic startle response through prepulse inhibition

The acoustic startle response can be used as a tool to assess the neuronal basis of behavioural plasticity because of the ability to positively and negatively modulate sensorimotor information processing (Koch et al., 1997; Koch, 1999). Sensitization and fear-potentiation are examples of modulations that enhance the ASR magnitude, while pleasure-attenuation, prepulse inhibition, and habituation modulate the ASR by diminishing its magnitude. Prepulse inhibition and habituation are of particular interest because of the biologically significant role they play in sensory gating mechanisms (Koch et al., 1997; Koch, 1999), and as such will be further discussed in this and subsequent sections.

Prepulse inhibition (PPI), a term coined by Ison and Hammond (1971), is the ability of a weak stimulus, which itself evokes no behavioural response, to briefly attenuate the startle reaction to a subsequent strong stimulus (Figure 2.2; Mongeluzi et al., 1998a; reviewed in Laurraui and Schmajuk, 2006). PPI is not learning-related because of its occurrence on the first trial (Mongeluzi et al., 1998a; Fendt et al., 2001), and the startle response across species can be attenuated by previous stimulation with a prepulse from various modalities including acoustic, tactile, and visual (Buckland et al., 1969; Pinckney, 1976; Mongeluzi et al., 1998a/b; Fendt et al., 2001). For instance, a 100msec vibrotactile prepulse delivered to marine mollusks *Tritonia diomedea* and *Aplysia californica* prior to a tail shock, prevents the escape swim response that these invertebrates undergo when startled (Mongeluzi et al., 1998a/b).
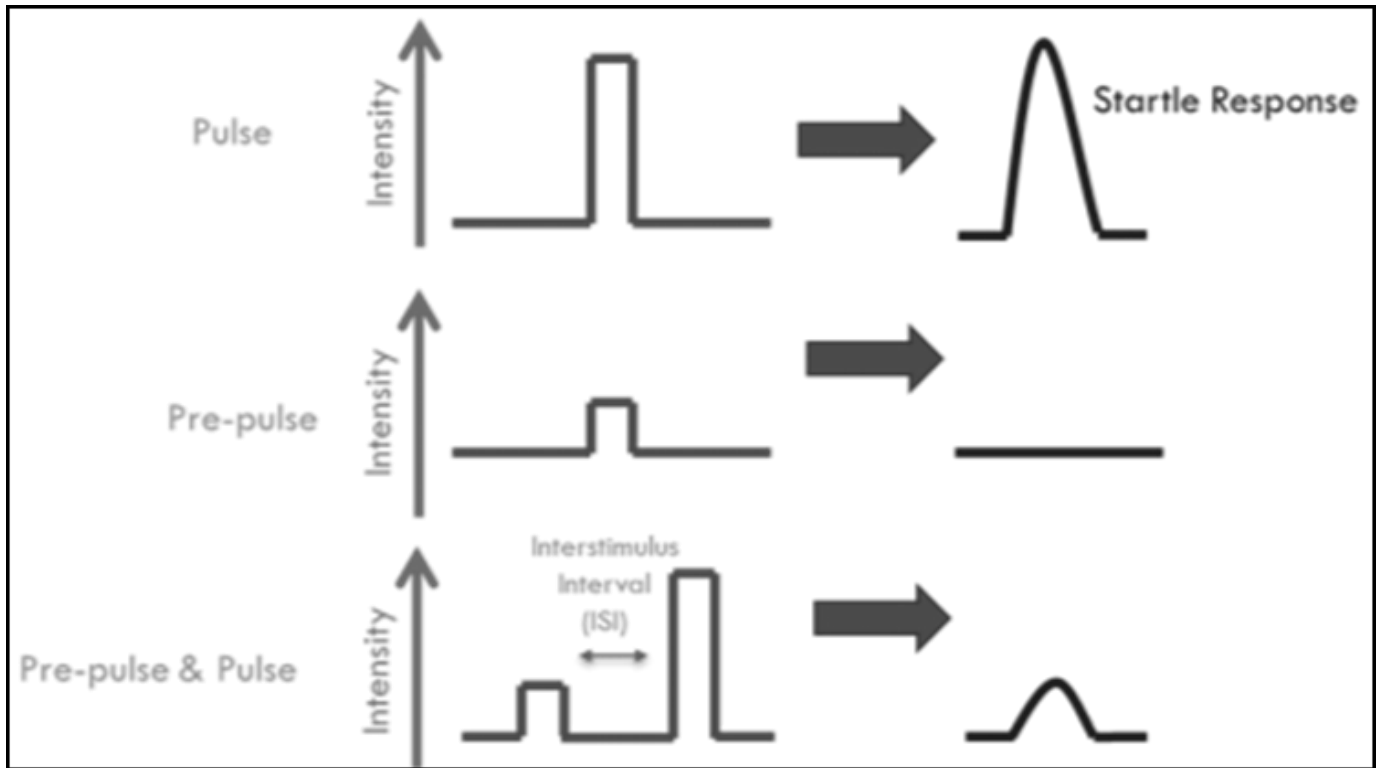
Figure 2.2 Schematic of prepulse inhibition where a weak, non-startling prepulse strongly attenuates the acoustic startle response to the following startling stimulus.

The biological significance of PPI, which in humans is measured as a change in the eye blink reflex – a component of the startle response (Li et al., 2009), is described in Graham's (1975) protection-of-processing theory. Graham briefly states that the low-intensity prepulse stimulus produces a detection reaction that triggers a gating mechanism, which transiently inhibits the distractive startle-like response that would disrupt perceptual processing of the lead stimulus. PPI is therefore an important modulation of startle that reduces distraction and prevents information overload in the brain (Koch et al., 1993; Fendt et al., 2001; Holmstrand and Sesack, 2011). As such, deficits in PPI are linked to a variety of neurological disorders such as Alzheimer's disease, Huntington's chorea, Tourette's syndrome, and especially Schizophrenia, due to the inability of these patients to suppress intrusive sensory, motor, and cognitive information (Braff et al., 1978; Geyer and Braff, 1982; Putzki, 2008).

PPI was first noted by Hoffman and Fleshler (1963) when they discovered that a continuous background noise had no effect on startle, however when the background noise was pulsed (0.5s on, 0.5s off), the startle response disappeared by 80%. Hoffman and Searle (1965) studied the inhibitory mechanisms of PPI in a more direct and controlled manner by varying prepulse intensities and the inter-stimulus-interval (ISI) – the time between the prepulse and the pulse. Using ISIs ranging from 10-4000msec, they concluded that inhibition of startle was maximum at shorter ISIs, with no inhibition observed below or above 20 and 1000msec, respectively. Thus, Hoffman and Searle were able to show that PPI is sensitive to temporal variables since it only occurs when the prepulse precedes the primary startle stimulus by a suitable interval, and that the magnitude of inhibition can be correlated with the intensity of the prepulse whereby higher intensities (up to the startle stimuli threshold) result in greater inhibitions. Based on their results, they cite three brain regions that may be responsible for the circuitry mediating PPI: the intratympanic reflex mediated by the reticular formation (Loeb, 1964), the oliveocochlear bundle (Desmedt, 1962), and the inferior colliculus (Prosser and Hunter 1936).

The hypothetical circuit for PPI was delineated through the conduction of numerous lesion and stimulation studies (reviewed in Fendt et al., 2001). Lesions of the inferior colliculus (IC) disrupted PPI by acoustic but not visual prepulses (Leitner and Cohen, 1985), and electrical stimulation of the IC simulated an acoustic prepulse and inhibited the startle response (Li and Yeomans, 2000), both of which provide evidence for the IC as a relay of auditory input to PPI-

mediating circuitry. The superior colliculus (SC) also plays a role in PPI and acts as the multimodal processing center in the circuit because of the direct input it receives from auditory, somatosensory, and visual nuclei (Meredith et al., 1992). The SC has also been shown to receive inhibitory GABAergic input from the substansia nigra pars reticulata (SNR) which is proposed to modulate PPI (Chevalier et al., 1981), and pharmacological stimulations by blocking GABA support this finding (Fendt, 1999). As for the IC, lesions of the SC prevented PPI (Fendt et al., 1994b) and electrical stimulations of this region mimicked PPI (Li and Yeomans, 2000). Since the SC projects to both the pedunculopontine tegmental nucleus (PPTg) and the laterodorsal tegmental nucleus (LTDg; Redgrave et al., 1987; Semba and Fibiger., 1992; Steiniger et al., 1992), lesions (Leitner et al., 1981) and electrical stimulations (Li and Yeomans, 2000) of these regions were undertaken to further reinforce their role in the PPI circuitry. Furthermore, a subpopulation of neuronal projections from the PPTg are shown to directly innervate the PnC giant neurons mediating startle, and inhibit their activation when a prepulse is present (Mitani et al., 1988; Lingenhöhl and Friauf, 1994; Bosch and Schmid, 2006). Interestingly, the PPTg is also proposed to act as a relay station between the PnC and higher order brain nuclei such as the nucleus accumbens and ventral pallidum, which may influence the modulation of PPI (Koch et al., 1993; Laurrauri and Schmajuk, 2006). This top-down modulation of PPI has been shown in a variety of animal experiments and functional magnetic resonance imaging studies in human subjects, to involve many more brain structures including but not limited to, the prefrontal cortex, thalamus, amygdala, hippocampus, striatum, and globus pallidum (reviewed in Swerdlow et al., 2001). In summary, these studies taken together allow for the hypothetical pathway for PPI to be outlined as per the representation in Figure 2.3.
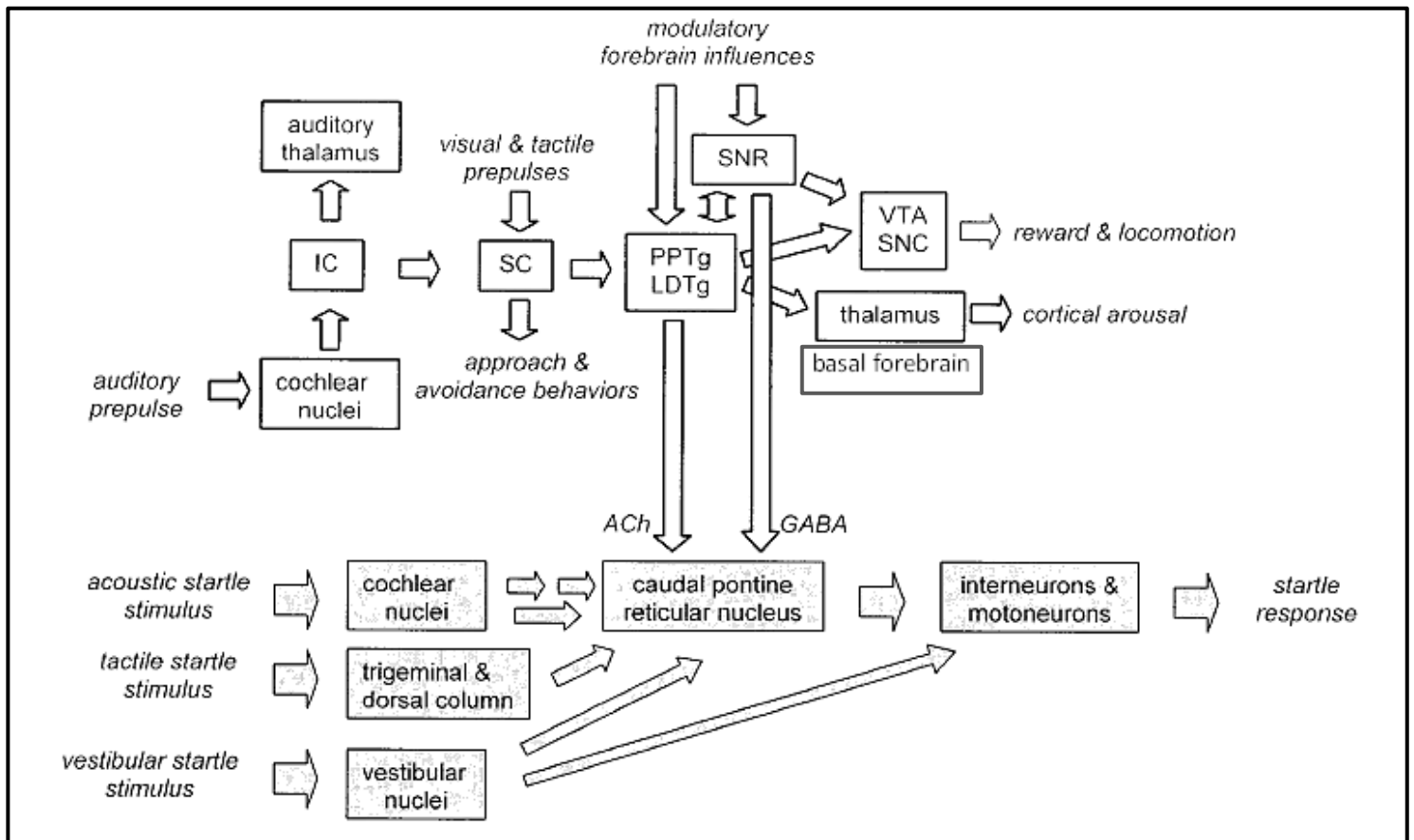
Figure 2.3 Schematic of the hypothetical circuit mediating PPI of the ASR. IC: inferior colliculus; SC: superior colliculus; PPTg/LDTg: pedunculopontine tegmental nucleus/laterodorsal tegmental nucleus; SNR: substansia nigra pars reticulate; SNC: substansia nigra pars compacta; VTA: ventral tegmental area; Ach: acetylcholine; GABA: γ-Aminobutyric acid (Fendt et al., 2001)

2.4 Cholinergic neurons in the pedunculopontine tegmental nucleus and their role in prepulse inhibition

As described in the previous section, the brain stem circuitry mediating PPI of the startle reflex is important for our understanding of neuropsychological disorders in which this pathway has been compromised. Thus knowledge of the neurotransmitter(s) involved in this modulation will aid in the comprehension of various drug effects on sensory gating and may provide insight into prophylactic targets in cases where a deficit is evident. Based on a wealth of literature, both inhibitory cholinergic and GABAergic neurotransmission have been proposed to be major participants in PPI (Fendt et al., 2001).

In 1988, Mitani and colleagues performed a series of tracing analyses to discern the identity of the PPTg/LDTg projections contacting PnC giant neurons, and believed to mediate PPI. Using a cat model, they used HRP conjugated to wheat germ agglutinin to retrogradely label neurons in the PPTg/LDTg from the PnC, as well as *Phaseolus vulgaris* leucoagglutinin anterograde transport to confirm projections from PPTg/LDTg to PnC. Combining these tracing techniques with the immunohistochemical staining of choline acetyltransferase (ChAT), a marker for cholinergic neurons, they discovered that 5% and 10% of the terminals from the PPTg and LDTg respectively, expressed the ChAT marker. This same tracing experiment coupled with ChAT immunohistochemistry was later conducted in rats (Semba et al., 1990; Grofova and Keane, 1991; Koch et al., 1993) with similar results, in addition to electrophysiological and neurotoxic lesioning tests. Recordings from PnC giant neurons in the presence of acetylcholine agonists acetyl-ß-methylcholine and carbachol revealed decreased responses as compared to controls, and quinolinic acid lesions of the cholinergic neurons in the PPTg significantly reduced PPI with no effect on ASR or habituation (Koch et al., 1993; Swerdlow and Geyer, 1993). Increasing evidence for the importance of cholinergic neurons in PPI was revealed through electron microscopy analysis which showed ChAT-positive varicosities from the PPTg terminating onto cell bodies and proximal dendrites of PnC giant neurons (Jones, 1990), and in rats fed a choline-free diet who showed behavioural signs of impaired PPI (Wu et al., 1993). Furthermore, the inhibitory role that these cholinergic neurons play was confirmed using whole-cell patch clamp recordings of PnC giant neurons in which excitatory postsynaptic

currents elicited by trigeminal and auditory fiber stimulations were inhibited by carbachol (Bosch and Schmid, 2006 and 2008), and in muscarinic receptor knockout mice who exhibited impaired PPIs (Gomeza et al., 2001). In both of these two studies, muscarinic receptor subtypes 4 and 2 were hypothesized to be involved.

No study has been able to completely block PPI following blockade of cholinergic input into the PnC (Leitner et al., 1981; Semba et al., 1990; Fendt et al., 1994b; Fendt, 1999; Li and Yeomans, 2000) and this suggests that while cholinergic release is important for PPI, it is not the sole neurotransmitter responsible for the mediation of this circuit. Using the $GABA_A$ receptor anatagonist bicuculline, the $GABA_B$ receptor antagonist phaclofen, and the muscarinic receptor antagonist scopolamine in Wistar rats and B6 mice, Yeomans et al. (2010) were able to show that both GABA receptors on PnC giant neurons mediate a part in PPI; $GABA_A$ receptors contributed to the peak of PPI and $GABA_B$ receptors were activated at long ISIs in synergy with the effects of cholinergic muscarinic receptors. This attenuation of PPI in the presence of GABA receptor antagonists supported a study conducted ten years prior by Koch and his colleagues (2000) who noted a 60% reduction in PPI when the SNR was lesioned. Combined, the results of these researchers suggest a role for inhibitory GABAergic projections from the SNR to PnC giant neurons in partially mediating PPI.

Neurons have been traditionally assumed to only release one classical neurotransmitter, however the evidence against this notion is increasing. Co-release of neurotransmitters has widespread implications for the activation of postsynaptic receptors and the potential for distinct modes of signaling (reviewed by Hnasko and Edwards, 2012). A subpopulation of cholinergic, retinal amacrine cells in chicks, rats, and rabbits, simultaneously excite and inhibit postsynaptic cells by their respective co-release of acetylcholine and GABA neurotransmitters (reviewed in Duarte et al., 1999). Cholinergic neurons in both the basal forebrain (Allen and al., 2006) and the striatum (Guzman et al., 2011) have also been shown to co-release transmitters, in this case acetylcholine and glutamate. In the basal forebrain, synaptically released acetylcholine exerts a negative-feedback inhibition on co-released glutamate (Allen and al., 2006), and in the striatum, selective elimination of the vesicular acetylcholine transporter (VaChT) has only marginal consequences on striatal-related tasks because co-released glutamate mediates most functions previously attributed to acetylcholine (Guzman et al., 2011).

Moreover, Spann and Grofova (1992) combined light and electron microscopy to show that the PPTg is composed of a mixture of cholinergic and non-cholinergic neurons. This finding was elaborated by Wang and Morales (2009) who used ChAT immunohistochemistry coupled with *in situ* hybridization of GAD and VGLUT2 mRNA transcripts, to demonstrate that the PPTg and LDTg both contain distinct populations of cholinergic, glutamatergic, and GABAergic neurons. Therefore, due to the abundance of experimental evidence, the hypothesis that cholinergic terminals projecting to the PnC co-release GABAergic or glutamatergic transmitters that combine to inhibit the startle response during PPI, is a plausible theory to exam.

2.5 Habituation as an intrinsic modulation of the acoustic startle response

Both PPI and habitation represent important sensorimotor gating mechanisms (Koch and Schnitzler, 1997; Koch, 1999; reviewed in Rankin et al., 2009). In contrast to PPI however, habituation is (mostly) and intrinsic modulation of the ASR which means that the underlying mechanism is located in the primary startle pathway itself (see below). First described by Prosser and Hunter (1936), habituation refers to the reduction in magnitude of the startle response following repetitive presentation of the startling stimulus (Figure 2.4). Habituation is termed the "simplest form of non-associative learning" because the response decrement does not rely on the presentation of a conditioned stimulus (Koch, 1999; Rankin et al., 2009), and it modulates the startle reflex in a wide variety of vertebrate and invertebrate models including the gill withdrawal reflex in *Aplysia* (Engel and Wu, 1998), the tap reversal response in *C.elegans* (Rankin et al., 1990), and the escape circuit in *Drosophila* (Castellucci et al., 1970). Habituation is an important gating mechanism that allows for the filtration of irrelevant stimuli in favor of more salient ones, thus comprehension of its mediating neuronal mechanism is an important prerequisite for understanding other forms of learning.
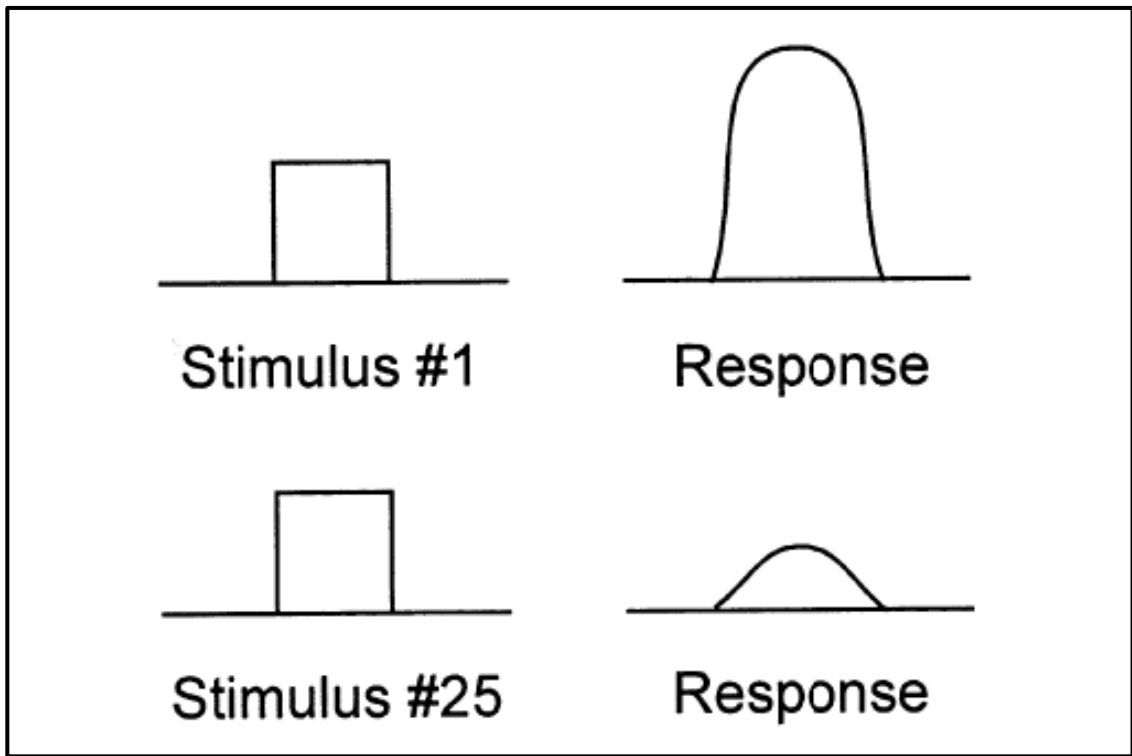
Figure 2.4 Schematic of the habituation of a startle response when a repetitive stimulus (#25) is given (Koch and Schnitzler, 1997).

The dual-process theory by Groves and Thompson (1970) is the most influential theory of habituation and describes the existence of two independent and opposing mechanisms (habituation and sensitization) whose net result is measured as the decline in response amplitude. This implies that any given startling stimulus evokes both sensitizing and habituating properties which are at competition with one another (Borszcz et al., 1989; Ornitz and Guthrie, 1989). A landmark paper by Thompson and Spencer (1966) characterized nine common features that habituation entails including spontaneous recovery (response decrement recovers upon stimulus withdrawal), dishabituation (response decrement to original stimulus increases when an alternate stimulus is presented), and stimulus specificity (response decrement to one modality, tactile or acoustic, is not generalized to a different modality (see also Simons-Weidenmaier et al., 2006)). Furthermore, because dishabituation is a characteristic of habituation, the latter can be differentiated from response decrements due to sensory adaptation or motor fatigue (Davis and File, 1984; Christofferson, 1997). These nine features remained relatively unchanged since they were first introduced in 1966, and in 2009, Rankin et al. saw the need to include one more consideration: long-term habituation (LTH).

LTH is the reduction in the ASR magnitude of the first trial amplitude across several days (between sessions), and is differentiated from short-term habituation (STH; most often referred to as simply "habituation") which typically occurs within a single test session (Koch, 1999; Rankin et al., 2009). Like STH, LTH is a non-associative learning process (Jordan et al., 2000) that shows stimulus modality specificity (Pilz et al., 2013) however, the neuronal mechanism underlying LTH is thought to be far more complex than STH and incorporate a variety of brain structures (Koch and Schnitzler, 1997; Rankin et al., 2009). STH occurs via an intrinsic mechanism within the primary ASR pathway but LTH suppresses ASR by an extrinsic mechanism outside of the stimulus response pathway, and includes brain regions such as the medial cerebellum (Leaton and Supple, 1986 and 1991; Lopiano et al., 1990) and the ventral periaqueductal gray (Borszcz et al., 1989). Despite lesion experiments implicating these various neuronal substrates in the mediation of LTH, the precise location in the primary ASR pathway where attenuation occurs remains unknown.

In the case of STH, any role of rostral brain structures were ruled out because decerebrated rats at the level of the inferior colliculus still preformed short-term, but not long-term, habituation

(Fox, 1979; Leaton et al., 1985). Pilz and Schnitzler (1996) discovered that STH occurred without increasing the ASR threshold and concluded that the mechanism for habituation must lie downstream from the region that determines the ASR threshold, most likely at the synapse between CRNs and PnC giant neurons. Lingenhöhl and Friauf (1994) furthered this theory by testing EPSPs generated by giant neurons in the presence of repetitive sensory stimulations, which resulted in decreased amplitudes. Moreover, habituation of startle-like responses was evident with electrical stimulation of only CRNs and not reticular neurons (Davis et al., 1982b), which again indicated the synapse between CRNs and cells in the PnC as the neural substrate for habituation. Weber et al. (2002) used rat brain slices to show that repeated action potentials (mimicking sensory afferent fibers during startle stimuli presentation) induced an exponential decay of the synaptic response amplitude in PnC giant neurons; this synaptic depression is hypothesized to be the neural correlate for STH. Based on these findings, two processes of synaptic depression are possible: either attenuation of the CRN presynaptic transmitter release or reduction of sensitivity of postsynaptic receptors on PnC giant neurons (Koch and Schnitzler, 1997). To determine which process of synaptic depression is most likely responsible for STH, Simons-Weidenmaier et al. (2006) conducted patch-clamp recordings in PnC giant neurons of rat and mice brain slices, following stimulation of auditory and trigeminal afferents. They proposed that since habituation was specific for each stimulus modality and not generalized between the two, a presynaptic mechanism is responsible for causing STH before signal integration from different pathways can occur in the PnC.

Since STH is suggested to occur via presynaptic depression of CRN afferents, the identity of the neurotransmitter involved in the mediation of auditory input to the reticular brainstem is of great interest. Acetylcholine (Yao and Godfrey, 1992), glycine, and GABA (Kolston et al., 1992), were ruled out as transmitter phenotypes of CRNs. Using electron microscopy, CRN axons were revealed to establish both en passant and terminal contacts in the PnC (Nodal and López, 2003). Based on the rounded morphology of these terminal vesicles and the asymmetric synapses they formed, it was concluded that they released excitatory transmitters. Ebert and Koch (1992) iontophoretically applied glutamate and both α-Amino-3-hydroxy-5-methyl-4-isoxazolepropionic acid (AMPA) and NMDA receptor antagonists to examine their effects on acoustically-evoked responses of PnC giant neurons. Glutamate caused an increase in the tone-evoked discharge rate of these neurons which was inhibited by both antagonists with a greater

reduction when the AMPA receptor antagonist was used. Using these same two antagonists, Miserendino et al. (1990) described an inhibition of the ASR in behaving rats. Therefore, the evidence compiled from these studies points to glutamate as the transmitter phenotype of CRNS (Krase et al., 1993).

2.6 BK channels and their potential role in habituation of startle

Since habituation involves a form of plasticity that calls for depression of excitatory neurotransmission, it is significant to gain insight into the molecular mechanisms which produce this reduction of depolarization in the synaptic terminal (Charpier et al., 1995). Large Ca^{2+}-activated potassium (K^+) channels, designated as Big K^+ or BK channels due to their 100-300pS sized single-channel conductance (Latorre and Miller, 1983; Marty, 1981), are hypothesized to be the key players in mediating presynaptic depression (reviewed in Cui et al., 2009) which is believed to be responsible for habituation.

BK channels are vastly expressed throughout the animal kingdom and they participate in a number of functions including regulation of neuronal transmitter release (Sailer et al., 2006; Sausbier et al., 2006; Wang, 2008), tuning of cochlear inner hair cells (Rüttiger et al., 2004; Pyott et al., 2007), and contractibility of both skeletal (Pallotta et al., 1981) and smooth musculature (Inoue et al., 1985). BK channels are heterooctamers composed of four α and (in mammals) four β subunits (Rüttiger et al., 2004). The α subunits each contain seven transmembrane domains (S0-S6) with S1-S4 as voltage-sensors and S5-S6 as pore-gate formers (Figure 2.5; Cui et al., 2009). The S0 domain secures the N-terminus to the extracellular side, and the carboxyl terminal contains two regulatory domains (RCK1 and Ca^{2+} bowl) important for Ca^{2+} - dependent channel gating (Wang, 2008). The β subunits are made up of two domains which control channel properties related to Ca^{2+}/toxin sensitivity (Farley and Rudy, 1988).
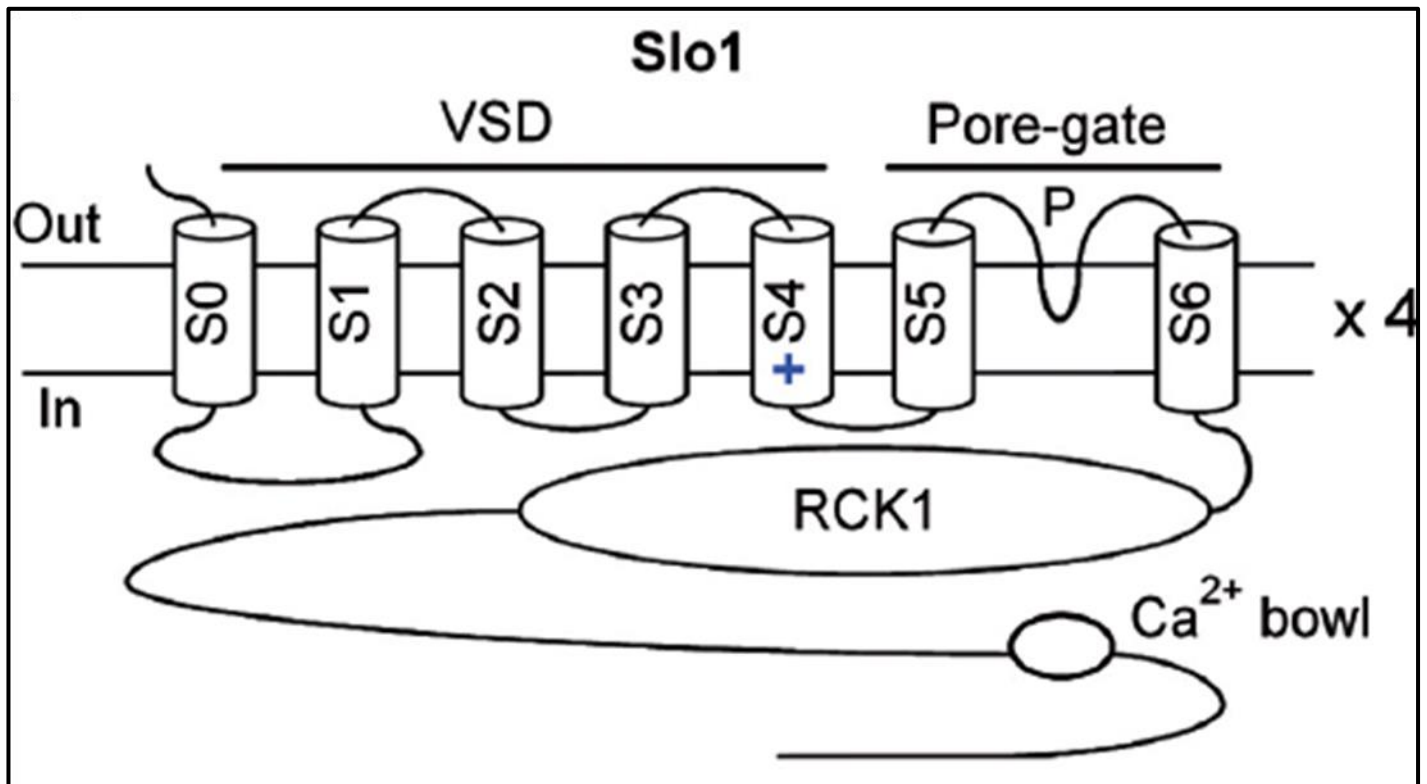
Figure 2.5 BK channel structural representation of the seven domains that form the α subunit (encoded for by the *Slo1* gene). VSD: voltage-sensor domain; P: pore loop; RCK1: regulatory domain for K^+ conductance (Cui et al., 2009).

The claim that BK channels are important modulators of membrane excitability at the presynaptic level (Robitaille et al., 1993; Xu and Slaughter, 2005) is supported by electron microscopy results localizing BK channels to presynaptic glutamatergic terminals in hippocampal pyramidal neurons (Sailer et al., 2006), and immunogold labeling of these channels in presynaptic cells (Hu et al., 2001). Furthermore, in retinal amacrine cells, BK channels are implicated in reciprocal synapse modulation of both pre- and postsynaptic signaling (Grimes et al., 2009), and in hippocampal/cortical nerve terminals, BK channels located at the presynaptic terminal were noted to selectively regulate the release of glutamate over GABA (Raffaelli et al., 2004; Martire et al., 2010).

Presynaptic BK channels serve as negative regulators of excitatory glutamatergic release and are able to efficiently regulate the activity-dependent accumulation of presynaptic Ca^{2+} because of their colocalization with the presynaptic Ca^{2+} channels (Gho and Ganetzky, 1992). Intracellular calcium accumulation, which is triggered by N-type Ca^{2+} channel depolarization (Katz et al., 1995) and leads to neurotransmitter release, is significantly increased in the presence of the BK channel blockers, Iberiotoxin and Charybdotoxin (Robitaille et al., 1993) or in conditions such as ischemia and epilepsy (Hu et al., 2001). Hyperpolarizing BK channels are therefore proposed to serve as emergency brakes which prevent this rise in intracellular calcium accumulation and ensuing excessive depolarization (Runden-Pran et al., 2002). Other than the need for high voltage and calcium, the exact mechanism for the activation of BK channels is not fully understood, however it is hypothesized that this is brought on as a result of phosphorylation of the channels (as seen in *C.elegans*) by the presynaptic Ca^{2+}/Calmodulin-dependent protein kinase II (CaMKII; Liu et al., 2007).

The role of BK channels in habituation was first described in *Drosophila* with mutations in the *slowpoke* (*Slo*) gene which encodes subunits implicated in channel modulation (Engel and Wu, 1998). Malfunctions of the BK channels in these flies led to a markedly reduced rate of habituation to a visually-induced jump response. The α pore-forming subunit of BK channels (Rüttiger et al., 2004) was abolished in *C.elegans* with a *Slo1* channel mutant, and these mutants were unable to habituate to a reversal reflex induced by a mechanical stimulus (Unpublished data, personal communication, Catharine Rankin). Moreover, Typlt et al. (2013) found that mice with a knock-out mutation for the *Slo1* gene had completely abolished STH but

unaffected LTH, reiterating the notion that LTH is mediated by an alternate circuit. Thus, in consistence with their physiological importance and molecular properties, BK channels acting on presynaptic glutamatergic afferents, are the likely mediators of CRN synaptic depression on PnC giant neurons, which is ultimately responsible for the habituation of startle (Figure 2.6).
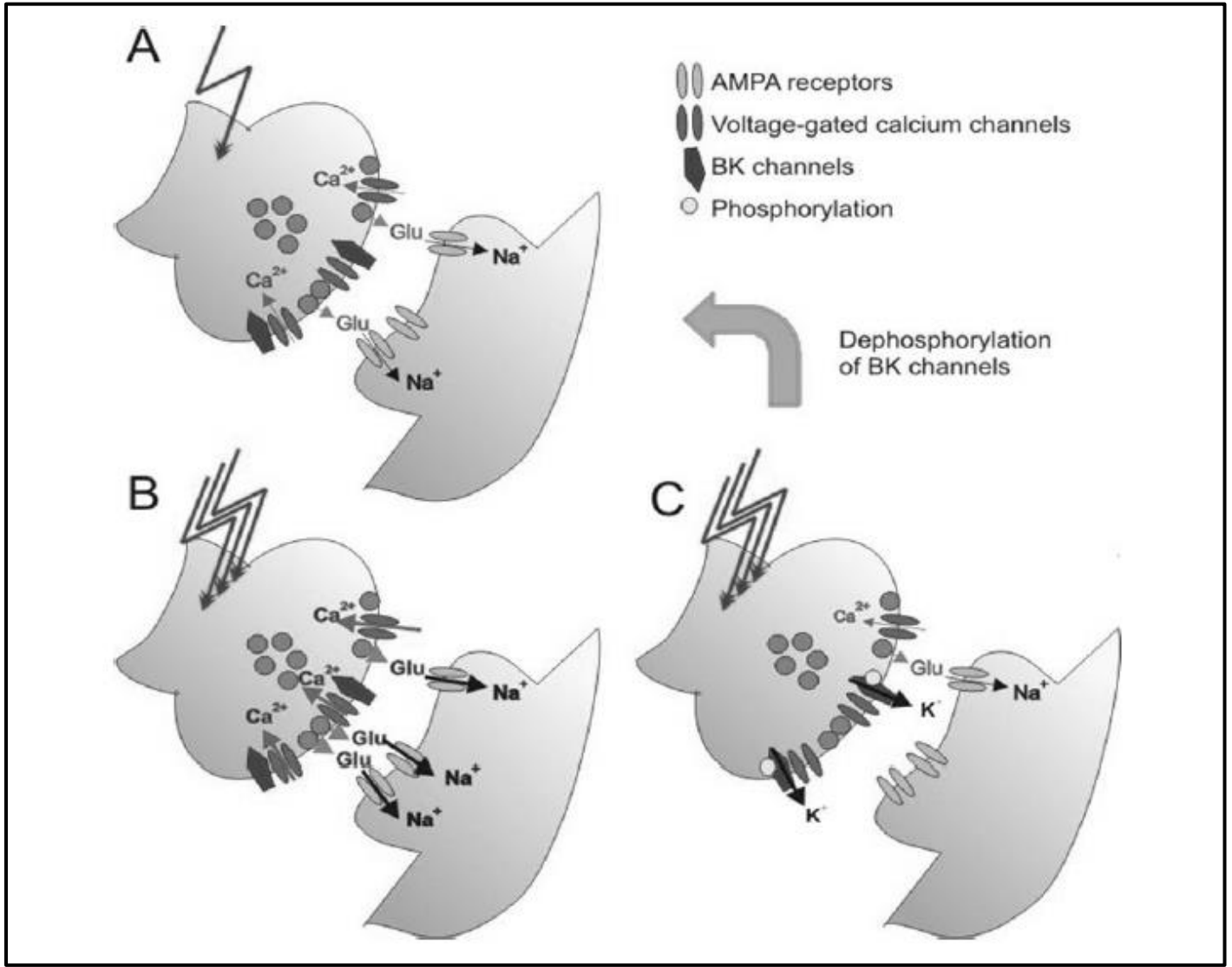
Figure 2.6 Hypothetical molecular mechanism of BK channel dependent regulation of transmitter release at the sensorimotor synapse in the PnC. *A.* Subthreshold synaptic transmission that would not lead to a postsynaptic action potential/startle response. *B.* Action potential bursts that lead to a suprathreshold activation of PnC giant neurons. Ca^{2+} starts to accumulate in the terminal leading to BK channel activation through possible phosphorylation. *C.* BK channel activation truncates further depolarization and calcium influx, reducing transmitter release which results in synaptic depression. Upon gradual dephosphoylation of BK channels, the synapse recovers to its original status (*A).*

3 Hypotheses and Objectives

This study was conducted to test the overall <u>hypothesis</u> that giant neurons within the PnC form the sensorimotor interface of the ASR pathway. More specifically, we hypothesized that these giant neurons are responsible for mediating the startle response and become activated in the presence of a startle stimuli. We additionally hypothesized that PnC giant neurons receive cholinergic input which may co-localize with GABAergic and/or glutamatergic markers, and that presynaptic glutamatergic afferents in contact with these giant neurons would co-express BK channel markers.

There were three main <u>objectives</u> to this work:

1. Confirm the location of giant neurons within the PnC by using Fluorogold retrograde labeling from the spinal cord and validate their function in mediating startle by looking at the expressions of immediate early genes c-Fos and Zif268/EGR-1, as well as the transcription factor pCREB, upon startle activation.

2. Demonstrate and quantify the co-localization of cholinergic terminals in the PnC with GABA and glutamate markers by performing triple labeling immunofluorescence using high affinity choline transporter 1 (CHT1), glutamate decarboxylase (GAD67), and vesicular glutamate transporter 1 (VGLUT1) as respective markers.

3. Show that glutamatergic terminals in the PnC express BK channels by performing dual labeling immunofluorescence using VGLUT1 and $K_{ca}1.1$ as respective markers.

* For the second and third objectives, subsequent staining was done using the neuronal biomarker NeuN in order to understand the relationship of these dual/triple labeled terminals with the startle mediating giant neurons.

4 Materials and Methods

Animal care and handling

A total of 19 adult (300-400g) male (n=5) and female (n=14) Sprague Dawley rats, obtained from Charles River Laboratories (Senneville, Quebec, Canada), were used for this study. Animals were housed at the animal care facility in Western University and kept in a temperature controlled room, on a 12/12 hour light/dark cycle, with access to food and water *ad libitum*. Animals used for behavioural testing were handled prior to the experiments to ensure familiarity with the handler and equipment used. All procedures were approved by the Western University Animal Care and Use Committees and conformed to Canadian Council on Animal Care research guidelines.

4.1 c-Fos, Zif268, and pCREB expression

Stereotaxic surgery

Fifteen male (n=2) and female (n=13) rats were used for this portion of the study. Fluorogold (FG) retrograde tracer (Fluorochrome, LLC, Denver, CO, USA) was injected into the spinal cord of rats to confirm the location of giant neurons within the PnC. The neuronal tracer was injected under deep anaesthesia, using a mixture of Xylacine (13%) and Ketamine (87%) administered intraperitoneally at a concentration of 1ml/kg. Where warranted, an additional injection of the anaesthetic (1/5th of the initial dosage), was given during the surgery. Following anaesthesia, animal furs were shaved off and skin was cleaned with soap, 70% ethanol, and iodine to ensure sterility. The head-positioning protocol referred to by Paxinos and Watson (2004) was used to place animals in a stereotaxic frame for spinal cord injections. For each animal, a midsagittal incision was made on the dorsal surface of the neck, and muscles within that region were removed to expose the laminae of the third and fourth cervical vertebrae. The lamina of the 4th cervical vertebrae was removed and spinal dura was punctured to facilitate subsequent tracer injections. Two pressure injections (1μL each) of FG (4% in saline) were made into the spinal cord bilaterally on either side of the dorsal vein between C3 and C4 (Nodal and López, 2003). On both sides, the first injection was made 1.6mm down from the dorsal surface of the spinal cord, followed by a second injection 0.8mm from the dorsal surface. Silk

sutures (PERMA-HAND®, Ethicon, Sommerville, NJ, USA) were used to close the wounds and animals were allowed a 4 day rest period prior to behavioural testing. Ketoprofen (0.35ml in 3ml saline) was subcutaneously given to animals following surgeries.

Behavioural testing

To test the effects of startle on IEG and pCREB expression in PnC giant neurons, animals were randomly divided into three treatment groups. Seven rats of Group 1 rats "Startle" received startle stimuli. Rats were placed in startle boxes (Med Associates Inc., St. Albans, Vermont, USA) and acclimated to white background noise at 65 dB for 5 minutes. Following acclimation, rats received either 10 (n=4) or 30 (n=3) startle stimuli (Figure 4.1) of 115dB, with an inter trial interval of 15 seconds. Rats remained in the boxes for a total of 60 minutes prior to transcardiac perfusion. Group 2 "Background Noise" rats (n=2) received only white background noise while in the startle boxes for 60 minutes prior to transcardiac perfusion. Group 3 "Silence" rats (n=6) were placed into the startle boxes without any background noise or sound for 60 minutes.
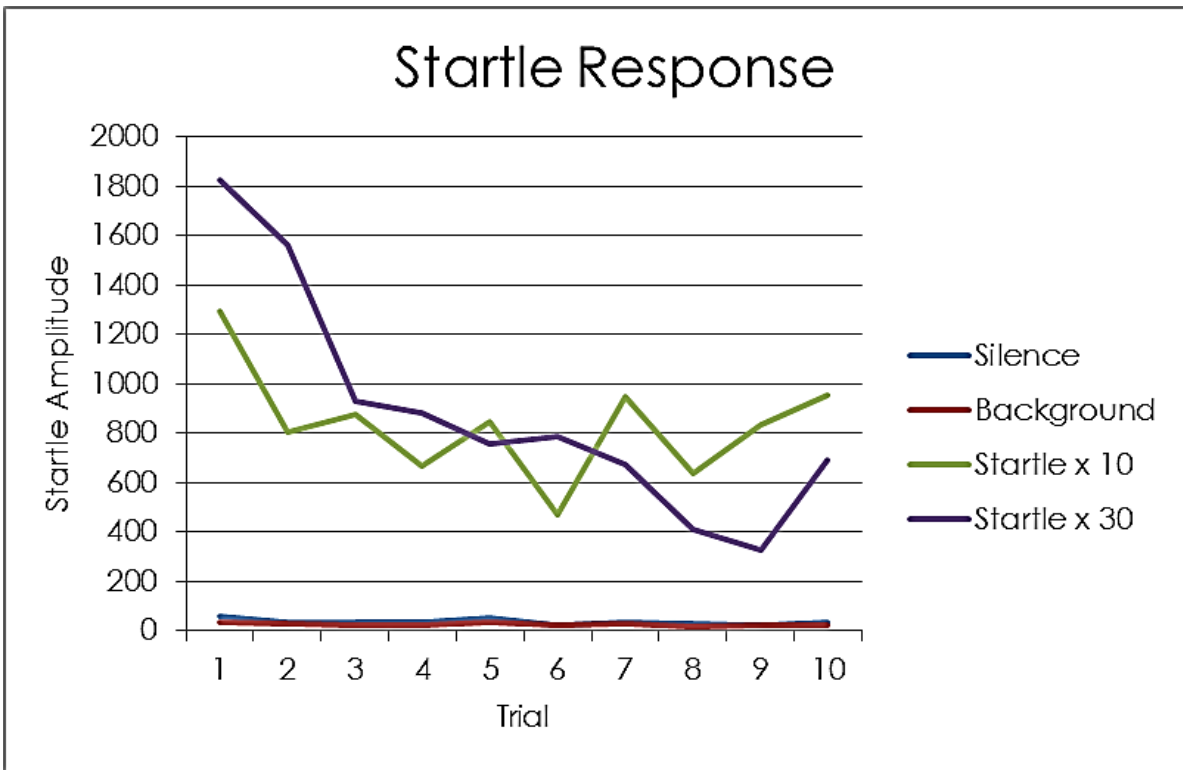
Figure 4.1 Startle response curves for the animals in Group 1 "Startle", Group 2 "Background Noise" and Group 3 "Silence". All animals were acclimated for 5 minutes. Group 1 animals received either 10 or 30 startle stimuli of 115dB, with an inter trial interval of 15 seconds. The first ten trials are shown averaged for all animals in each group. Group 2 rats received only a background noise and Group 3 rats were not given any sound. All rats remained in the boxes for a total of 60 minutes. Only Group 1 rats exhibited a startle response, corrected for the gain factor (gain = 1).

Tissue Processing

Animals were perfused intracardially using 50mls of 0.9% saline, followed by 500ml of 4% paraformaldehyde (PFA) in 0.1M phosphate buffer (PB), while under sodium pentobarbital anaesthesia (54 mg/kg, i.p.). Brains were harvested and post-fixed in the PFA mixture for 1h after which they were immersed in 15% sucrose in 0.1M PB and stored overnight at 4˚C. The following day, brainstems were sliced at the level of the PnC [Bregma 10.20mm, Interaural - 1.20mm, Paxinos and Watson, 2004, Figure 4.2] using a freezing microtome (KS34S, Micron, Walldorf, Germany) creating coronal tissue sections of 40μm in thickness. Parallel series (6-12) of each animal brain were collected and stored at -20˚C in cryoprotectant solution (30% sucrose, 30% ethylene glycol, and 5% of 0.01% sodium azide in 0.1M PB). Free floating tissue sections were thoroughly washed in 0.1M phosphate-buffered saline (PBS; pH 7.35-7.45) prior to immunohistochemical stainings, as well as in between the various incubations.

Figure 4.2 Brainstem slice showing the PnC. The coordinates of the PnC are located at Bregma 10.20mm and Interaural -1.20mm as per Paxinos and Watson, 2004. The PnC is highlighted by the blue rectangle and can easily be distinguished in a tissue section by locating the facial/VII cranial nerves (red arrows).

Immunohistochemistry

All immunohistochemical incubations were performed at room temperature. The expression of c-Fos was tested across all animals of the "Startle", "Background Noise", and "Silence" groups, Zif268/EGR-1 in only the three "Startle" group animals that received 30 stimuli, and pCREB in these same three animals, as well as an additional three rats from Group 3 "Silence". To ensure destruction of endogenous peroxidases, sections were extensively washed in 0.1M PBS and exposed to 1% H_2O_2 in PBS (Caledon Laboratories Ltd., Georgetown, ON, Canada) for 10 minutes. Sections were subsequently blocked in PBS+ solution (0.1M PBS plus 0.4% Triton X-100 and 0.1% bovine serum albumin both from Fisher Scientific, Ottawa, ON, Canada) for 1 hour, followed by overnight incubation in PBS+ with the respective primary antibodies for c-Fos [rabbit polyclonal antibody, 1:1000; sc-52 Santa Cruz Biotechnology, Santa Cruz, CA, USA], Zif268/EGR-1 [rabbit polyclonal, 1:1000; sc-110 Santa Cruz Biotechnology, Santa Cruz, CA, USA], or pCREB [Ser 133 mouse monoclonal, 1:1000; 1B6 Cell Signalling Technology, Beverley, MA, USA]. Figures 4.3, 4.4, and 4.5 show respective in-house positive controls performed for each antibody. Following primary antibody incubation, sections were incubated in PBS+ with their respective biotinylated secondary antibodies, goat anti-rabbit or goat anti-mouse (1:500; Vector Laboratories, Burlingame, CA, USA) for 1 hour. Signal amplification was achieved by bathing sections in PBS+ with avidin-biotin horseradish peroxidase (ABC elite, 1:500; Vector Laboratories, Burlingame, CA, USA) for 1 hour, followed by 10 minutes in PBS containing Biotinylated Tyramine (BT, 1:250, Perkin Elmer, Woodbridge, ON, Canada) and 3% H_2O_2. Biotin was subsequently tagged with a fluorescent dye by incubating sections for 30 minutes in PBS with Alexa Fluor (AF) 633-conjugated streptavidin (1:200; Life Technologies, Burlington, ON, Canada) followed by a short rinse with 0.1M PB. Sections were then mounted onto plus-charged glass slides using Gelatin A (0.3% in ddH_2O) and cover-slipped with Vectashield mounting medium (Vector Laboratories, Burlingame, CA, USA) to prevent photobleaching.
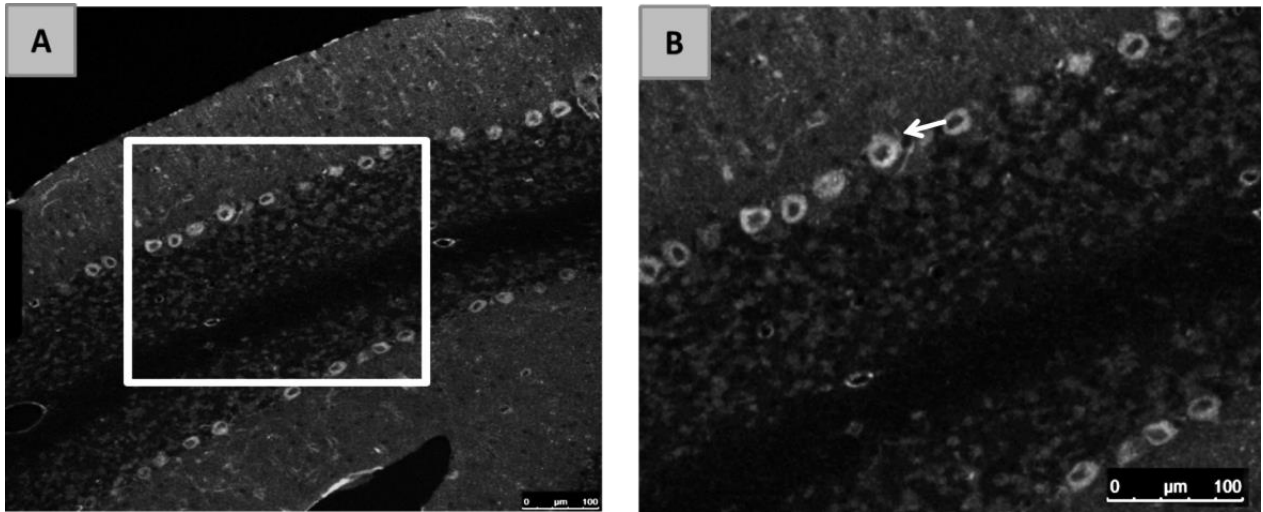
Figure 4.3 Positive control for c-Fos staining. *A.* Positive tissue control showing c-Fos staining in the soma of cerebellar Purkinje cells (Lärkfors et al., 1996). *B.* Magnified image of the region enclosed by the white rectangle in *A.* The arrow points to one brightly labeled c-Fos stained cell body. Scale bars indicate 100μm in both *A* and *B.*
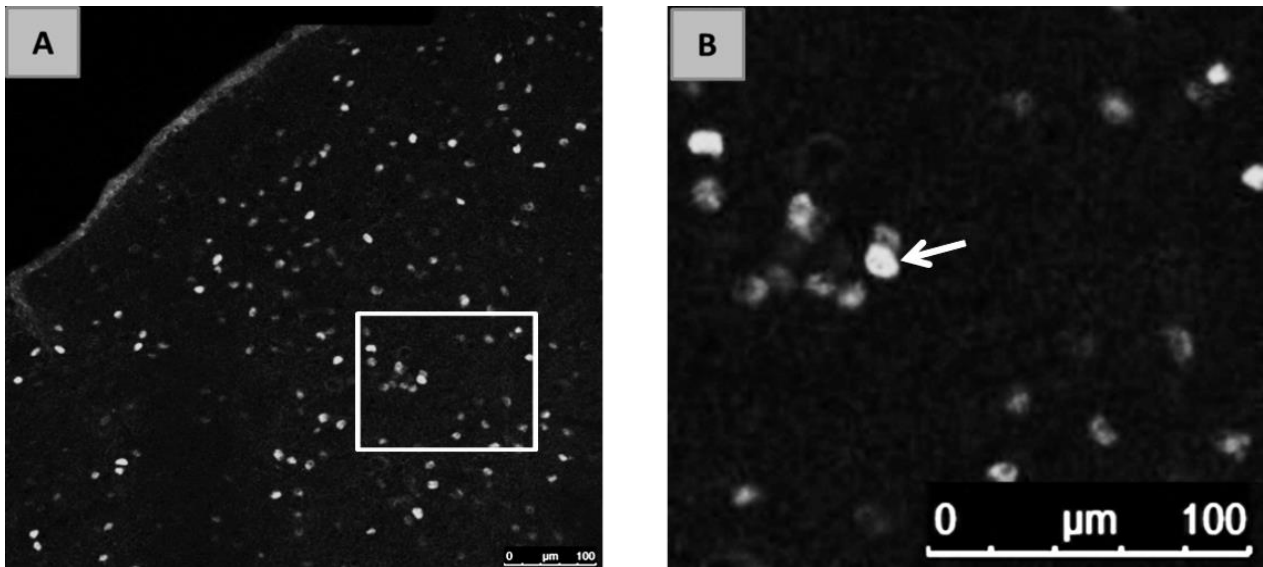
Figure 4.4 Positive control for Zif268/EGR-1 staining. *A.* Positive tissue control showing Zif268/EGR-1 staining in the central nucleus of the inferior colliculus (CIC; Illing et al., 2002). *B.* Magnified image of the region enclosed by the white rectangle in *A.* The arrow points to a brightly labeled Zif268/EGR-1 stained neuron. Scale bars indicate 100μm in both *A* and *B.*

Figure 4.5 Positive control for pCREB staining. *A*. Positive tissue control showing pCREB staining in the central nucleus of the inferior colliculus (CIC; Illing et al., 2002). *B*. Magnified image of the region enclosed by the white rectangle in *A*. The arrow points to brightly labeled pCreb stained neurons. Scale bars indicate 100μm in both *A* and *B*.
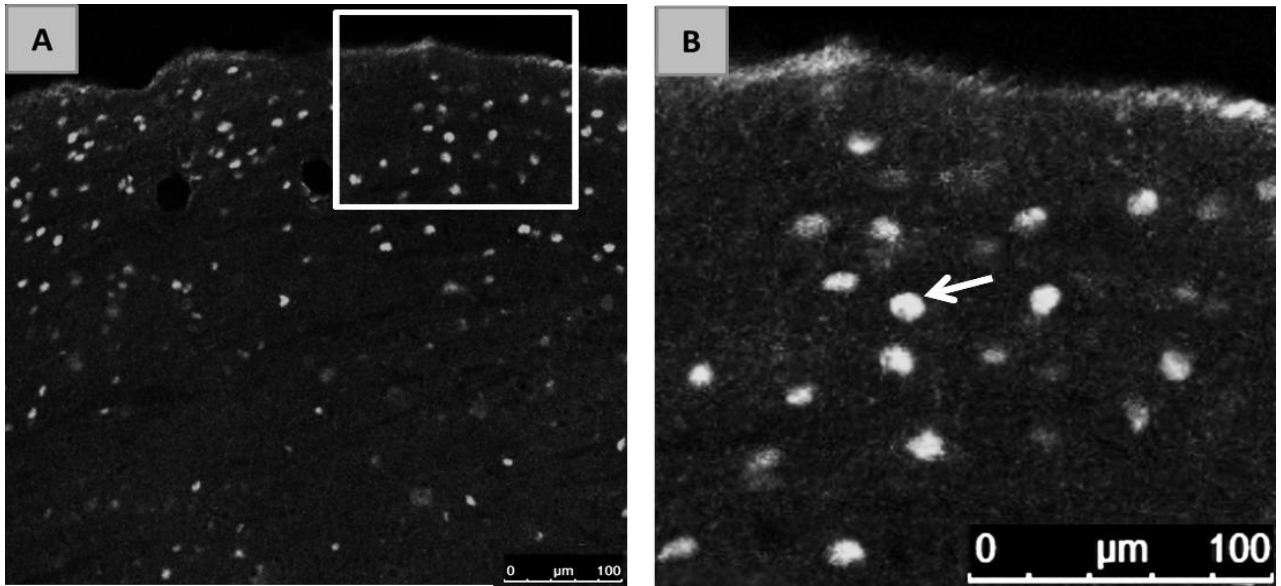
Data analysis

c-Fos expression was examined using all sections from a single series in each of the fifteen animals tested and compared across the different treatment groups. Specifically, the PnC, vestibular (MVeMC/MVePC), and trigeminal motor (Mo5) regions were isolated for analysis (Paxinos and Watson, 2004). The expression of Zif268/EGR-1 in the PnC was analyzed using all sections from a second series in the three startle animals tested. pCREB expression was analyzed using a third parallel series from the animals tested for Zif268/EGR-1, along with a parallel series of sections from Group 3 "Silence" treated animals. All images were captured with an SP5 TCS II Confocal Microscope (Leica Microsystems, Concord, ON, Canada) and LAS AF 2.6 software (Leica Microsystems, Concord, ON, Canada) using various objectives (5x, 20x, 40x, and 63x magnification). The 458nm Argon laser was used to excite FG (excitation max – 370nm); FG's wide emission band (350-750nm) due to two emission peaks (430, 610nm) was filtered to only include signal between 464-550nm. The 633nm laser line was used to excite AF 633 (excitation max – 631nm) and the emission filters selected (670nm-792nm) included the emission peak (647nm) and excluded overlap with FG signals (Figures 4.6 and 4.7). 10% power was used for each laser and the gain/offset were fixed across all sections. In addition, resolution and signal intensity were increased for all images by setting the line average to 4 and frame accumulation to 2, respectively. While no alterations were made to actual images, representative images of c-Fos and Zif268/EGR-1 expression patterns were adjusted (brightness and contrast) for enhanced viewer observation before inclusion in the results. Only pCREB images were counted and subjected to statistical analyses. Giant neuron size was determined by calculating the maximum (length) and minimum (width) soma diameters of 20 regular sized FG labelled neurons within the PnC, perpendicular to each other. The means and standard deviations (SD) of both were calculated, and neurons whose maximum and minimum soma diameters were 3 SD away from the mean were regarded as outliers and characterized as giant neurons. Thus, PnC giant neurons exhibit maximum and minimum diameters that both exceed 36μm and 25μm, respectively. Based on this criteria, 15 giant neurons across the 3 startle treated animals and 11 across the 3 silence treated animals were selected and manually counted to determine the percentage of PnC giant neurons in each case that express nuclear pCREB. The expression of pCREB within the various brainstem regions (PnC, vestibular, motor, and inferior colliculus) was analyzed by using data from three separate

images (63x magnification), for each animal, in each area. The number of pCREB positive cells in each image was counted using Image Pro Premier software (Media Cybernetics, Rockville, MD, USA) with threshold adjustments made to only include signals between the 40-190 grayscale range (French et al., 2008). Statistical analysis for all data (expressed as mean ± SEM) was done using IBM SPSS Statistics 20 software, and an independent t-test or a non-parametric Mann-Whitney U test comparing the means of startle treated animals to the silence treated ones was performed. Statistical significance was determined at a p-value of 0.05 ($\alpha=0.05$).
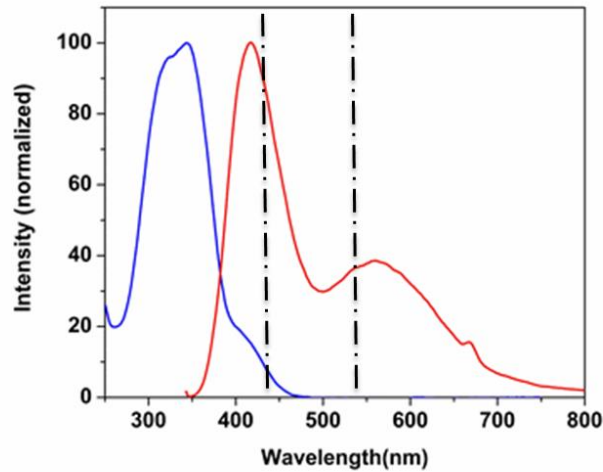
Figure 4.6 Fluorogold excitation and emission spectra. The excitation spectrum of FG is indicated by the blue line and the emission by the red line. Fluorogold is maximally excited at 370nm and exhibits two emission peaks, 430nm and 610nm. Dashed vertical lines represent filters selected to collect signal from 464-550nm. (Image courtesy of AAT Bioquest, 2006).
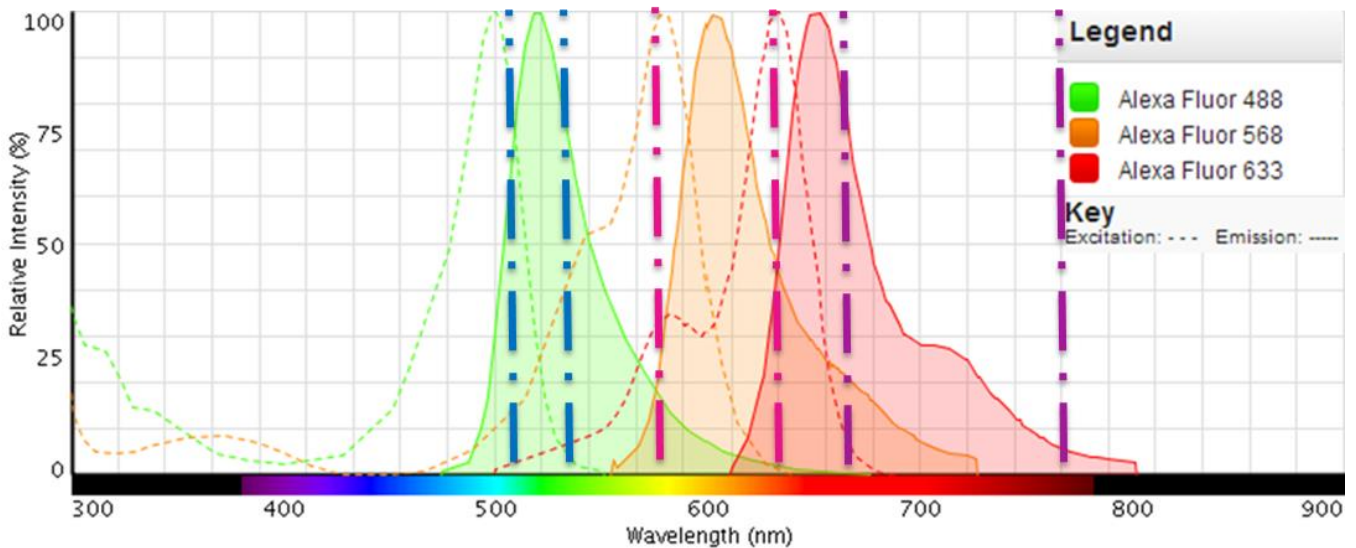
Figure 4.7 Excitation and emission spectra of the various Alexa Fluors used: 488, 568, and 633. AF 488 is maximally excited at 499nm and exhibits an emission peak at 520nm (green). AF 568 is maximally excited at 578nm and exhibits an emission peak at 603nm (orange). AF 633 is maximally excited at 631nm and exhibits an emission peak at 647nm (red). Filters selected to collect signal from AF 488, 568, and 633 are represented by blue (510-535nm), pink

(590-620nm), and purple (670-792nm) dashed vertical lines, respectively. (Image courtesy of Fluorescence SpectraViewer, Life Technologies, 2014).

4.2 CHT1, VGLUT1, and GAD67 expression

Triple immunofluorescence

Two male and one female rat were used for this portion of the study. These animals did not undergo FG injection or behavioural testing procedures, but were perfused using the above protocol for immediate staining. Tissue was processed as described in section 4.1 and triple immunofluorescence staining was performed at room temperature. A single series of each animal was used to test the combined expression of CHT1, VGLUT1, and GAD67 markers within the PnC. Immunohistochemistry was done as per the above protocol, with a few minor adjustments. CHT1 labeling was done by using a rabbit anti-CHT1 polyclonal antibody [1:10000; Courtesy of Dr. Jane Rylett, Western University, London, ON, CANADA, Figure 4.8] followed by a biotinylated goat anti-rabbit secondary (1:500; Vector Laboratories, Burlingame, CA, USA). ABC elite, BT, and AF 633-conjugated streptavidin (1:200; Life Technologies, Burlington, ON, Canada) were used subsequently to complete staining. VGLUT1 labeling was done using a guinea pig anti-VGLUT1 polyclonal antibody [1:1000, Millipore, Billerica, MA, USA, Figure 4.10] followed by a biotinylated goat anti-guinea pig secondary antibody (1:500; Vector Laboratories, Burlingame, CA, USA). ABC elite, BT, and AF 488-conjugated streptavidin (1:200; Life Technologies, Burlington, ON, Canada) were used subsequently to complete staining. GAD67 labeling was done by using a mouse anti-GAD67 monoclonal antibody [1:500; Millipore, Billerica, MA, USA, Figure 4.9] followed by AF 568-conjugated goat anti-mouse secondary antibody (1:200; Life Technologies, Burlington, ON, Canada). Sections were then mounted onto positively-charged glass slides using Gelatin A (0.3% in ddH$_2$O) and cover-slipped with Vectashield mounting medium (Vector Laboratories, Burlingame, CA, USA) to prevent photobleaching. For negative controls the primary antibody was omitted which resulted in the absence of labeling at the respective wavelength (Figure 4.11).
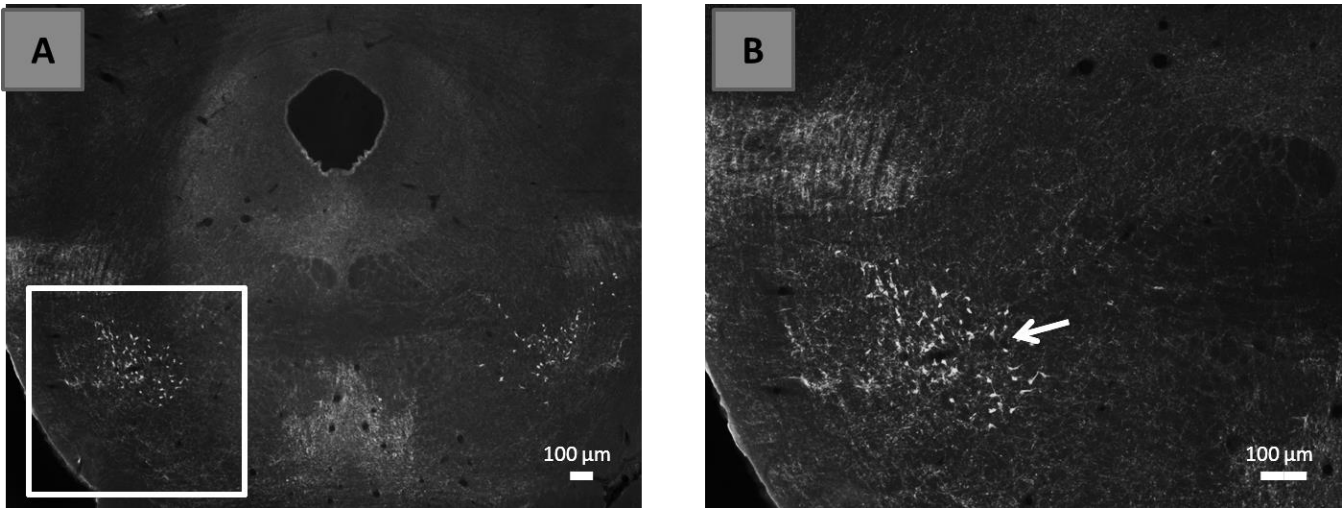
Figure 4.8 Positive control for CHT1 staining (polyclonal rabbit antibody). *A*. Positive tissue control showing CHT1 staining in the pedunculopontine tegmental nucleus (PPT; Koch et al., 1993; Mitani et al., 1988). *B*. Magnified image of the region enclosed by the white rectangle in *A*. The arrow points to brightly labeled cholinergic neurons. Scale bars indicate 100μm in both *A* and *B*.
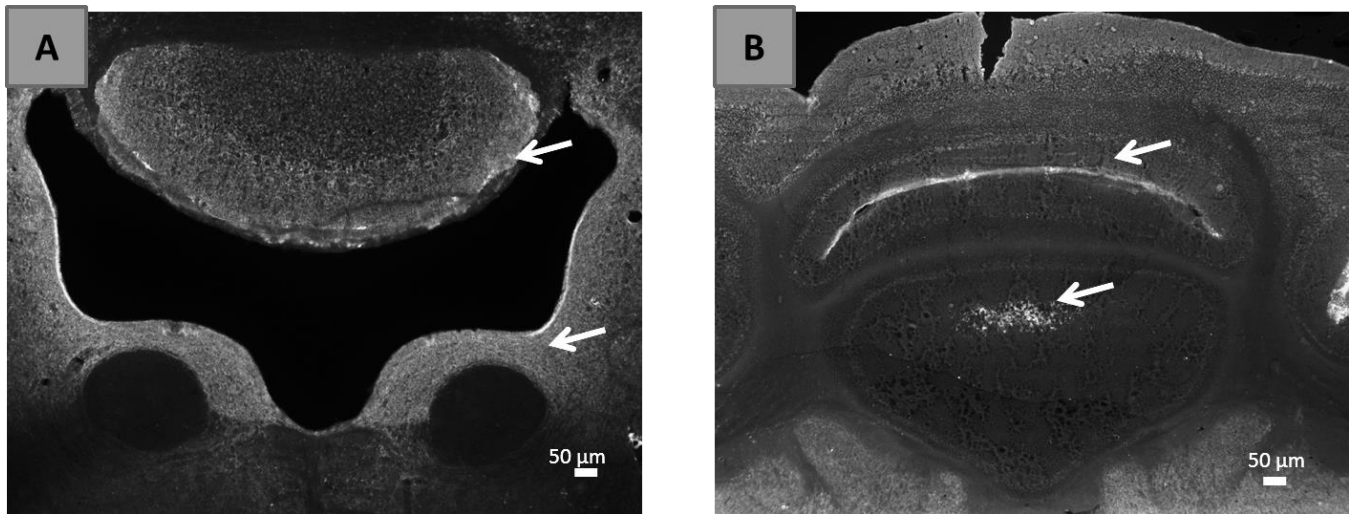
Figure 4.9 Controls for GAD67 staining. *A –B*. Positive tissue control showing GAD67 staining in the cerebellum, specifically in Purkinje and granule cells (Escapez et al., 1994; Kaufman et al., 1991). Arrows indicate areas with brightly labeled GAD67. Scale bars indicate 50μm in both *A* and *B*.
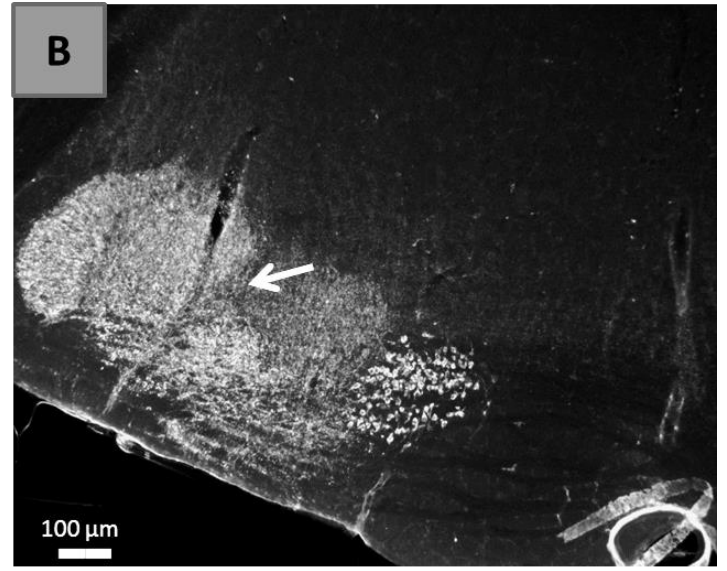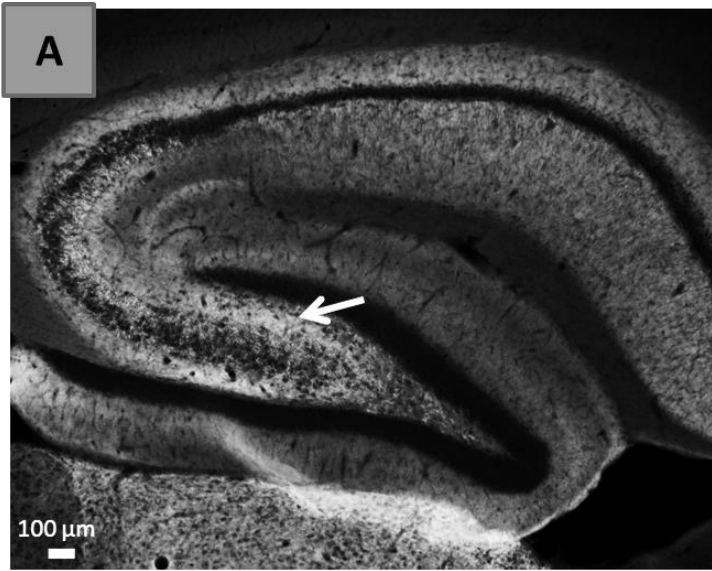
Figure 4.10 Positive control for VGLUT1 staining. *A*. Positive tissue control showing VGLUT1 staining (arrow) in a sagittal slice of the hippocampus (Antonucci et al., 2012). *B*. An alternate positive control for VGLUT1 showing staining (arrow) in the lateral superior olivary (LSO) nucleus of the brainstem (Billups, 2005). Scale bars indicate 100μm in both *A* and *B*.
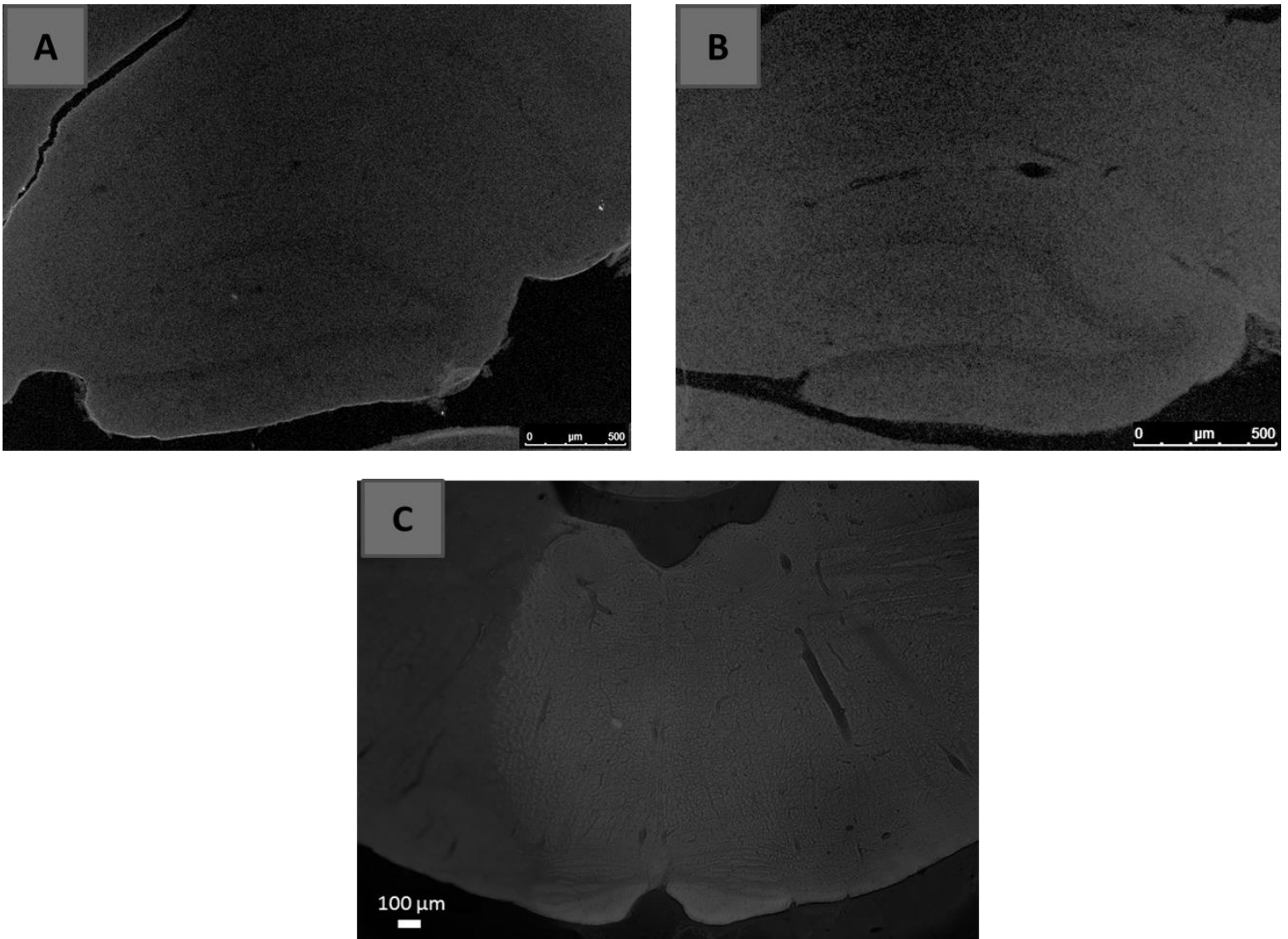
Figure 4.11 Negative controls for Alexa Fluorochromes. *A*. Hippocampal section showing no unspecific labeling from the Alexa Fluor 488 when no primary antibody was included in the staining. Contrast this image with Figure 4.9a. *B*. Hippocampal section showing no unspecific labeling from the Alexa Fluor 568 when no primary antibody was included in the staining. *C*. Negative control showing no unspecific labeling from the Alexa Fluor 633 in the absence of a primary antibody. Contrast this image with Figure 4.9b. Scale bars indicate 500μm in both *A* and *B;* 100μm in *C*.

Data analysis

A single series of each animal was used to test the combined expression of CHT1, VGLUT1, and GAD67 markers within the PnC. Z-series images ($63 \times$ magnification) were acquired at 0.60 μm intervals with SP5 TCS II Confocal Microscope (Leica Microsystems, Concord, ON, Canada) using LAS AF 2.6 software (Leica Microsystems, Concord, ON, Canada). The 488nm Argon laser was used to excite AF 488 (excitation max – 499nm) and the emission filters were selected only include signal between 510-535nm. The 543nm laser was used to excite AF 568 (excitation max – 578nm) and the emission filters were selected to only include signal between 590-620nm. The 633nm laser line was used to excite AF 633 (excitation max – 631nm) and the emission filters were selected to only include signal between 670-792nm. Filters were chosen to reduce as much overlap as possible between the three lasers while still maintaining sufficient signal detection (Figure 4.7). 20% power was used for the Argon and 633nm laser, 40% for the 543nm laser, and the gain/offset were fixed across all sections. In addition, resolution and signal intensity were increased for all images by setting the line average to 4 and frame accumulation to 2, respectively. While no alterations were made to actual images, representative images of CHT1, VGLUT1, and GAD67 expression patterns were adjusted (brightness and contrast) for enhanced viewer observation before inclusion in the results. The z-series acquired from each animal consisted of anywhere between 30-50 steps. Three planes were chosen for analysis by dividing the number of total steps into quartiles, and selecting the planes that make up the end of the 1st (Q_1), 2nd (Q_2), and 3rd (Q_3) quartiles. The merged images for the three different quartiles in each of the three animals were imported into Image Pro Premier (Media Cybernetics, Rockville, MD, USA) for analysis. The software was used to split the combined triple immunofluorescence image into three separate channels (red, green, and blue). Threshold adjustments were made to only include signals between various grayscale ranges (French et al., 2008), dependent on antibody strength and intensity (CHT1: 70-190, VGLUT1: 40-190, GAD67: 50-190). Once threshold filters were selected, a masked image was composed to exclude background noise and unwanted signals. Using the program's automated counter, combinations of two (CHT1+VGLUT1, CHT1+GAD67, VGLUT1+GAD67) channels were analyzed to determine the percentage of single or colocalized immunostained markers within the PnC. Since the Image Pro Premier only allows for colocalization to be determined between two channels, triple labeling of markers (CHT1+VGLUT1+GAD67) was manually

counted using the LAS AF Lite software (Leica Microsystems, Concord, ON, Canada). Descriptive statistics for all data (expressed as mean ± SEM) was done using IBM SPSS Statistics 20 software.

4.3 CHT1 and VGLUT1/GAD67 expression on NeuN-labeled giant neurons

Triple immunofluorescence

A second and third series of tissue sections, from the same animals processed above in section 4.2, were used for this portion of the study. One series was used to test the combined expression of CHT1, NeuN, and VGLUT1 and the other, CHT1, NeuN, and GAD67, within the PnC. Immunohistochemistry was performed as previously described. CHT1 labeling was done by using a rabbit anti-CHT1 polyclonal antibody (1:10000; Courtesy of Dr. Jane Rylett, Western University, London, ON, CANADA) followed by a biotinylated goat anti-rabbit secondary antibody (1:500; Vector Laboratories, Burlingame, CA, USA). ABC elite, BT, and AF 633-conjugated streptavidin (1:200; Life Technologies, Burlington, ON, Canada) were used to complete staining. Labeling of either VGLUT1 **OR** GAD67 was then performed using a guinea pig anti-VGLUT1 polyclonal antibody (1:1000, Millipore, Billerica, MA, USA) followed by a biotinylated goat anti-guinea pig secondary (1:500; Vector Laboratories, Burlingame, CA, USA) **OR** a mouse anti-GAD67 monoclonal antibody (1:500; Millipore, Billerica, MA, USA) followed by a biotinylated goat anti-mouse secondary antibody (1:500; Vector Laboratories, Burlingame, CA, USA). ABC elite, BT, and AF 488-conjugated streptavidin (1:200; Life Technologies, Burlington, ON, Canada) were used subsequently to complete staining. NeuN labeling was performed last using a mouse anti-NeuN monoclonal antibody [1:1000; Millipore, Billerica, MA, USA, Figure 4.12] followed by AF 568-conjugated goat anti-mouse secondary antibody (1:200; Life Technologies, Burlington, ON, Canada). Sections were then mounted onto plus-charged glass slides using Gelatin A (0.3% in ddH$_2$O) and cover-slipped with Vectashield mounting medium (Vector Laboratories, Burlingame, CA, USA) to prevent photobleaching.
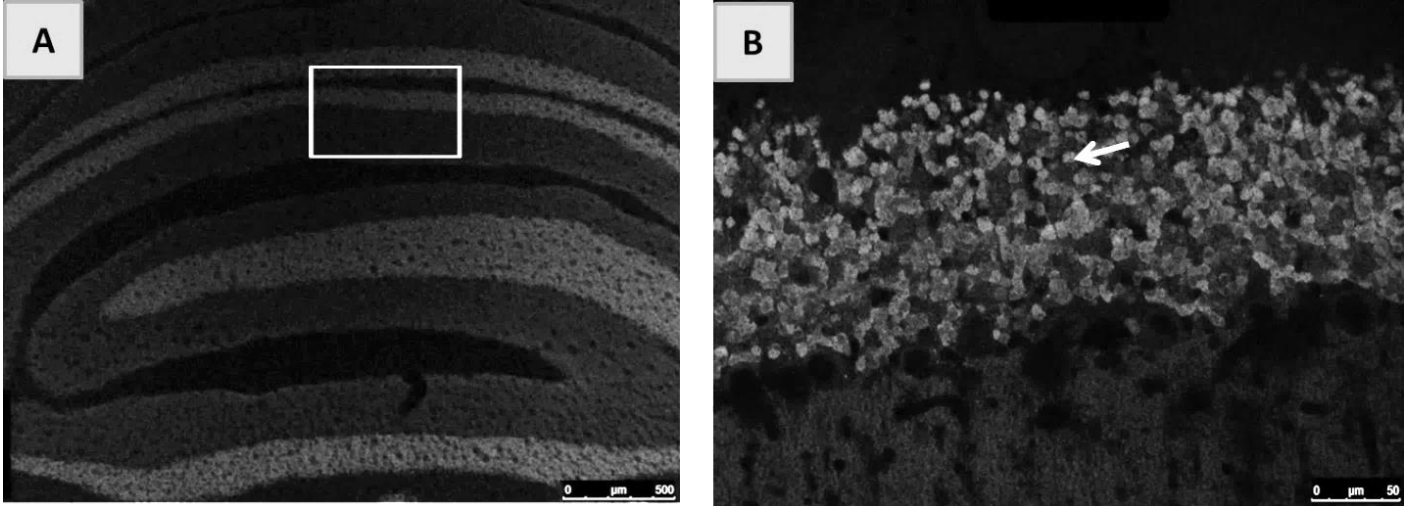
Figure 4.12 Control for NeuN staining. *A.* Positive tissue control showing NeuN staining in the inner granule cells of the cerebellum (Guo et al., 2011). *B.* Magnified image of the region enclosed by the white rectangle in *A.* The arrow points to brightly labeled NeuN stained cells. Scale bars indicate 100µm in *A* and 50µm in *B.*

Data analysis

A single series of each animal was used to test the combined expression of CHT1 and VGLUT1 cells contacting PnC giant neurons, and another was used to test that of CHT1 and GAD67. Z-series images were acquired as indicated in the previous section using all of the same laser settings. Again, no alterations were made to actual images except those adjustments necessary to enhance image visualization (brightness and contrast). The z-series acquired from each animal for the two separate series consisted of anywhere between 30-50 steps. This time, instead of three planes, three giant neurons (according to the above established criteria), from the section where their nucleoli were visible were chosen for analyzing contact on neuronal soma. Only one giant neuron was chosen for analyzing contact on proximal dendrites since not all giant neurons exhibited proximal dendrites due to incomplete filling of dendrites by NeuN labeling techniques. The merged images for the three giant neurons in each of the three animals for both series were imported into Image Pro Premier (Media Cybernetics, Rockville, MD, USA). The autotracing tool was used to trace a perimeter around each giant neuron and crop out any background information. The software was then used to split the combined triple immunofluorescence image into three separate channels (red, green, and blue). Threshold adjustments were made to only include signals between various grayscale ranges (French et al., 2008), dependent on antibody strength and intensity (CHT1: 70-190, VGLUT1: 40-190, GAD67: 50-190). Once threshold filters were selected, a masked image was composed to exclude background noise and unwanted signals. Using the program's manual counter function, the number of individually stained CHT1 synaptic terminals or those dually labeled with either VGLUT1 or GAD67 markers, contacting NeuN-labeled giant neurons were recorded. The location where contact occurred (soma or proximal dendrite) was also taken into account. Descriptive statistics for all data (expressed as mean ± SEM) were done using IBM SPSS Statistics 20 software.

4.4 BK Channel and VGLUT1/GAD67/CHT1 expression on NeuN-labeled giant neurons

Triple immunofluorescence

A fourth, fifth, and sixth series of tissue sections, from the same animals as processed in section 4.2, were used for this portion of the study. One series was used to test the combined expression of BK Channel, NeuN, and VGLUT1, another BK, NeuN, and GAD67, and a third, BK Channel, NeuN, and CHT1, within the PnC. Once more, immunohistochemistry was performed as previously described. BK Channel labeling was done by using a rabbit anti-K_{Ca} 1.1 polyclonal antibody [1:1000; Alomone Labs, Jerusalem, Israel, Figgure 4.13] followed by a biotinylated goat anti-rabbit secondary antibody (1:500; Vector Laboratories, Burlingame, CA, USA). ABC elite, BT, and AF 633-conjugated streptavidin (1:200; Life Technologies, Burlington, ON, Canada) were used subsequently to complete staining. Triton X was omitted in all solutions used to process BK immunohistochemistry. Labeling of either VGLUT1 **OR** GAD67 **OR** CHT1 was next completed using a guinea pig anti-VGLUT1 polyclonal antibody (1:1000, Millipore, Billerica, MA, USA) followed by a biotinylated goat anti-guinea pig secondary antibody (1:500; Vector Laboratories, Burlingame, CA, USA) **OR** a mouse anti-GAD67 monoclonal antibody (1:500; Millipore, Billerica, MA, USA) followed by a biotinylated goat anti-mouse secondary antibody (1:500; Vector Laboratories, Burlingame, CA, USA) **OR** a mouse anti-CHT1 monoclonal antibody [1:1000, Millipore, Billerica, MA, USA, Figure 4.14] followed by a biotinylated goat-anti mouse secondary (1:500; Vector Laboratories, Burlingame, CA, USA). ABC elite, BT, and AF 488-conjugated streptavidin (1:200; Life Technologies, Burlington, ON, Canada) were used subsequently to complete staining. NeuN labeling was performed last using a mouse anti-NeuN monoclonal antibody (1:11000; Millipore, Billerica, MA, USA) followed by AF 568-conjugated goat anti-mouse secondary antibody (1:200; Life Technologies, Burlington, ON, Canada). Sections were then mounted onto positively-charged glass slides using Gelatin A (0.3% in ddH$_2$O) and cover-slipped with Vectashield mounting medium (Vector Laboratories, Burlingame, CA, USA) to prevent photobleaching.
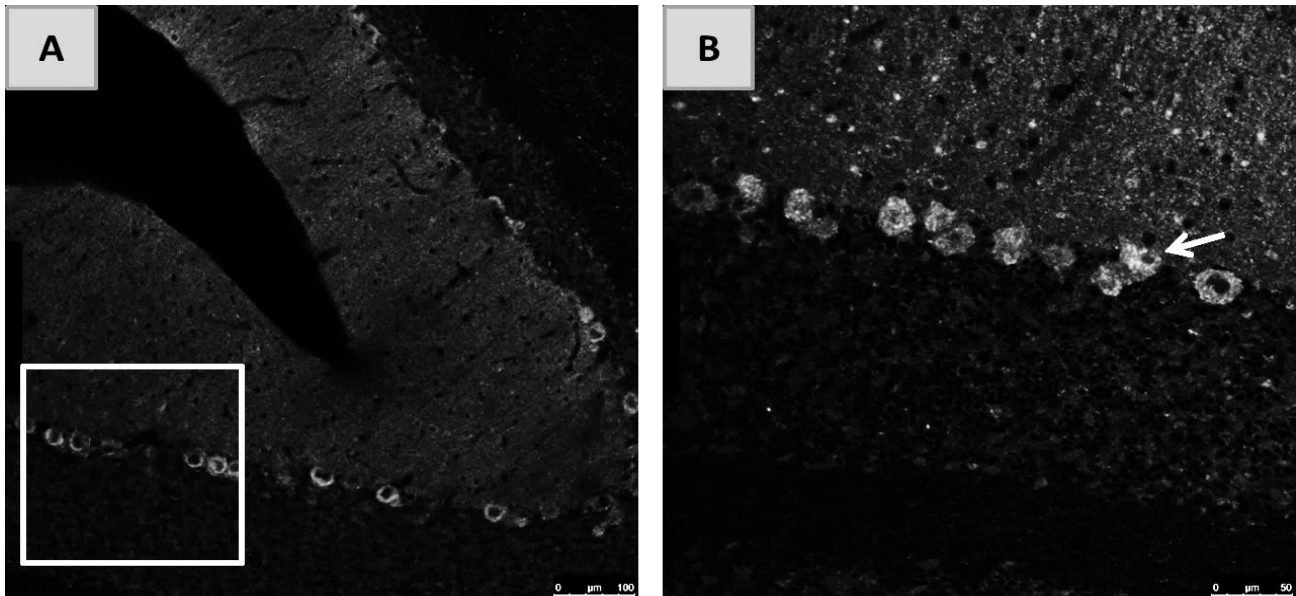
Figure 4.13 Positive control for BK Channel staining. *A.* Positive tissue control showing BK staining in the cerebellar Purkinje cells (referenced in Sausbier et al., 2006). *B.* Magnified image of the region enclosed by the white rectangle in *A.* The arrow points to brightly labeled BK stained cells. Scale bars indicate 100μm in *A* and 50μm in *B.*

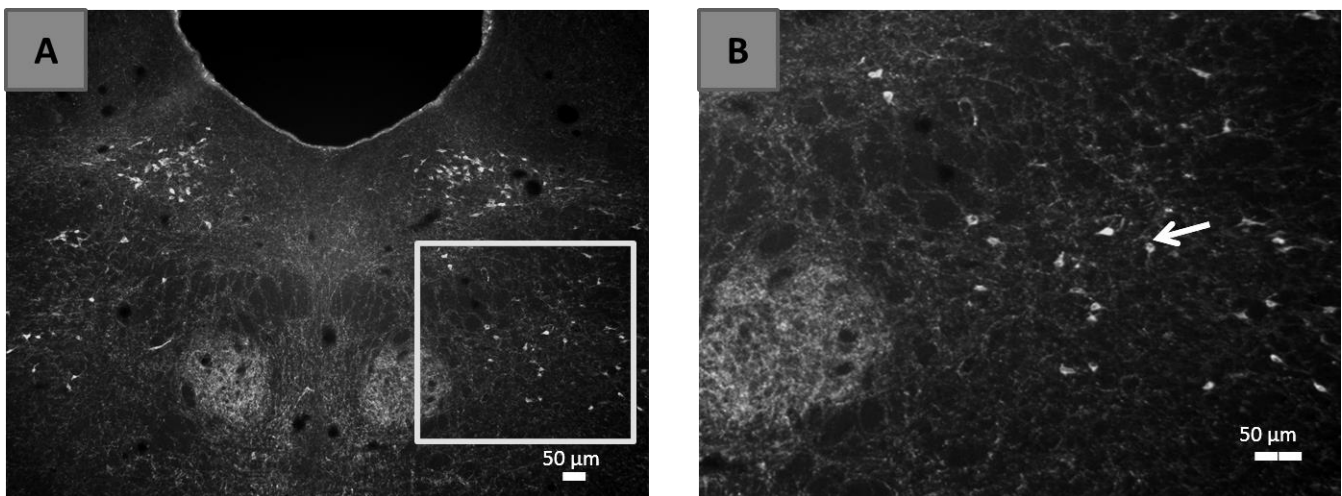**Figure 4.14** Positive control for CHT1 staining (monoclonal mouse antibody). *A.* Positive tissue control showing CHT1 staining in the pedunculopontine tegmental nucleus (PPT; Koch et al., 1993; Mitani et al., 1988). B. Magnified image of the region enclosed by the white rectangle in A. The arrow points to brightly labeled cholinergic neurons. Scale bars indicate 50μm in both A and B.

Data analysis

A single series of each animal was used to test the combined expression of BK and VGLUT1, another BK and GAD67, and a third BK and CHT1. In this case two separate analyses were conducted: one to determine the percentage of the respective colocalization within the PnC, and another to quantify the number of co-labeled synaptic terminals contacting a given the PnC giant neuron. For the first analysis, the NeuN channel was ignored and only dual staining of BK and VGLUT1, GAD67, or CHT1, was looked at. Z-series images were acquired as indicated in the previous section using all of the same laser settings. Again, no alterations were made to actual images except those adjustments necessary to enhance image visualization (brightness and contrast). The z-series acquired from each animal for the two separate series consisted of anywhere between 30-50 steps. As described above, three planes per animal were chosen for analysis based on quartiles. The merged images for each of the three different quartiles and for each of the unique staining combination (from three different animals) were imported into Image Pro Premier (Media Cybernetics, Rockville, MD, USA) for analysis. The software was used to split the combined triple immunofluorescence image into three separate channels (red, green, and blue). Threshold adjustments were made to only include signals between various grayscale ranges (French et al., 2008), dependent on antibody strength and intensity (BK: 40-190, VGLUT1: 40-190, GAD67: 50-190, CHT1: 70-190). Once threshold filters were selected, a masked image was composed to exclude background noise and unwanted signals. Using the program's automated counter, combinations of two channels (BK+VGLUT1, BK+GAD67, BK+CHT1) were analyzed to determine the percentage of single or dual labeled synaptic terminals that exist within the PnC.

For the second analysis, three giant neurons with a visible nucleolus were chosen. The merged images for each giant neuron, from the various series and animals used, were imported into the Image Pro Premier software. The autotracing tool was used to trace a perimeter around each giant neuron and crop out any background information. The software was then used to split the combined triple immunofluorescence image into three separate channels (red, green, and blue). Threshold adjustments were made to only include signals between various grayscale ranges (French et al., 2008), dependent on antibody strength and intensity (BK: 40-190, VGLUT1: 40-

190, GAD67: 50-190, CHT1: 70-190). Once threshold filters were selected, a masked image was composed to exclude background noise and unwanted signals. Using the program's manual counter function, the number of terminals labeled with only one antibody (BK, VGLUT1, GAD67, or CHT1), or dually labeled (BK+VGLUT1, BK+GAD67, BK+CHT1) that came into contact with NeuN-labeled giant neurons, were recorded. The location where contact occurred (soma or proximal dendrite) was also recorded. Descriptive statistics for all data (expressed as mean ± SEM) was done using IBM SPSS Statistics 20 software.

5 Results

5.1 Giant neurons within the PnC mediate the startle response

The location of giant neurons within the PnC was confirmed by injecting a retrograde tracer, 4% Fluorogold, into the spinal cord of 13 adult Sprague-Dawley rats [see Materials and Methods]. Fluorogold labelled all neurons in within the reticular formation as well as vestibular, auditory, trigeminal motor, and raphe nuclei that project to the injection site in C3/C4 segments of the cervical spinal cord (Figure 5.1). Giant neurons were distinguished from their counterparts based on their location within the PnC and size. The mean length (maximum) and width (minimum) soma diameters of regular neurons (n=20) were determined to be $23.70 \pm 0.95\mu m$ and $15.4 \pm 0.74\mu m$, respectively (Figure 5.2A). Neurons three standard deviations away from these means with a length $> 36\mu m$ and a width $> 25\mu m$, were considered to be giant (see Materials and Methods). As such, the mean length and width soma diameters of giant neurons (n=73) were determined to be $48.71 \pm 0.88\mu m$ and $31.69 \pm 0.70\mu m$, respectively (Figure 5.2B).
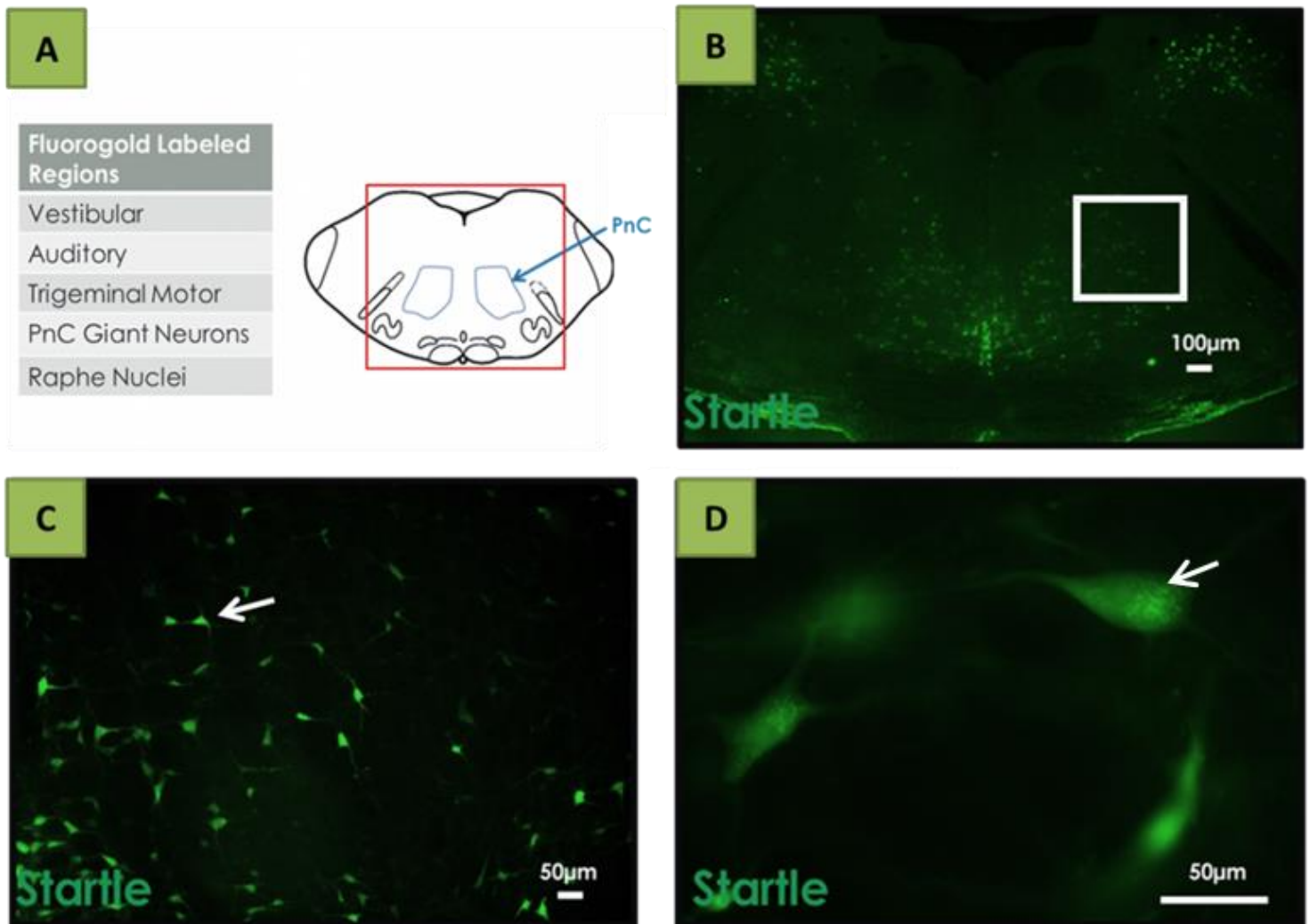
Figure 5.1 Fluorogold tracing effectively labels PnC giant neurons. *A.* Schematic of brainstem slice; PnC region is shown in blue. *B.* Region depicted by the red rectangle in *A.* All of the brightly lit neurons project to C3/C4 region of the spinal cord where Fluorogold was injected. *C.* Magnified image of the PnC area outlined in *B.* The criss-cross pattern of the reticular formation can be seen as well as a mixture of giant (arrow) and non-giant neurons. *D.* Magnified image of *C.* where the giant neurons of interest can be seen (>36μm; arrow). Scale bars indicate 100μm in *B* and 50μm in both *C* and *D.*
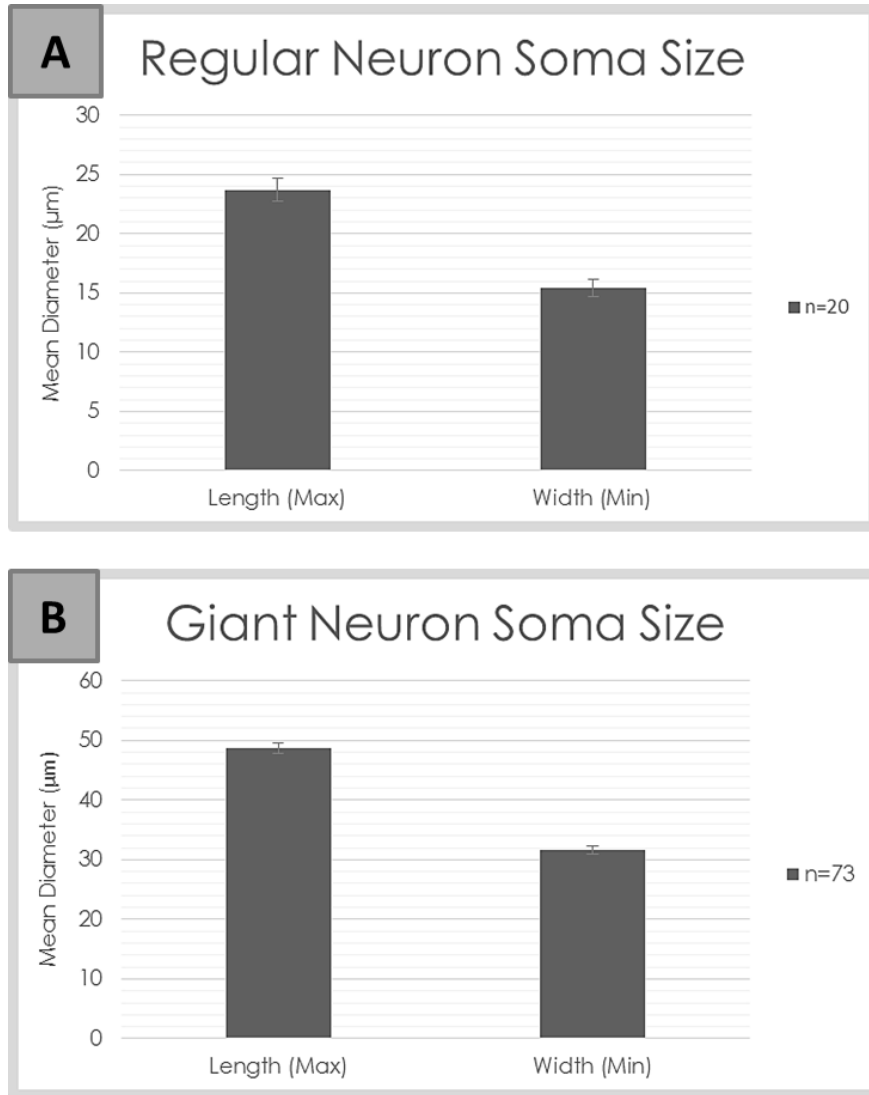
Figure 5.2 Maximum (length) and minimum (width) soma diameters (mean ± SEM) of labeled regular (*A.*) and giant (*B.*) neurons within the PnC. Legends represent number of neurons measured for each type.

The function of giant neurons, specifically their role in mediating startle, was tested by analyzing the expression of two immediate early genes, c-Fos and Zif268/EGR-1, as well as the active, thus phosphorylated, form of the transcription factor CREB, in animals that were startled. Positive tissue controls for all antibodies used can be found in the Materials and Methods section. c-Fos expression was seen in the Mo5 trigeminal motor nuclei of startled rats (n=7) but not those treated with background noise (n=2) or silence (n=3) (Figure 5.3). Activity dependent expression of c-Fos was seen within the vestibular nuclei of startled and background noise but not silence treated animals (Figure 5.4). Interestingly, c-Fos was not seen in the Fluorogold-labeled PnC giant neurons of startled animals nor in the animals treated with background noise or silence (Figure 5.5). Similar to its counterpart c-Fos, Zif268/EGR-1 was not expressed in Fluorogold-labeled PnC giant neurons of startled animals (n=3) (Figure 5.6).
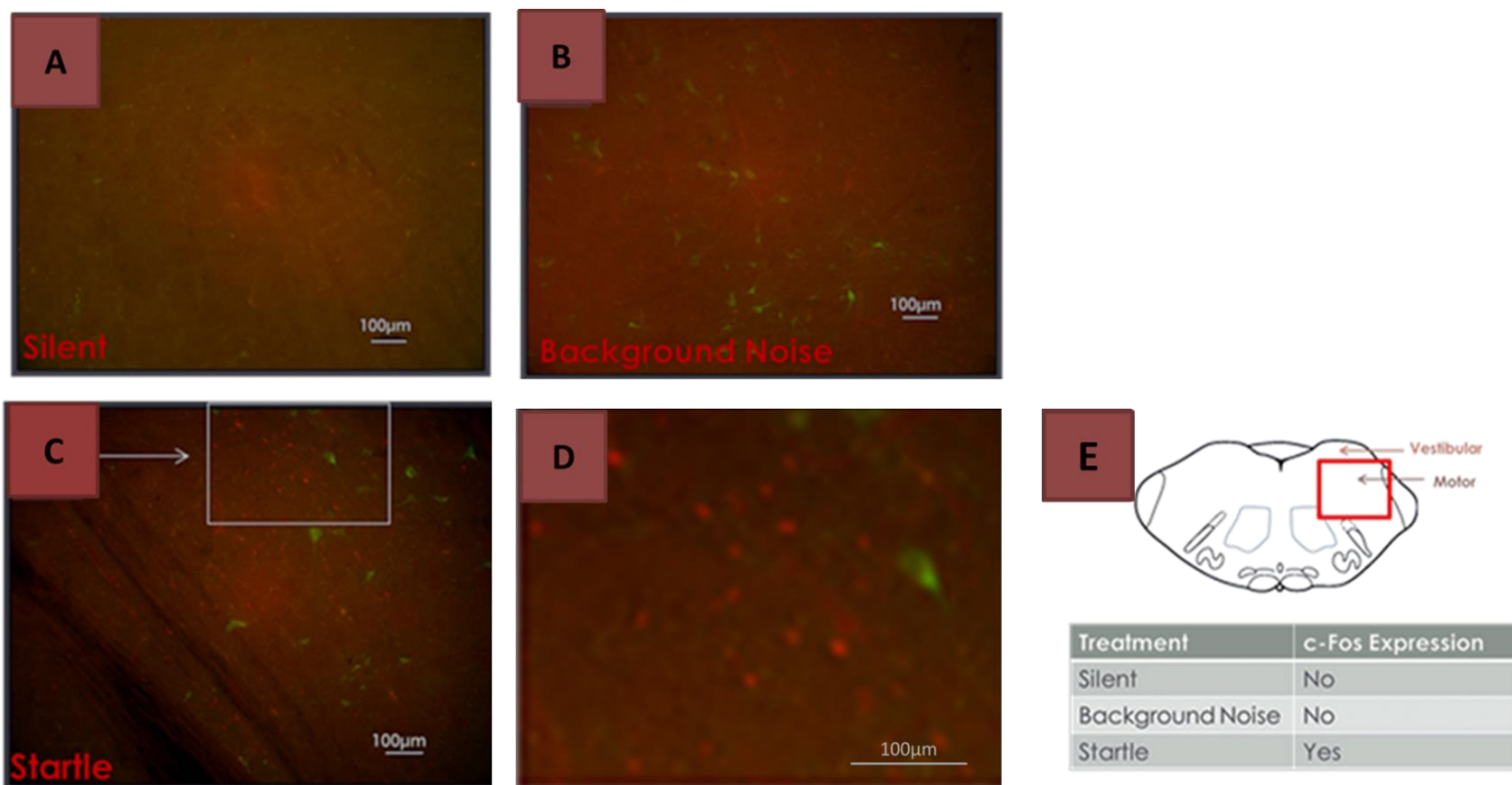
Figure 5.3 c-Fos expression (red) within motor nuclei is seen in startled animals (*C;* n=7) but not in animals subjected to background noise (*B;* n=2) or silence (*A;* n=3) animals. *D.* Magnified image of the area outlined in *C* indicating c-Fos expression. *E.* A schematic brainstem slice where the red rectangle depicts the region shown in *A-C*. The motor region shown is the motor trigeminal (Mo5) nuclei. Fluorogold labeled neurons (green) are seen in *B* and *C*. Scale bars indicate 100μm in all images.
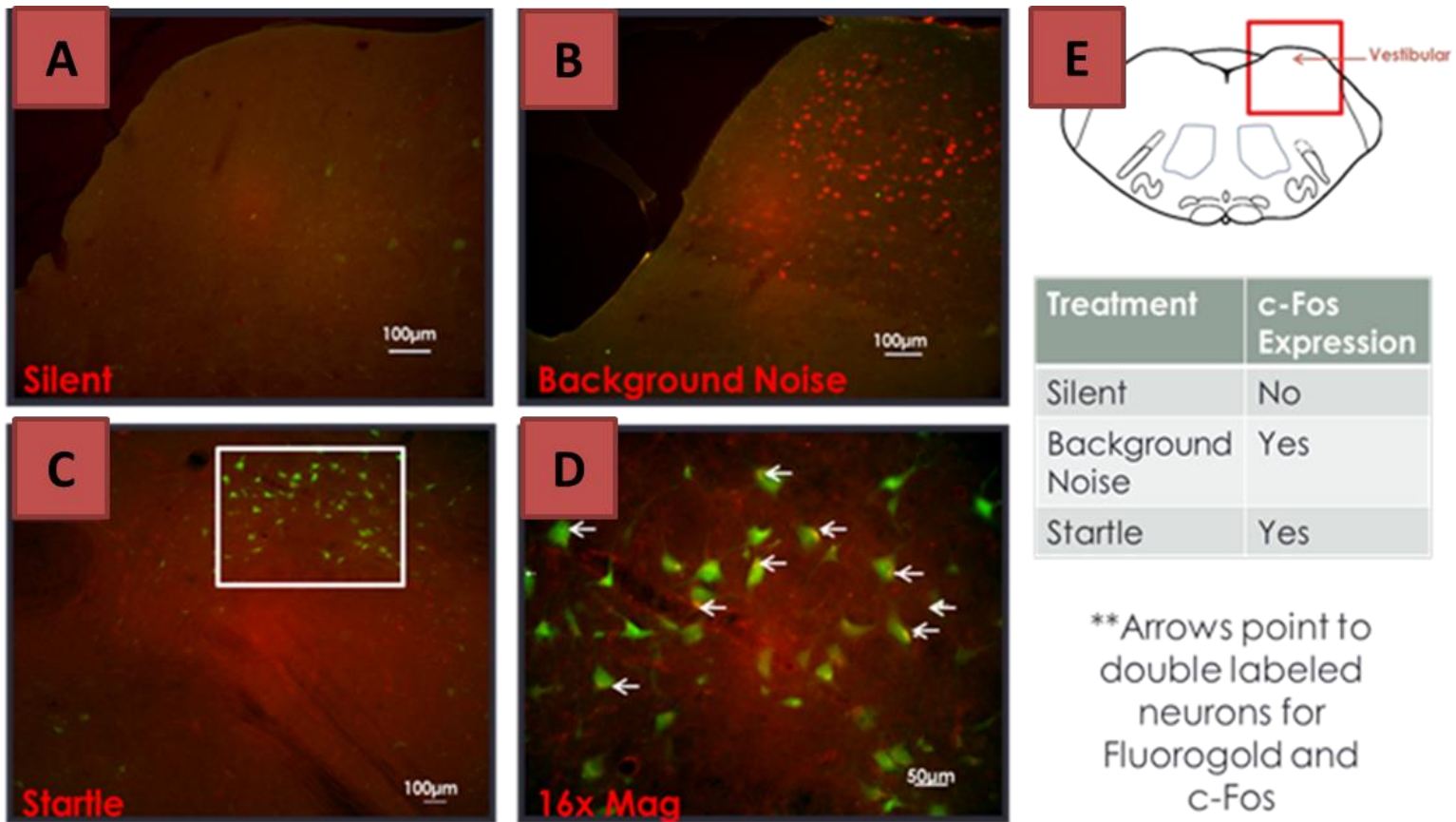
Figure 5.4 Activity-dependent expression of c-Fos (red) is not seen in the vestibular nuclei of silence (n=3) treated animals *A.* but is seen in background noise (n=2) *B.* and startle (n=7) *C.* treated animals. *D.* The image shown is a magnification of the area outlined in *C.* Double labeling for Fluorogold and c-Fos is seen in startled animals (white arrows*). E.* A schematic brainstem slice where the red rectangle depicts the region shown in *A-D.* Scale bars indicate 100μm in *A*, *B* and *C;* 50μm in *D.*

Treatment	c-Fos Expression
Silent	No
Background Noise	No
Startle	No
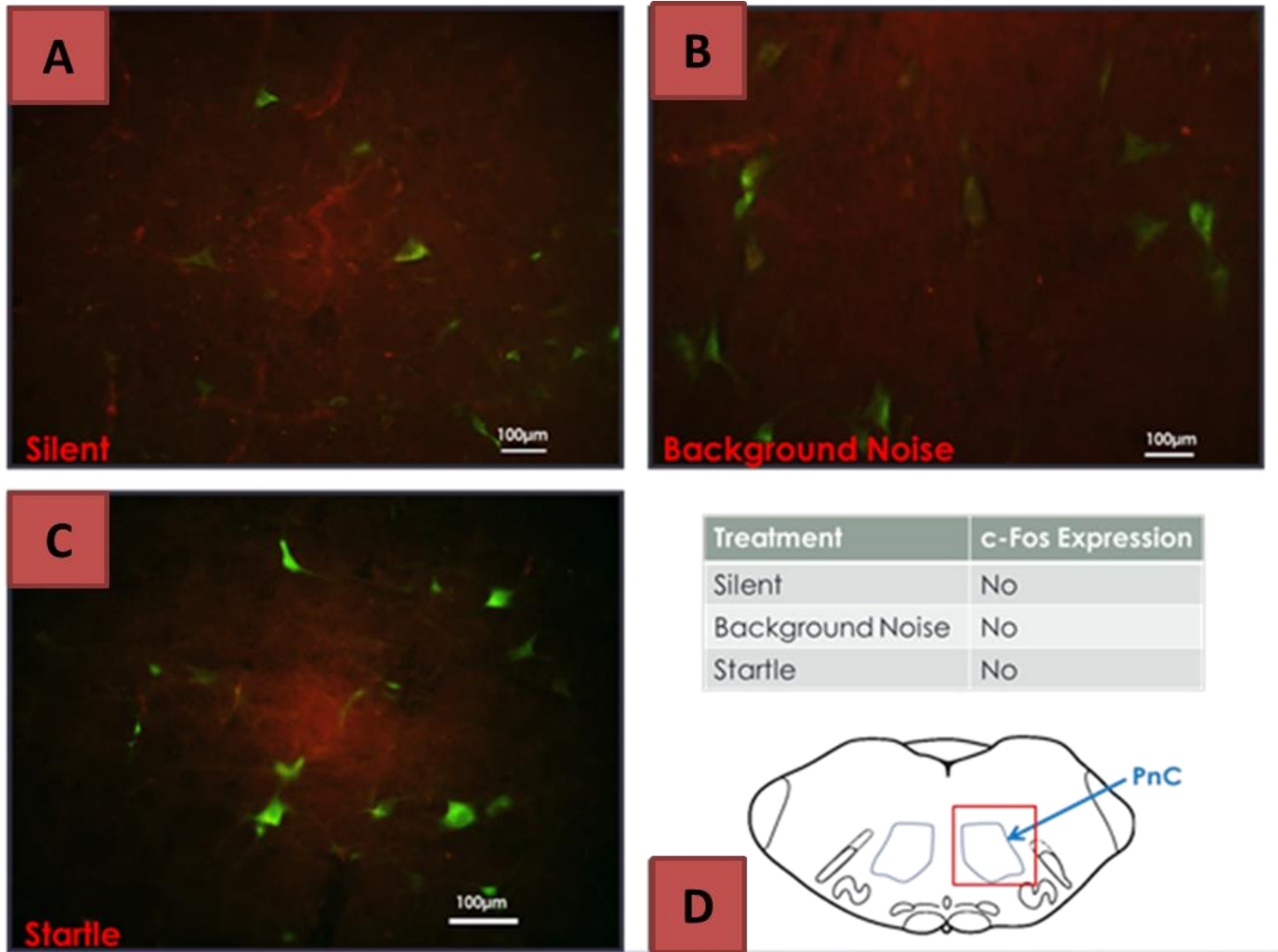
Figure 5.5 PnC giant neurons do not express c-Fos (red) in startled (n=7) *C.*, background noise (n=2) *B.* nor silence (n=3) treated animals *A*. Giant neurons are labeled with Fluorogold (green) in *A-C. D.* A schematic brainstem slice where the red rectangle depicts the region shown in *A-C.* Scale bars indicate 100µm in all images.
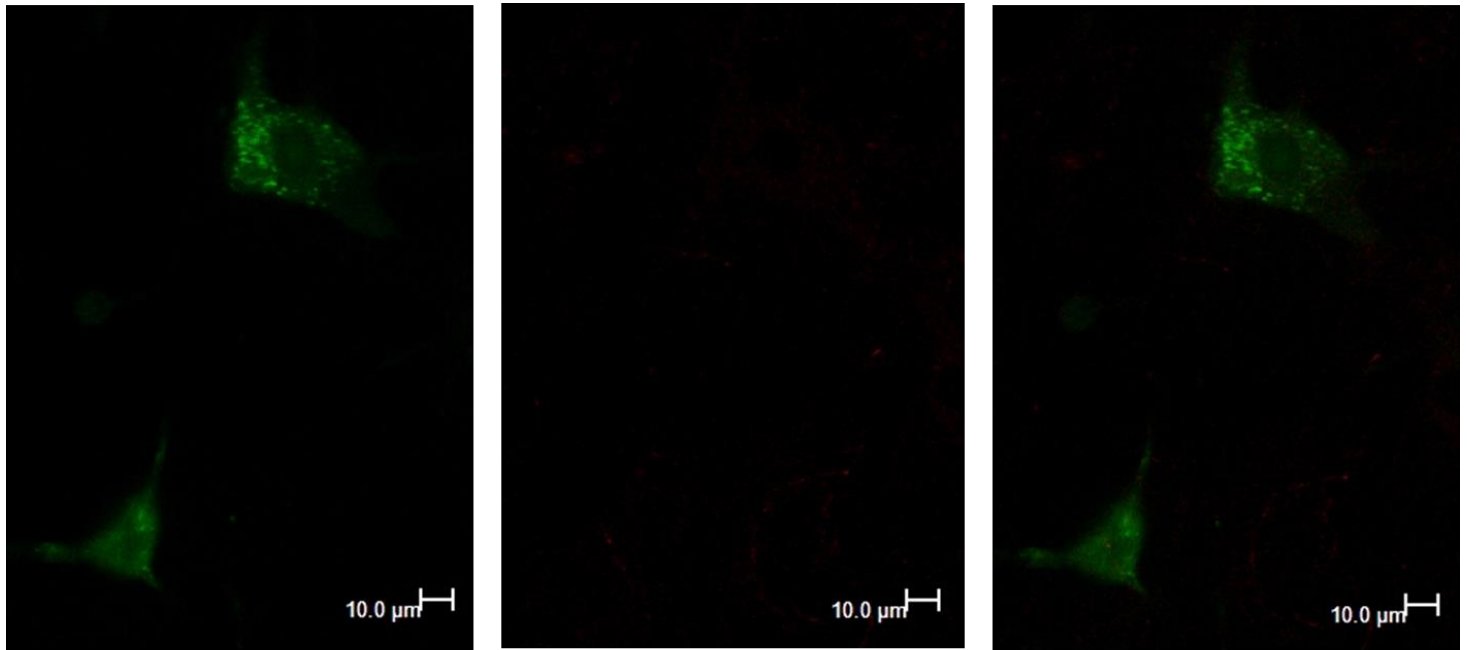
| Fluorogold | Zif268/EGR1 | Merged Image |

Figure 5.6 PnC giant neurons do not express Zif268 (EGR-1) in startled animals (n=3). Giant neurons are labeled with Fluorogold (green) and Zif268 staining is labeled with Alexa Fluor-568 (red). Scale bars indicate 10μm in all panels.

Phosphorylation status of CREB within PnC giant neurons of startle or silence treated animals was subsequently tested (Figure 5.7A/B). Fifteen PnC giant neurons across three startle treated animals and eleven giant neurons across three silence treated animals were used in the analysis. Giant neurons in startle treated animals showed a significantly higher percentage of nuclear pCREB expression as compared to those in silence treated animals [startle = 53 ± 0.13% with a mean rank of 16.43, silent = 0% with a mean rank of 9.50, Mann-Whitney U test, U=38.50, Z =-2.85, p=0.004, Figure 5.7C]. No significant main effect of treatment was observed when comparing the mean length [startle = 45.37 ± 1.83µm, silent = 47.17 ± 2.26µm, independent t-test, t(24)=0.58, p=0.566, Figure 5.7D] and width [startle = 29.98 ± 1.60µm, silent = 32.24 ± 1.29µm, independent t-test, t(24)=1.11, p=0.279, Figure 5.7D] soma diameters of giant neurons that show phosphorylated CREB (pCREB) in startle or silence treated animals .
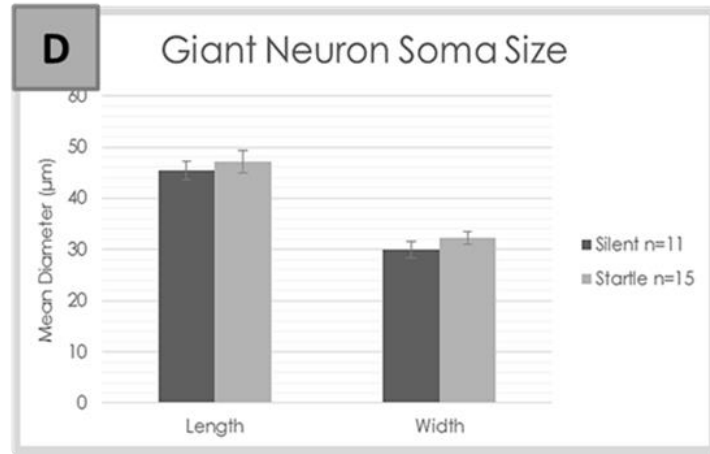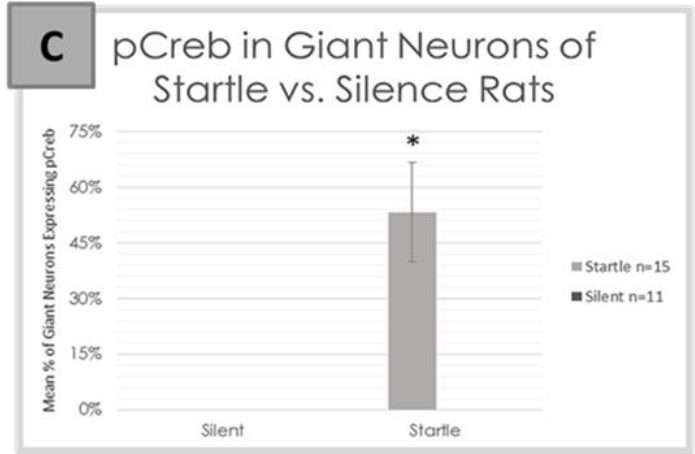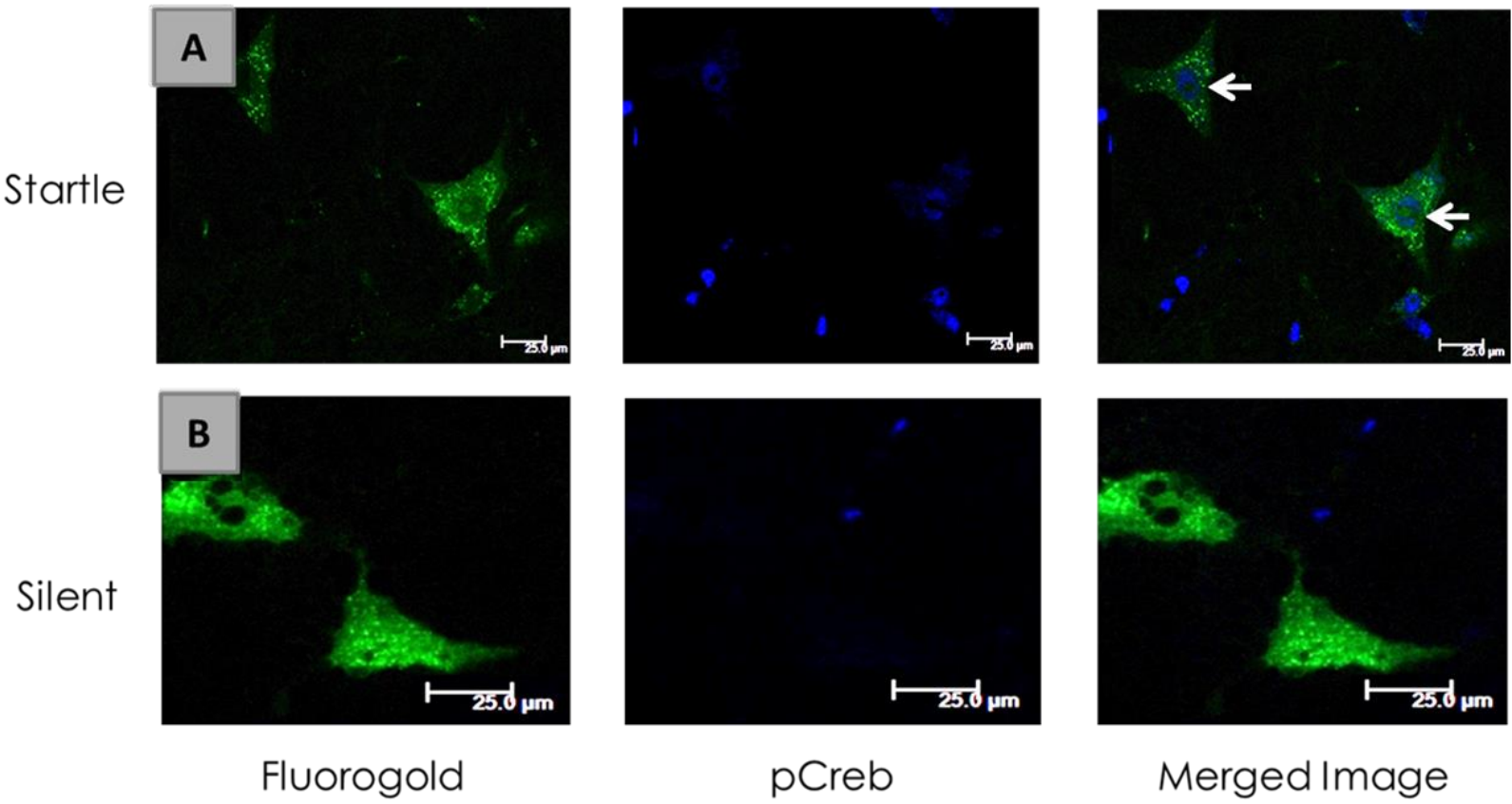
Figure 5.7 pCREB labeling within PnC giant neurons of startle or silence treated animals. *A.* PnC giant neurons (green) of startle treated animals show pCREB (blue) within their nuclei; arrows in the merged image point to dual labeling. *B.* PnC giant neurons (green) of silence treated animals do not express pCREB (blue) within their nuclei. Merged image shows lack of dual labeling. *C.* Percentage (mean ± SEM) of giant neurons within the PnC that express pCREB in their nuclei. A significant main effect of treatment was observed; asterisks above bars depict significantly different means (Mann-Whitney U test, $p < 0.05$). *D.* Maximum (length) and minimum (width) soma diameters (mean ± SEM) of giant neurons in startle or silence treated animals. No significant main effect of treatment was observed (independent t-test, $p < 0.05$). Legends represent the number of neurons analyzed in three animals for each group. Scale bars indicate 25μm in all images.

pCREB labeling was also generally assessed in all of the neurons that make up the PnC (giant and non-giant) as well as in various brainstem regions including the inferior colliculus, vestibular nuclei, and trigeminal motor area of startle (n=3) or silence (n=3) treated animals (Figure 5.8A-D). No significant main effect of treatment was seen on the mean number of pCREB neurons within the PnC [startle = 6.67 ± 2.40, silent = 0.33 ± 0.33, independent t-test, t(4)=2.61, p=0.059, Figure 5.8E], indicating that increased pCREB expression in PnC giant neurons is not sufficient to generally increase its expression within the area due to the relatively low number of giant neurons as compared to non-giant ones. A significant main effect of treatment was also not observed in either the inferior colliculus [startle = 73.33 ± 3.18, silent = 70.33 ± 11.05, independent t-test, t(4)=0.26, p=0.807, Figure 5.8E] or the vestibular nuclei [startle = 87 ± 6.56, silent = 91 ± 6.43, independent t-test, t(4)=0.44, p=0.686, Figure 5.8E]. A significant increase in the mean number of pCREB neurons within the trigeminal motor area was seen in the startle treated animals as compared to the silent [startle = 39 ± 2.89, silent = 19 ± 0.58, independent t-test, t(4)=6.79, p=0.002, Figure 5.8E]
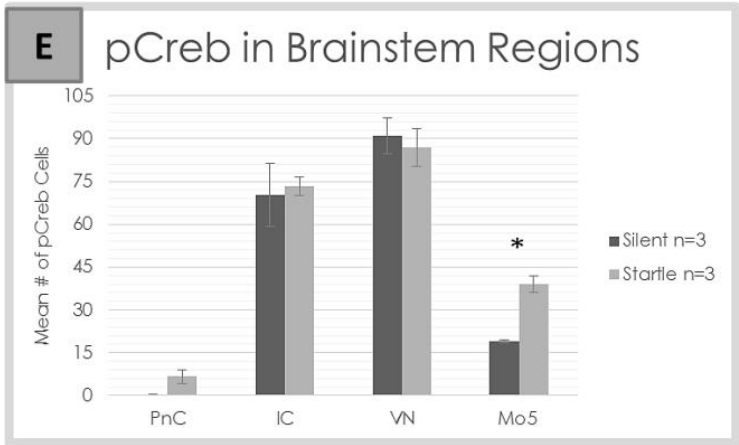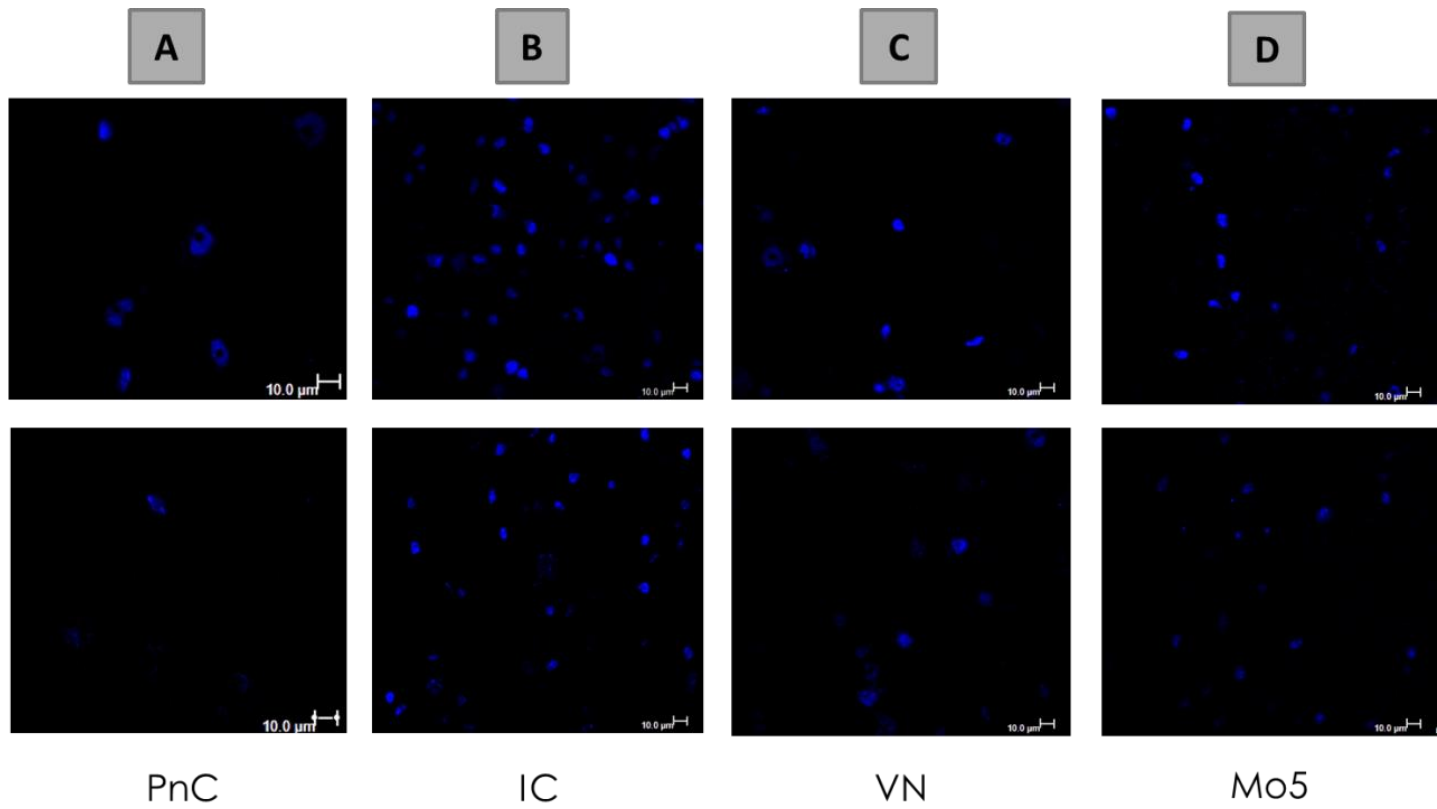
Figure 5.8 pCREB labeling within brainstem regions of startle or silence treated animals. *A.* Expression pattern of pCREB (blue) in representative images of various brainstem regions in startle or silence treated animals including, *A.* pontine caudal reticular nucleus (PnC), *B.* inferior colliculus (IC), *C.* vestibular nuclei (VN), and *D.* motor nucleus of the trigeminal nerve (Mo5). *E.* Percentage (mean ± SEM) of pCREB cells expressed within various brainstem regions of startle or silence treated animals. A significant main effect of treatment was observed in the Mo5 region. Legend represents the number of animals analysed for each treatment type. Asterisks above bars depict significantly different means (independent t-test, $p < 0.05$). Scale bars indicate 10μm in all images.

5.2 A subpopulation of cholinergic terminals co-label for glutamate or GABA synaptic markers

Cholinergic neurons in the PPT/LTD have been reported to project to the PnC and potentially innervate PnC giant neurons. We here visualized the cholinergic terminals in the PnC and tested whether they also possess glutamate and or GABA synaptic markers, using triple labeling immunohistochemistry with antibodies against markers for glutamate (VGLUT1), GABA (GAD67), and acetylcholine (CHT1). As described in the Materials and Methods, three planes were analyzed out of a z-stack confocal image of 30-50 sections in each of three animals (n=9). A subpopulation of CHT1 labeled axon terminals within the PnC were shown to co-express either VGLUT1 or GAD67 (Figure 5.9A/B). A proportion of colocalized VGLUT1 and GAD67 cells were also seen within the PnC (Figure 5.9C), as well as rare instances where cholinergic terminals expressed both VGLUT1 and GAD67 (Figure 5.9D). The total percentage of terminals in the PnC that show co-expression of CHT1 with VGLUT1 was determined to be $34.88 \pm 4.91\%$ as compared to single labeled cholinergic ($21.98 \pm 6.18\%$) and glutamatergic ($43.13 \pm 10.48\%$) markers (Figure 5.10A). The total percentage of PnC terminals that show a dual labeling for CHT1 and GAD67 markers was determined to be $17.81 \pm 2.03\%$ as compared to single labeled cholinergic ($28.61 \pm 8.02\%$) and GABAergic ($53.58 \pm 8.80\%$) markers (Figure 5.10B). Colocalization of VGLUT1 and GAD67 markers was also observed at a percentage of $32.86 \pm 2.16\%$, with $37.06 \pm 4.73\%$ and $30.08 \pm 4.92\%$ single labeled glutamatergic and GABAergic markers, respectively (Figure 5.10C). The number of cholinergic terminals that expressed both VGLUT1 and GAD67 markers was manually counted across the images analyzed and determined to be 13.44 ± 5.50 cells (Figure 5.10D). The percentage of cholinergic terminals in the PnC that co-express either VGLUT1 or GAD67 was also analyzed. The proportion of CHT1-labeled terminals that colocalized with VGLUT1 markers was $69.59 \pm 6.59\%$ as opposed to those that do not [$30.41 \pm 6.59\%$, Figure 5.11A]. The proportion of CHT1-labeled terminals that co-express GAD67 markers was $45.82 \pm 6.11\%$ as compared with single labeled CHT1 terminals [$54.18 \pm 6.11\%$, Figure 5.11B].
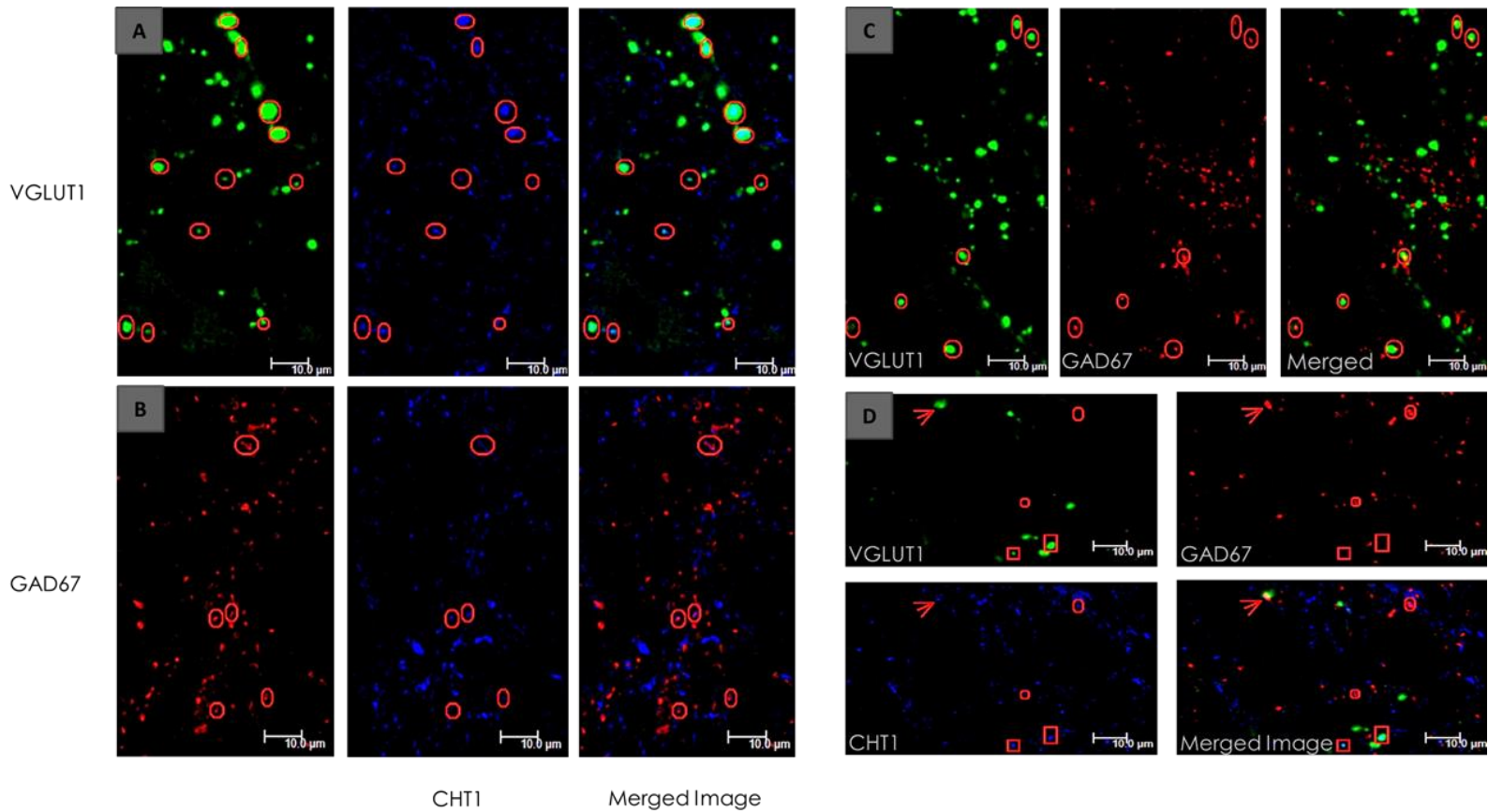
Figure 5.9 Glutamatergic or GABAergic colocalization on cholinergic terminals within the PnC. A subpopulation of CHT1 terminals (blue) within the PnC co-express either *A.* VGLUT1 or *B.* GAD67 (green). *C.* Colocalized VGLUT1 (green) and GAD67 (red) cells within the PnC. Red circles depict areas of colocalization in each representative image. *D.* Triple labelling of VGLUT1 (green), GAD67 (red) and CHT1 (blue) cells. Squares depict areas of cholinergic and glutamatergic dual labeling and circles those of cholinergic and GABAergic double labeling. Labeling for all three markers is represented by the arrowhead. All images are single planes in a z-stack taken of about 30-50 steps; thickness of section is 0.6μm. Scale bars indicate 10μm in all images.
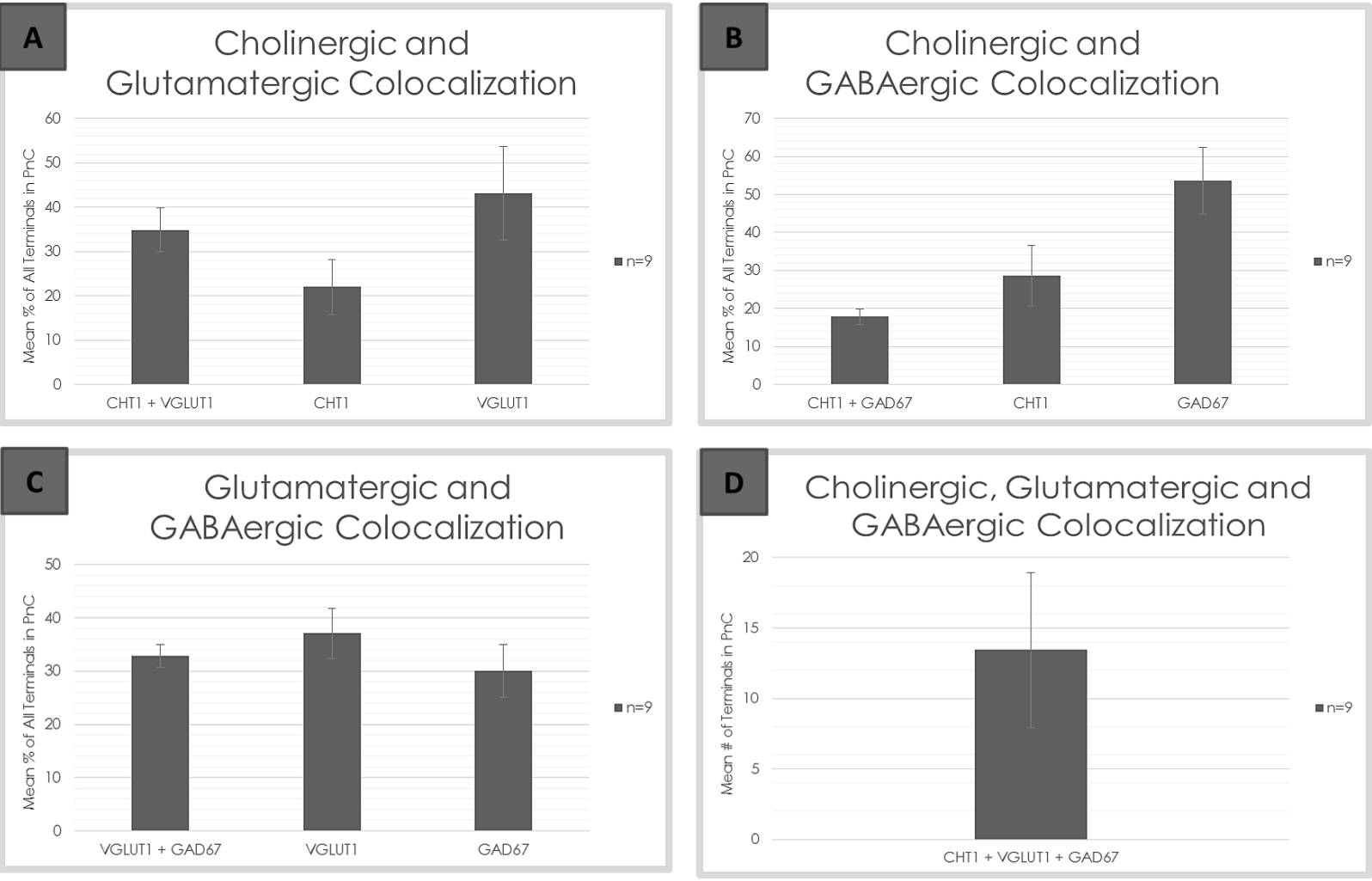
Figure 5.10 Percentage (mean ± SEM) of the total number of terminals in the PnC that show co-expression of CHT1 with VGLUT1 and/or GAD67. *A*. Percent colocalization of cholinergic and glutamatergic markers in the PnC as compared to single markers labeled. *B*. Percent colocalization of cholinergic and GABAergic markers in the PnC as compared to single markers labeled. *C*. Percent colocalization of glutamatergic and GABAergic markers in the PnC as compared to single markers labeled. *D*. Number (mean ± SEM) of cells labeled with all three markers (CHT1, VGLUT1, and GAD67) in the PnC. The legend represents the number of single z-stack planes analyzed, across three animals, for each combination.
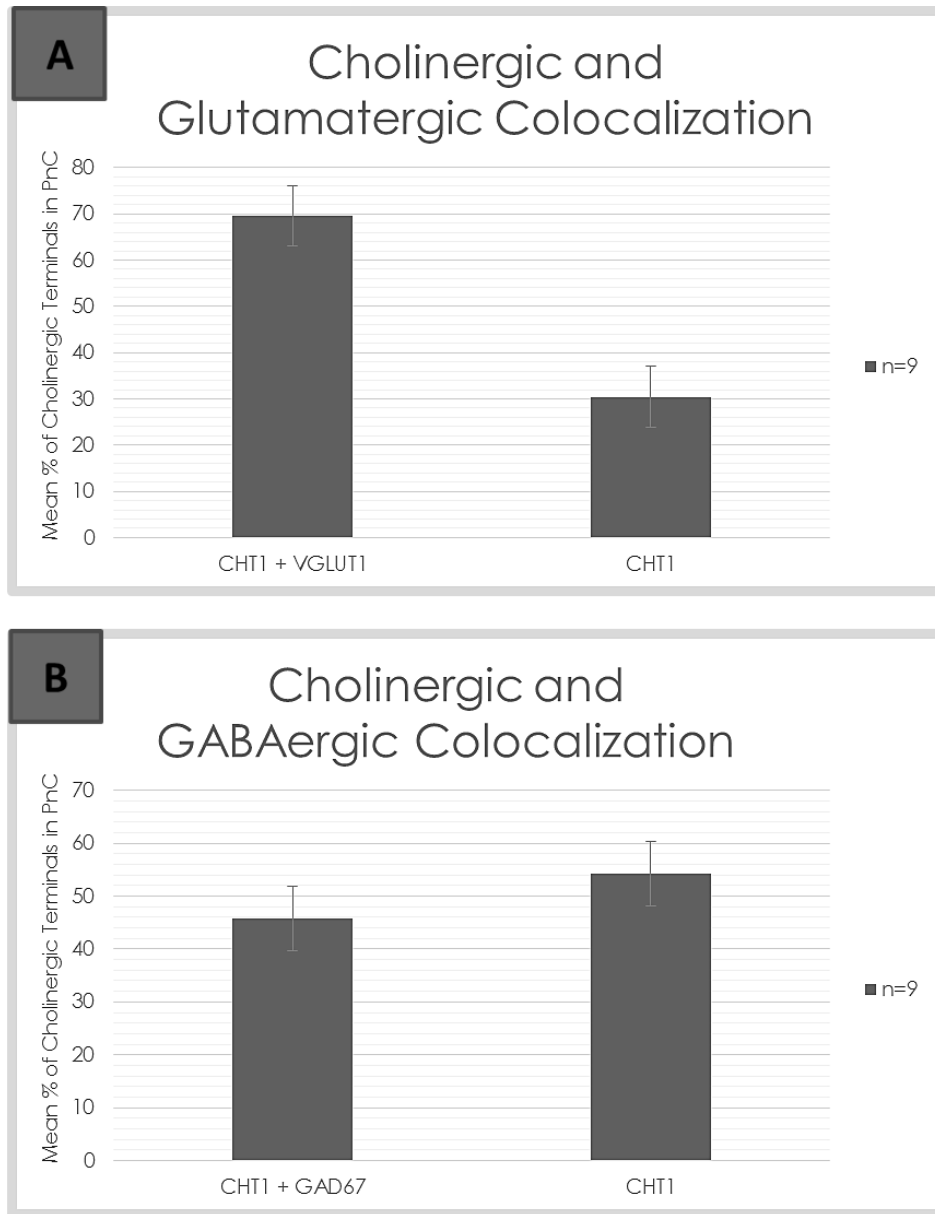
Figure 5.11 Percentage (mean ± SEM) of cholinergic terminals in the PnC that co-express VGLUT or GAD67. *A*. Percent of PnC cholinergic terminals that co-express glutamatergic markers as compared to those that do not. *B*. Percent of PnC cholinergic terminals that co-express GABAergic markers as compared to those that do not. The legend represents the number of single z-stack planes analyzed, across three animals, for each combination.

In order to understand the relationship of these dual-labeled cholinergic terminals with the startle mediating giant neurons, subsequent staining was done using the neuronal biomarker, NeuN. Fluorogold could not be used in conjunction with the colocalization stainings due to inherent limitations with its emission spectrum. The emission spectrum of Fluorogold overlaps with two of the three secondary Fluorochromes used and as such was replaced with NeuN. NeuN staining can be seen within the PnC labeling both our giant neurons of interest along with other neurons within the vicinity (Figure 5.12A). As expected, all neurons labeled with Fluorogold are also marked with NeuN, however not all NeuN-stained cells are Fluorogold positive (Figure 5.12B/C). Interestingly, while NeuN has been shown to mainly stain the nuclei of neurons and the cytoplasm to a lesser extent, PnC giant neurons seem to express an abundance of cytoplasmic NeuN.
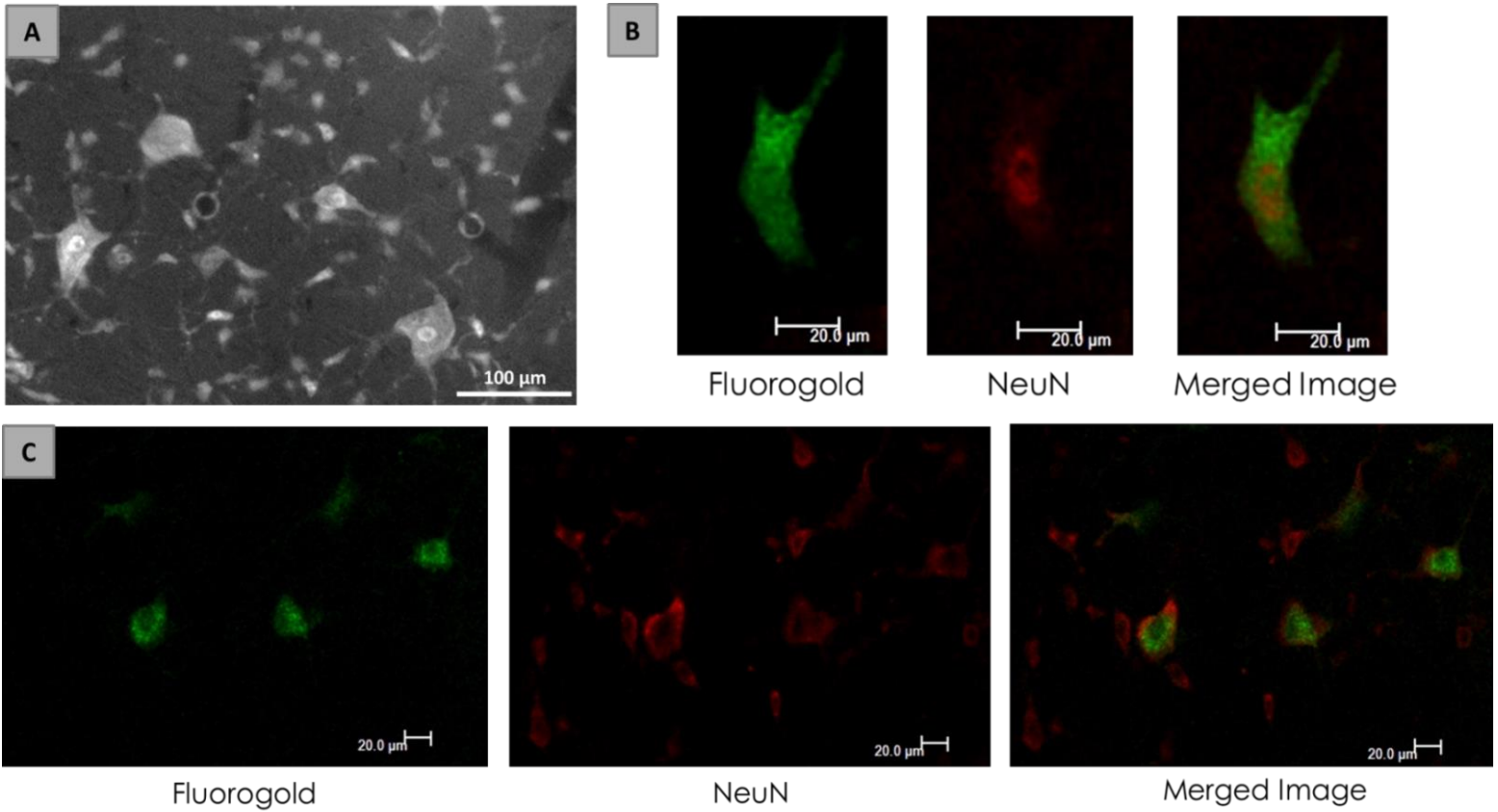
Figure 5.12 NeuN (Neuronal Nuclei) is a neuronal nuclear antigen that is commonly used as a biomarker for neurons. *A*. NeuN staining can be seen in the PnC labeling both our giant neurons of interest and other neurons within the vicinity. *B*. The green image shows Fluorogold labelled neurons and the red image shows those same neurons labeled by NeuN. The last image in the series is a merge between Fluorogold and NeuN. *C*. NeuN (red) stains far more neurons in the PnC than those labelled with the Fluorogold retrograde tracer (green) which is limited to only those neurons that project to the C3/C4 spine. Scale bars indicate 100μm in *A,* and 20μm in *B* and *C*.

Glutamatergic or GABAergic colocalization on cholinergic terminals contacting PnC giant neurons was tested by using triple labeling immunohistochemistry with antibodies against NeuN, CHT1, and either VGLUT1 or GAD67. A subpopulation of presynaptic cholinergic terminals outlining the NeuN-labeled giant neurons co-express either glutamate (Figure 5.13A/B) or GABA (Figure 5.13C/D). The number of dual or single-labeled cholinergic terminals in either case were counted and the place of contact, giant neuron soma or proximal dendrite, was noted. For terminals contacting the soma, three giant neurons were analyzed in each of three animals (n=9); for terminals contacting proximal dendrites, one giant neuron was analyzed in each of three animals (n=3) (see Materials and Methods). The number of cholinergic terminals that contact the soma and co-express glutamate markers was determined to be 0.89 ± 0.35, those that co-express GABA markers 3.00 ± 1.18, and those that don't express either markers 2.89 ± 0.90 (Figure 5.14A). For cholinergic terminals contacting proximal dendrites, none were observed to co-express glutamate markers, 1.33 ± 0.33 co-expressed GABA markers, and 3.00 ± 2.52 remained singly labeled (Figure 5.14B).
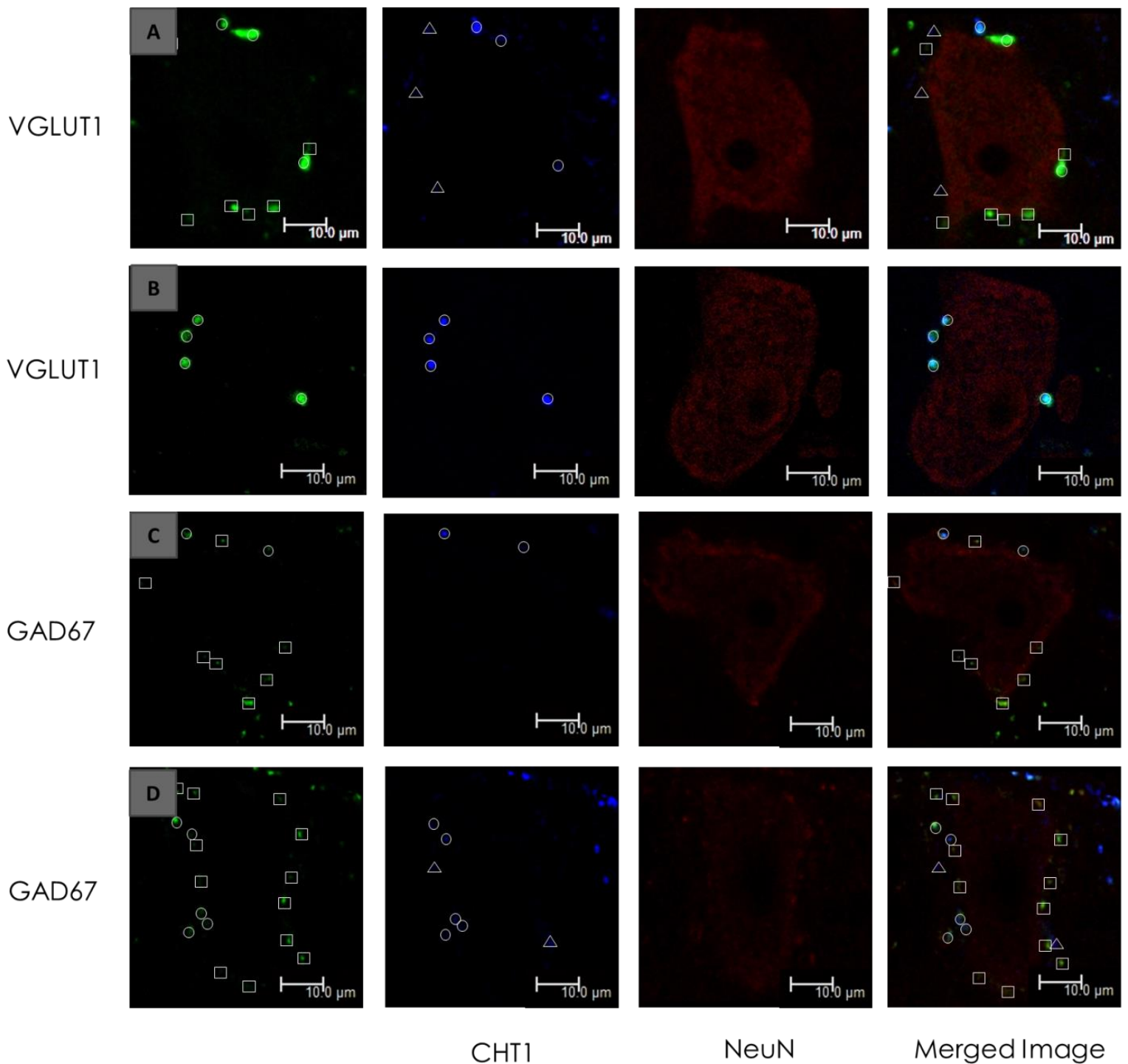
Figure 5.13 Colocalization of glutamatergic or GABAergic markers on cholinergic terminals in contact with PnC giant neurons. *A.*and *B.* each show isolated images of representative giant neurons with dual CHT1 and VGLUT1 labeling. VGLUT1 (green) is expressed on CHT1 terminals (blue) that are localized presynaptically as they border giant neurons stained for with NeuN (red). *C.* and *D.* each show isolated images of representative giant neurons with dual CHT1 and GAD67 labeling. GAD67 (green) is expressed on presynaptic CHT1 terminals. All images are single planes in a z-stack taken of about 30-50 steps; thickness of each section is 0.6μm. Cholinergic terminals in contact with giant neurons are outlined with triangles, VGLUT1 or GAD67 with squares, and any colocalization with circles. Scale bars indicate 10μm in all images.
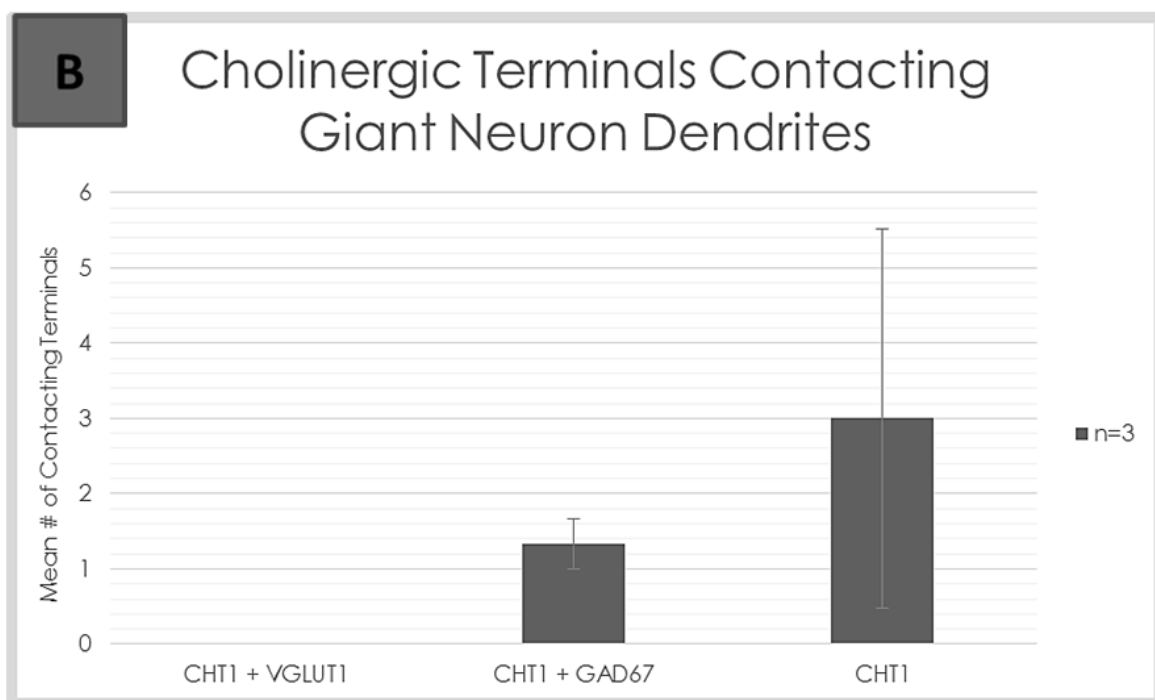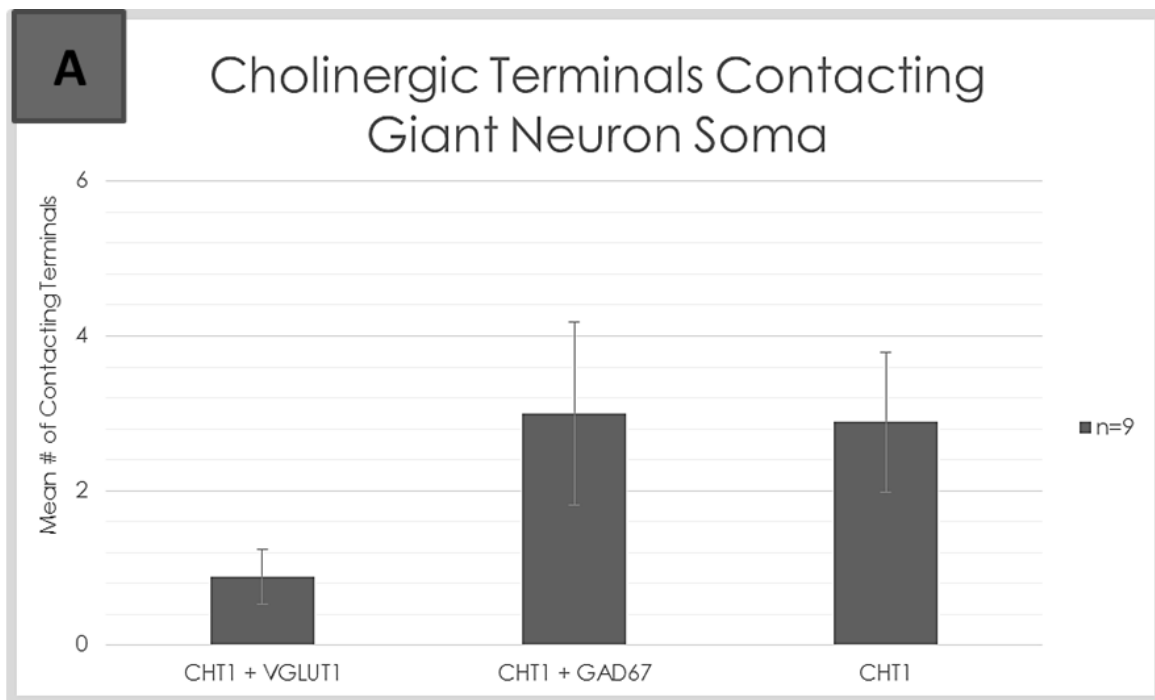
Figure 5.14 Number (mean ± SEM) of single-labeled or glutamatergic/GABAergic-expressing cholinergic terminals contacting the *A.* soma or *B.* proximal dendrite of PnC giant neurons. Legends represent the number of giant neurons analyzed, across three animals, for each combination.

5.3 BK channels implicated in habituation are localized on auditory glutamatergic afferents

Habituation is thought to occur as a result of the hyperpolarizing effect of BK channels that are hypothesized to be expressed on the sensory afferents that converge onto PnC giant neurons. Thus, BK channel colocalization on glutamatergic, GABAergic, and cholinergic terminals within the PnC was tested by using double labeling immunohistochemistry with antibodies against markers for BK channel (Kca1.1) and either VGLUT1, GAD67, or CHT1. As in section 5.2, three planes were analyzed out of a z-stack confocal image of 30-50 sections in each of three animals (n=9). A subpopulation of glutamatergic (Figure 5.15A), GABAergic (Figure 5.15B), and cholinergic (Figure 5.15C) terminals within the PnC were shown to co-express BK channels. The percentage of glutamatergic, GABAergic, and cholinergic terminals in the PnC that co-express BK channels was analyzed. The proportion of VGLUT-labeled terminals that colocalized with BK markers was $85.83 \pm 3.69\%$ as opposed to those that do not [$14.17 \pm 3.69\%$, Figure 5.16A]. The proportion of GAD67-labeled terminals that co-express BK markers was $94.97 \pm 4.23\%$ as compared with single labeled GAD67 terminals [$5.03 \pm 4.23\%$, Figure 5.16B]. Finally, the percentage of cholinergic terminals that co-localize with BK markers was determined to be $98.71 \pm 0.80\%$ as opposed to those that do not [$1.29 \pm 0.80\%$, Figure 5.16C].

VGLUT1

GAD67

CHT1

BK Channel　　　Merged Image
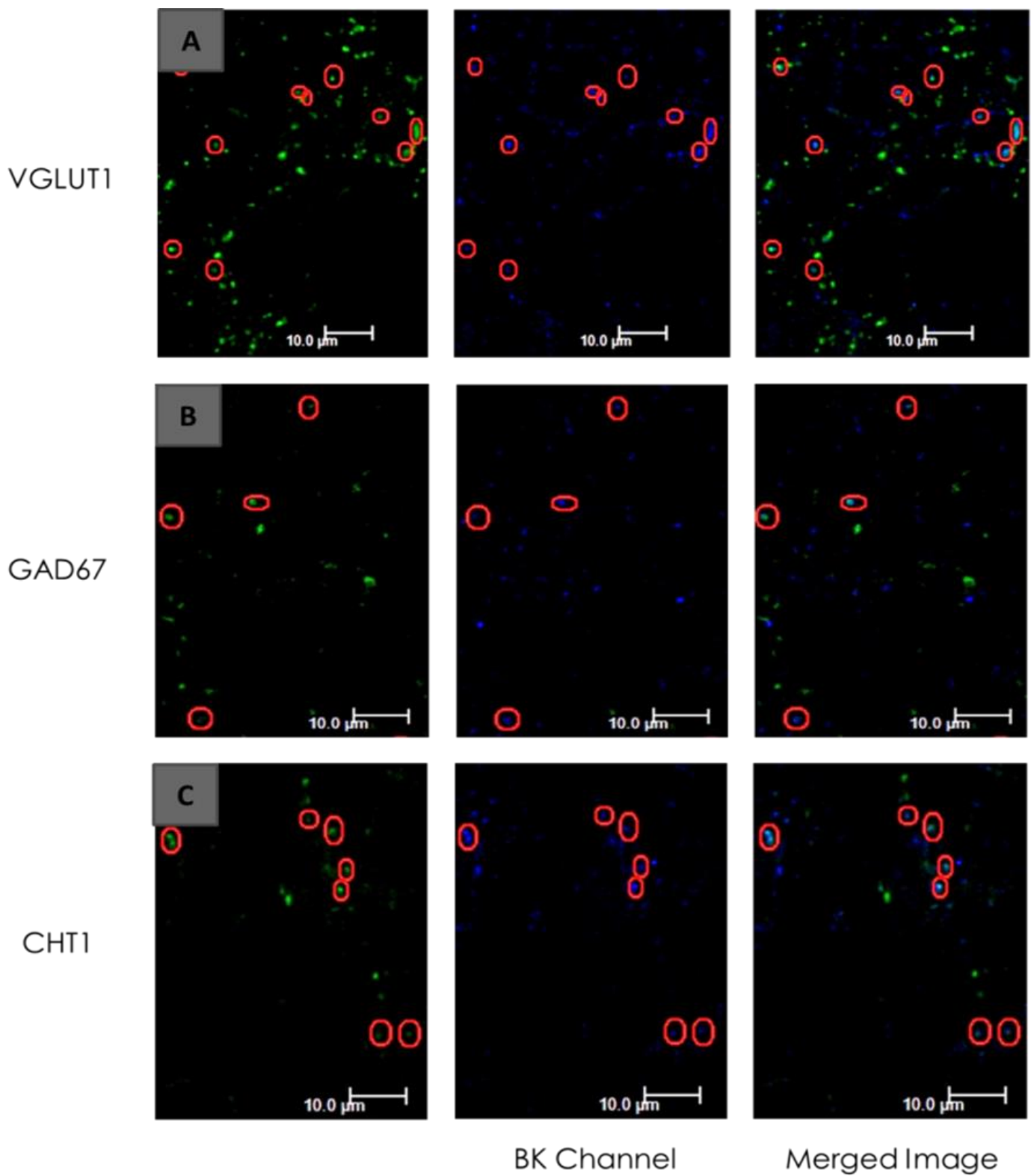
Figure 5.15 BK channel colocalization on glutamatergic, GABAergic, or cholinergic terminals within the PnC. BK channels (blue) are expressed on *A*. VGLUT1, *B*. GAD67, or *C*. CHT1 terminals (green) that are located within the PnC. Red circles depict areas of colocalization in each representative image. All images are single planes in a z-stack taken of about 30-50 steps; thickness of each section is 0.6μm. Scale bars indicate 10μm in all images.
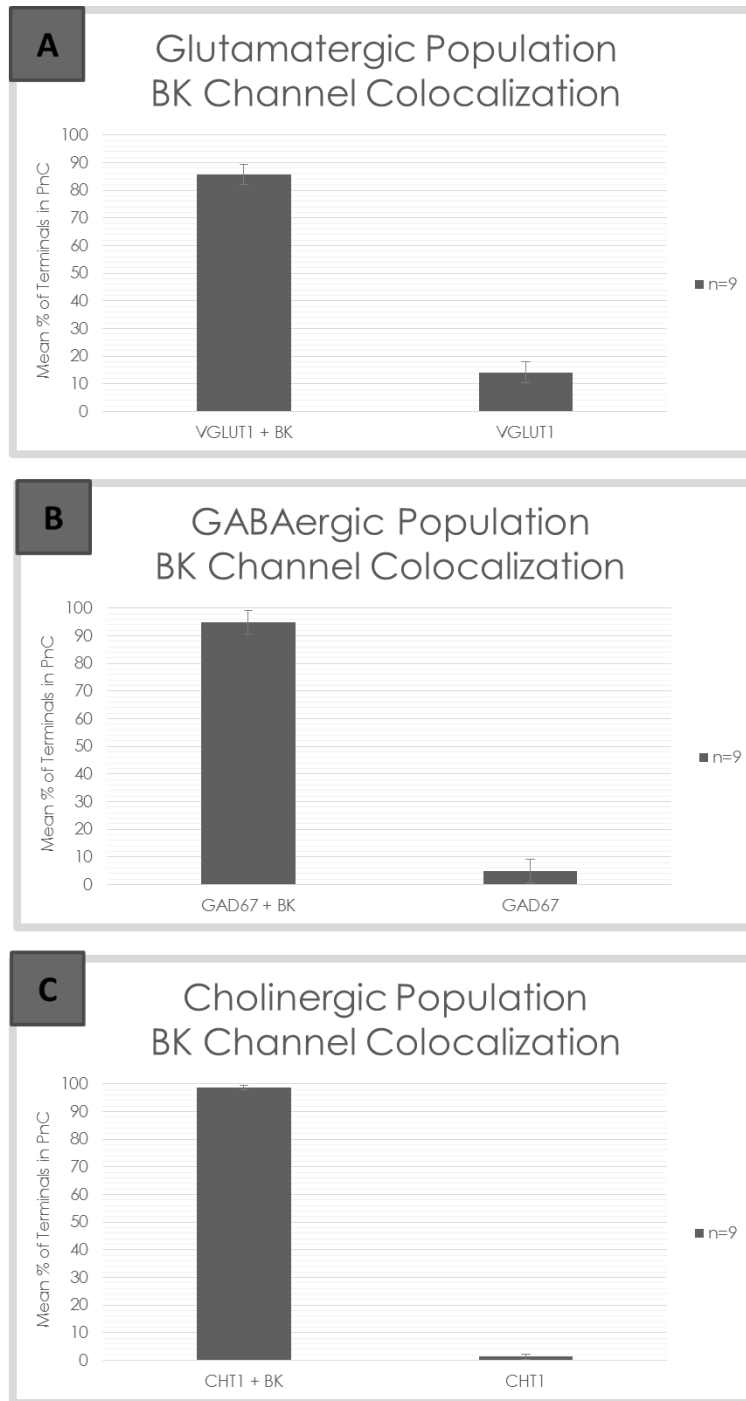
Figure 5.16 Percentage (mean ± SEM) of glutamatergic, GABAergic or cholinergic terminals in the PnC that express BK channels. *A.* Percent of PnC glutamatergic terminals that co-express Bk channel markers as compared to those that do not. *B.* Percent of PnC GABAergic terminals that co-express BK channel markers as compared to those that do not. *C.* Percent of PnC cholinergic terminals that co-express BK channel markers as compared to those that do not. The legend represents the number of single z-stack planes analyzed, across three animals, for each combination.

In order to understand the relationship of BK-expressing terminals with the startle mediating giant neurons, subsequent staining was done using the neuronal biomarker, NeuN. BK channel colocalization on glutamatergic, GABAergic, and cholinergic terminals contacting PnC giant neurons was tested by using triple labeling immunohistochemistry with antibodies against NeuN, Kca1.1, and either VGLUT1, GAD67 or CHT1. BK channels were shown to be localized on a subpopulation of presynaptic glutamatergic (Figure 5.17), GABAergic (Figure 5.18A/B), and cholinergic (Figure5.18C/D) terminals outlining the NeuN-labeled giant neurons. The number of dual-labeled cells in either case was counted and the place of contact, giant neuron soma (Figure 5.19A) or proximal dendrite (Figure 5.19B), was noted. For cells contacting the soma, three giant neurons were analyzed in each of three animals (n=9); for cells contacting proximal dendrites, one giant neuron was analyzed in each of three animals (n=3) (see Materials and Methods). The number of glutamatergic terminals that contact the soma and co-express BK channel markers was determined to be 3.00 ± 0.68, as compared to 1.00 ± 0.25 non BK channel-expressing glutamatergic terminals. The number of GABAergic terminals that contact the soma and co-express BK was 12.89 ± 2.36 as compared to 7.89 ± 2.23 single-labeled GABA terminals. Finally, the number of cholinergic terminals that co-express BK was also analyzed and determined to be 10.33 ± 1.95, with 2.89 ± 0.90 CHT1 terminals not expressing the BK channel marker. For BK channel-expressing terminals contacting proximal dendrites, 2.00 ± 1.00 was observed to be glutamatergic, 7.00 ± 0.58 GABAergic, and 4.33 ± 0.88 cholinergic. The number of single-labeled glutamatergic, GABAergic, and cholinergic terminals contacting proximal dendrites were determined to be 0.67 ± 0.33, 1.67 ± 0.67, and 3.00 ± 2.52, respectively.

Figure 5.17 BK channel colocalization on glutamatergic terminals in contact with PnC giant neurons. *A.* BK channels (blue) are expressed on VGLUT1 (green) terminals that are localized presynaptically as they border giant neurons stained for with NeuN (red). *B.* and *C.* each show isolated images of representative giant neurons with dual BK and VGLUT1 labeling. BK channels in contact with giant neurons are outlined with triangles, VGLUT1 with squares, and any colocalization of the two with circles. All images are single planes in a z-stack taken of about 30- 50 steps; thickness of each section is 0.6μm. Scale bars indicate 25μm in *A.* and 10μm in both *B.* and *C.*

NeuN   BK Channel   VGLUT1   Merged Image

| | BK Channel | NeuN | Merged Image |
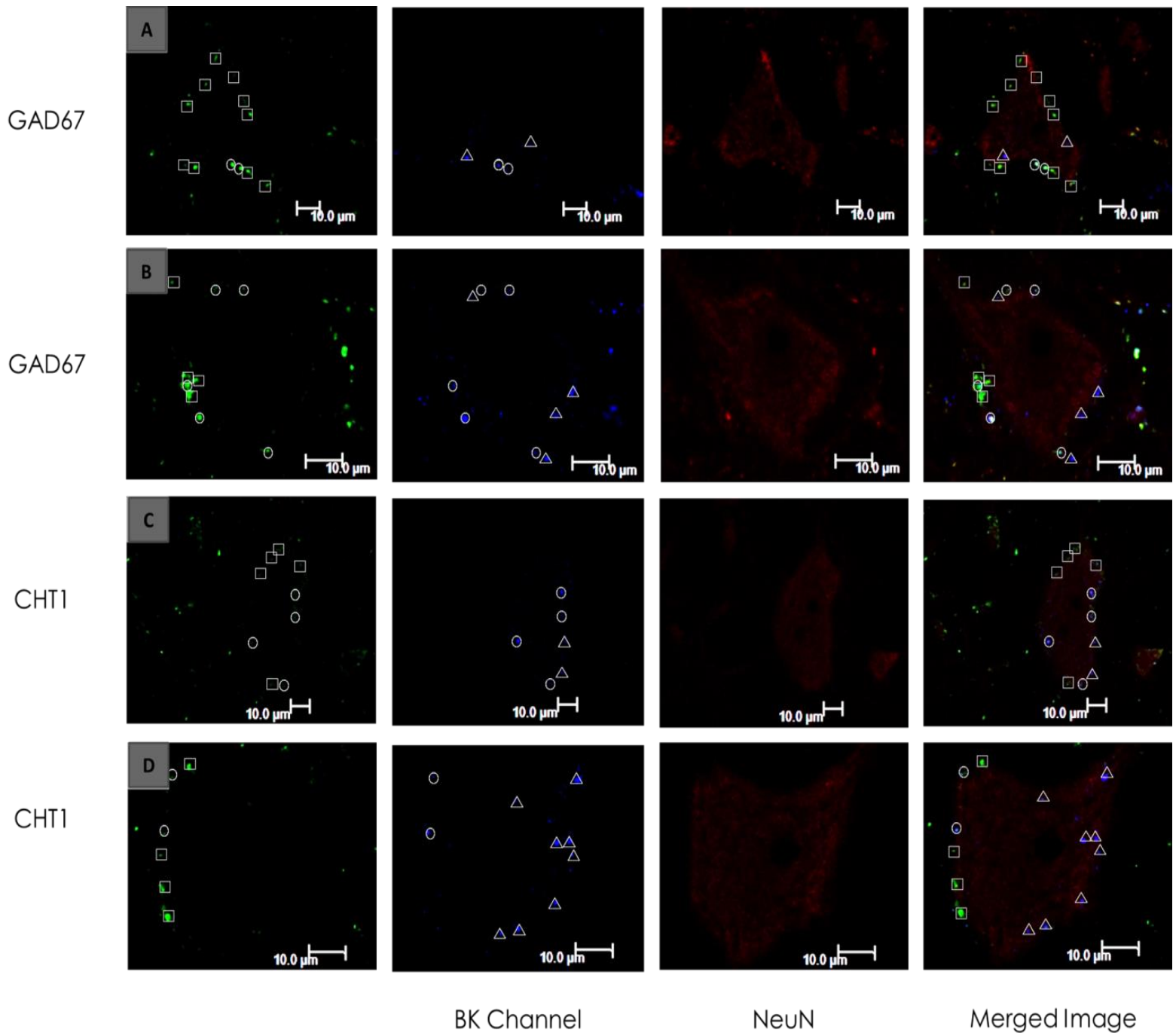
Figure 5.18 BK channel colocalization on GABAergic or cholinergic terminals in contact with PnC giant neurons. *A.*and *B.* each show isolated images of representative giant neurons with dual BK and GAD67 labeling. BK channels (blue) are expressed on GAD67 terminals (green) that are localized presynaptically as they border giant neurons stained for with NeuN (red). *C.* and *D.* each show isolated images of representative giant neurons with dual BK and CHT1 labeling. BK channels are expressed on presynaptic CHT1 terminals (green). All images are single planes in a z-stack taken of about 30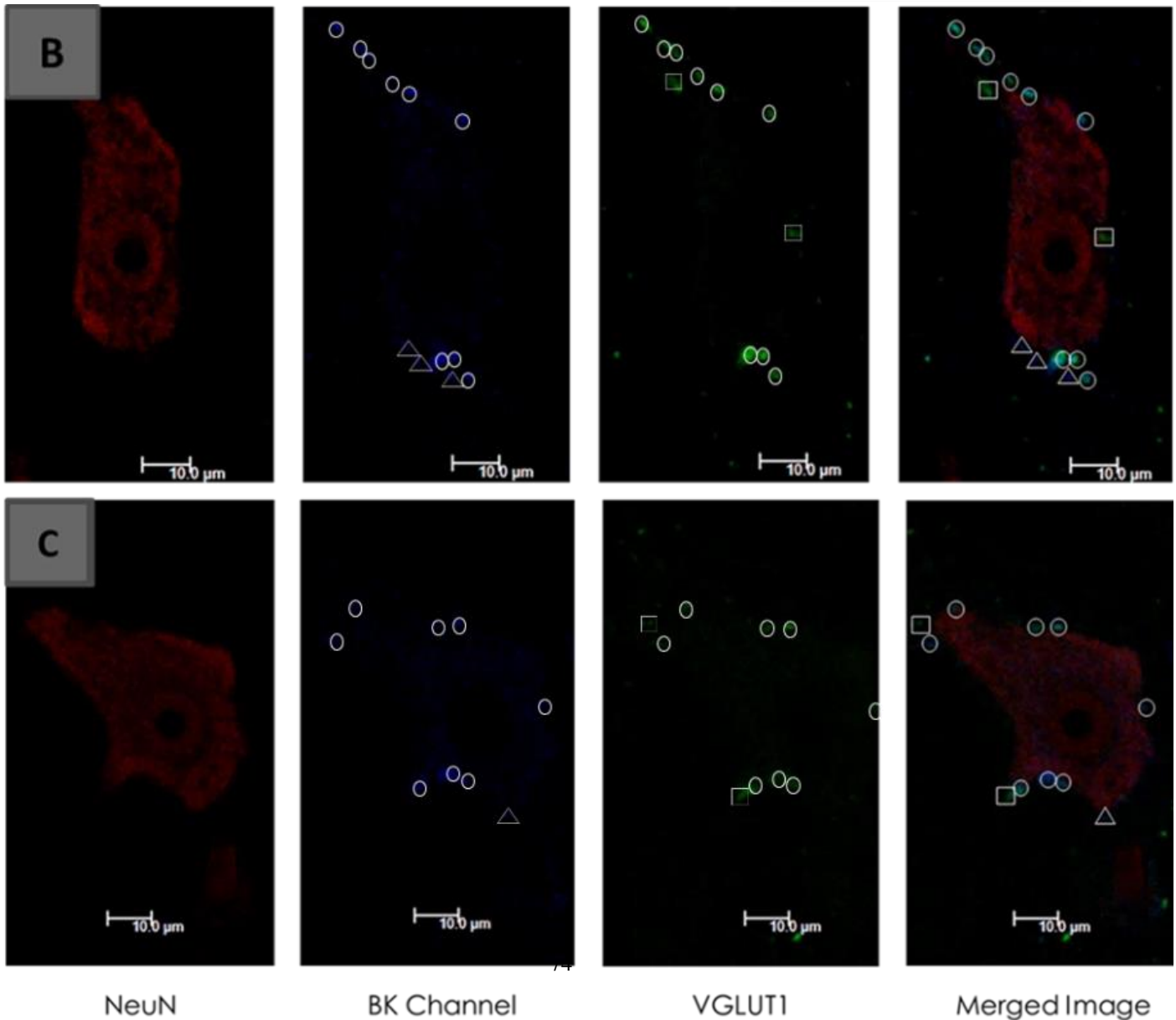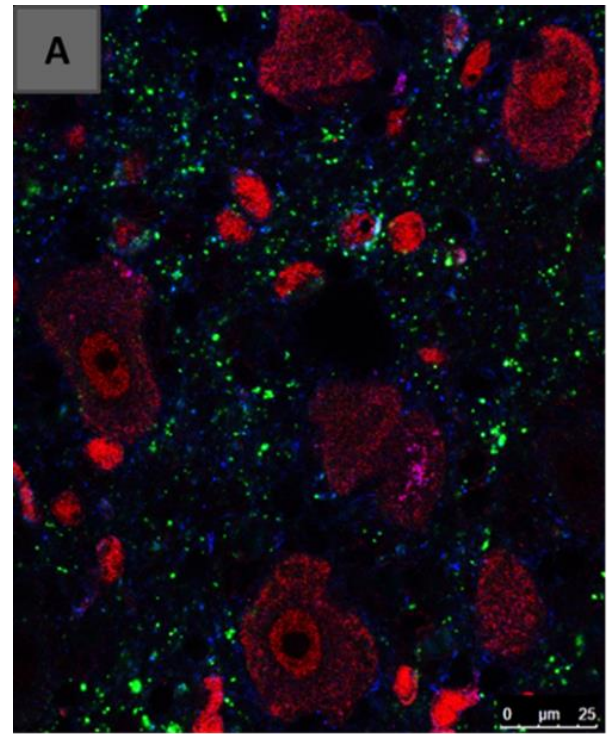-50 steps; thickness of each section is 0.6μm. BK channels in contact with giant neurons are outlined with triangles, GAD67 or CHT1 with squares, and any colocalization with circles. Scale bars indicate 10μm in all images.
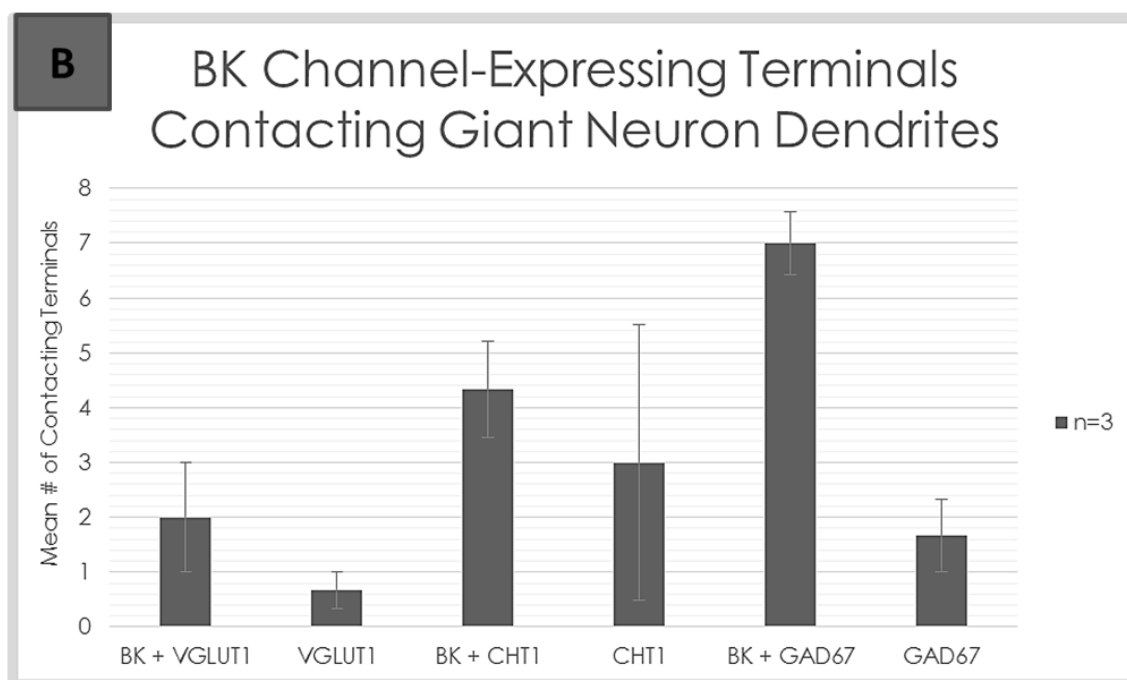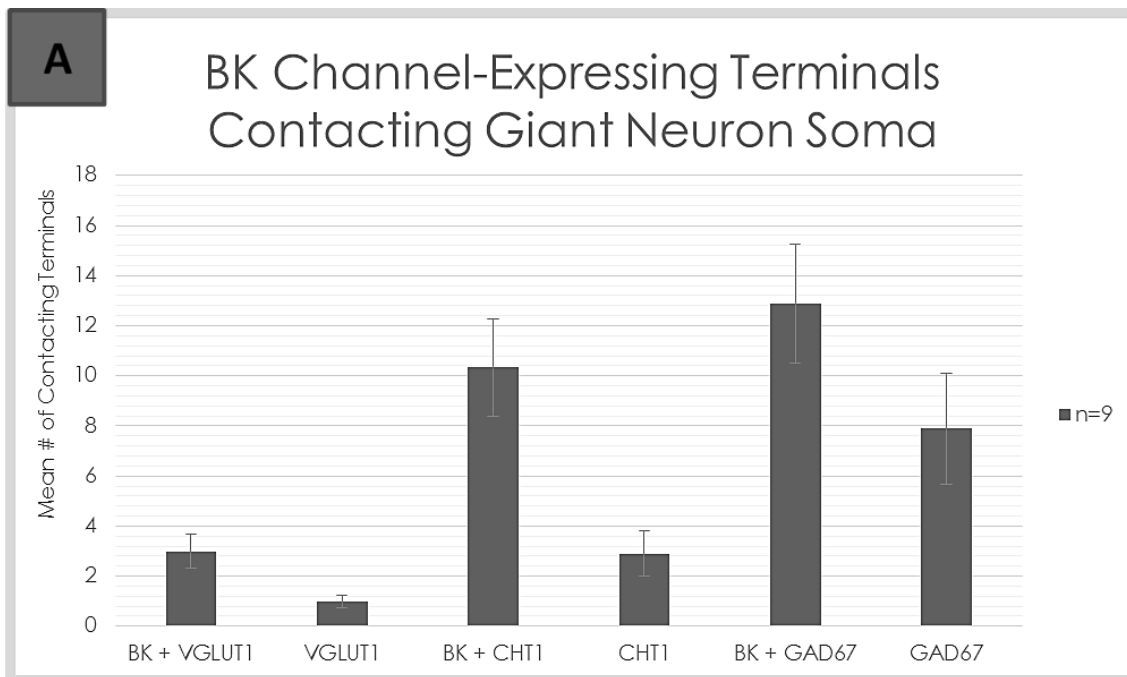
Figure 5.19 Number (mean ± SEM) of single-labeled or BK channel-expressing glutamatergic, GABAergic and cholinergic terminals contacting the *A.* soma or *B.* proximal dendrite of PnC giant neurons. Legends represent the number of giant neurons analyzed, across three animals, for each combination.

6 Discussion

6.1 Giant neurons within the PnC mediate the startle response

Based on the wealth of academic studies conducted using morphological identification, electrophysiology, targeted lesioning, and/or tracing techniques, giant neurons within the PnC are hypothesized to form the sensorimotor interface of the acoustic startle response and, as important relay centers of sensory stimuli, mediate startle (Koch et al., 1992; Lingenhöhl and Friauf, 1994; Yeomans and Frankland, 1996; Yeomans et al., 2002). One of the aims of this present study is to further solidify the pivotal role of giant neurons in ASR by using Fluorogold (FG) retrograde labeling from the spinal cord to confirm their location within the PnC, and by looking at the expression patterns of immediate early genes (IEGs) to validate their function in mediating startle.

In order to label the maximum number of giant neurons, FG was injected into the spinal cord at the cervical level since at this level reticulospinal axons either project directly to the injection site or they run through it innervating more caudal spinal cord segments (Nodal and López, 2003). Retrogradely labeled neurons were found within the PnC (Figure 5.1; the region dorsal to the superior olivary complex, ventral to the motor trigeminal nucleus, and within 2 mm medial to the facial cranial nerve; Koch et al., 1992; Lee et al., 1996; Yeomans and Frankland, 1996) and classified as giant neurons based on their maximum ($48.71 \pm 0.88\mu m$) and minimum ($31.69 \pm 0.70\mu m$) soma diameters (Figure 5.2B; Lingenhöhl and Friauf, 1994; Nodal and López, 2003; Weber et al., 2008).

One of the characteristics of PnC giant neurons is their high threshold to acoustic stimuli, which implies that these neurons do not respond to weak sounds, like human voice or laboratory noises, and only generate action potentials at sound intensities (>80 dB) that will elicit an ASR (Wu et al., 1988; Lingenhöhl and Friauf, 1994; Yeomans and Frankland, 1996). Therefore, giant neurons should only become activated (as measured indirectly by the expression of IEGs) in animals presented with a starting stimulus and not those of controls who received either background noise or silence. IEGs are the first genes activated that link membrane events with neuronal nuclei and they are rapidly induced by a variety of electrical or chemical signals (Cirelli and Tononi, 2000; Perez-Cadahía et al., 2011). The protein products of IEGs can

activate downstream targets because they act as transcription factors, regulating the expression of other genes (Cirelli and Tononi, 2000; Perez-Cadahía et al., 2011). c-*fos*, a nuclear proto-oncogene (Dragunow and Robertson, 1987) is one such IEG whose protein product c-Fos can be used as a tool to detect activity changes and plasticity within neurons (Hoffman and Lyo, 2002). c-*fos* encodes a DNA binding transcription factor having a zinc finger motif and is rapidly and transiently induced in many cells following exposure to a number of physiological stimuli, consequently, it is commonly used to study patterns of neuronal activation (Tian and Bishop, 2002).

The presence of c-Fos was seen within the trigeminal motor (Mo5) nuclei of startled animals but not in those of background or silence control animals (Figure 5.3). Retrograde labeling studies in the rat (Vornov and Sutin, 1983) and rabbit (Kolta et al., 2000) have demonstrated that the Mo5 region receives extensive bilateral noradrenergic input from the PnC which might be involved in locomotor functions (Mori, 1995). Therefore, because PnC giant neurons are hypothesized to be activated in response to startling stimuli, it makes sense for the Mo5 nuclei of startled animals to show c-Fos expression since PnC activation would be expected to enable noradrenergic projections to activate the Mo5. c-Fos expression was found within the vestibular nuclei (VN) of both startle and background noise treated animals but not in animals who received no acoustic input (Figure 5.4). This activity-dependent expression of c-Fos, based on the presence of an acoustic stimulus, coincides with the work done by McCue and Guinan (1997) who demonstrate that a proportion of neurons within the mammalian vestibular system exhibit sound-evoked activity. Their findings however indicate that acoustically responsive vestibular neurons respond to sound with higher thresholds than cochlear neurons (>90 dB), which contrasts our results indicating expression of c-Fos in the VN of background treated animals.

In alignment with our predictions, c-Fos expression was not observed in the PnC of control-treated animals, however unexpectedly, c-Fos expression was also not seen in the PnC of startled animals. This lack of c-Fos expression within the PnC has also been demonstrated by Palmer and Printz (1999) who used a 12.5 psi airpuff (containing both acoustic and tactile stimulus modalities) to elicit startle. Although they could not explain this interesting finding, they suggested that strain differences among animals may play a role since fluctuating c-Fos

expression patterns were observed in hypothalamic and medullary nuclei of Spontaneous Hypertensive rats and Wistar Ryoto rats. While c-Fos is a robust marker for neuronal activity (Malakhova and Davenport, 2001; Maloney et al., 2000), its use poses many problems, one of which is the time course of c-Fos elevation and decay (Dragunow and Robertson, 1987). This temporal pattern of c-Fos induction varies depending on the brain region and can be observed within the dentate gyrus 30 minutes following seizure-induction, but is only seen in hippocampal pyramidal cells 4 hours after the onset of seizure. Dragunow and Faull (1989) further report that neurons in certain brain regions do not show elevation of c-Fos regardless of the stimulus and despite certainty of activation (e.g. substantia nigra). These neurons potentially lack the biochemical messengers that regulate c-*fos* activation and thus do not show c-Fos even when they are active. Furthermore, the expression of c-Fos in granule and glial cells within the rat cerebellum following chemical or electrical stimulation, and its expression in molecular layer cells following only chemical and not electrical stimulation (despite neuronal activation by both stimuli types) demonstrate that c-Fos expression is stimulus-dependent (Tian and Bishop, 2002). Reisch et al. (2007) used electrical intracochlear stimulation to explain why c-Fos expression cannot be equated with electrophysiological activity; c-Fos expression was seen in the four auditory brainstem regions tested (ventral cochlear nucleus, dorsal cochlear nucleus, lateral superior olive, and central nucleus of the inferior colliculus) however, the spiral ganglion cells in the cochlea that drive these other auditory neurons failed to express c-Fos. Finally, Dragunow and Faull (1989) also suggest that c-Fos induction can be blocked or interfered with in the presence of ketamine and barbiturates. Taken together, these studies suggest a variety of reasons why c-Fos expression was not observed in the PnC of startled animals, and they add evidence to the understanding that negative c-Fos results does not indicate a lack of structural activation by stimulation.

Another integral step in the molecular cascades that underlie synaptic plasticity is the expression of early growth response 1 (Egr-1), a member of the IEG family with a GSG motif (Reisch et al., 2007). Egr-1 is also known as NGFI-1, Krox-24, Zif268, and can be expressed in regions following a seizure (Lanahan and Worley, 1998). Like its counterpart c-Fos, Zif268/Egr-1 was also not present in the PnC giant neurons of started animals (Figure 5.6). This coincides with studies that show a good correlation of Zif268 expression with that of c-Fos,

despite their differential structural properties and regulatory mechanisms (Reisch et al., 2007; Perez-Cadahía et al., 2011).

Since both IEGs used were not expressed in the PnC of giant neurons upon startle stimulation, an alternative approach to monitor neuronal changes in activity was carried out by using signal transduction intermediates like pCREB (Hoffman and Lyo, 2002). Unlike c-Fos, cAMP-response-element-binding protein (CREB) is expressed in all brain cells (Carlezon et al., 2005) and is essential in a variety of nervous system functions including circadian entrainment, growth and survival, neuroprotection and synaptic plasticity (Lonze and Ginty, 2002; Benito and Barco, 2010). The phosphorylation of CREB at serine 133 (Cirelli and Tononi, 2000) activates a cascade that involves CREB-binding protein (CBP) recruitment, and assembles a larger transcription complex which then promotes RNA synthesis (Carlezon et al., 2005). Thus, phosphorylation status of CREB within PnC giant neurons of startle or silence treated animals was subsequently tested, and a significantly higher percentage of nuclear pCREB expression was seen in the giant neurons of startled animals as compared to those subjected to silence (Figure 5.7). This finding is in alignment with our hypothesis that these neurons are only activated in response to a startling stimulus and since only about half of the giant neurons labeled with FG expressed pCREB (~53%), our data support the current understanding that not all of the giant neurons within the PnC are required for startle and the subpopulation that respond to an initial startle stimulus may not be the same group activated during a subsequent startle (Yeomans and Frankland, 1996). No significant main effect of treatment was seen in the mean number of pCREB neurons within the PnC (giant and non-giant), which indicates that increased pCREB expression in PnC giant neurons is not sufficient to generally increase its expression within the area due to the relatively low number of giant neurons as compared to non-giant ones (Figure 5.8). A significant main effect of treatment was also not seen in the inferior colliculus or the vestibular nuclei, however a greater number of pCREB neurons were observed within the Mo5 nuclei of startle treated animals as compared to controls, and this is consistent with c-Fos expression patterns (Figure 5.4; Figure 5.8).

The discrepancy between the positive pCREB and negative c-Fos expression within PnC giant neurons of startled animals can perhaps be explained based on an understanding of their signal transduction pathway (Figure 6.1; Hoffman and Lyo, 2002). There are two separate regulatory

pathways for the activation of c-*fos*, one through pCREB and another through serum response factor; the former is a secondary messenger cascade that is induced as a result of neurotransmission/depolarization (Greenberg et al., 1986). Briefly, Ca^{2+} influx can occur as a result of membrane depolarization via voltage-sensitive calcium channels (eg. L-type) or in the case of glutamatergic transmission, Ca^{2+} influx can occur via cation-permeable ion channels that open when glutamate binds to ionotropic receptors (eg. NMDA). Ca^{2+} then binds to the calcium binding protein calmodulin (CaM) and the Ca^{2+}-CaM complex go on to activate a variety of kinases (CaMKI, CaMKII, CaMKIV) which each have the capacity to phosphorylate CREB (Lonze and Ginty, 2002). Thus, the expression of pCREB without c-Fos may suggest an initial phase of neuronal and synaptic modification, since the former transcription factor is upstream of the latter, and a protocol using a longer time course for the expression of c-Fos (>60 minutes) may remedy this discrepancy.
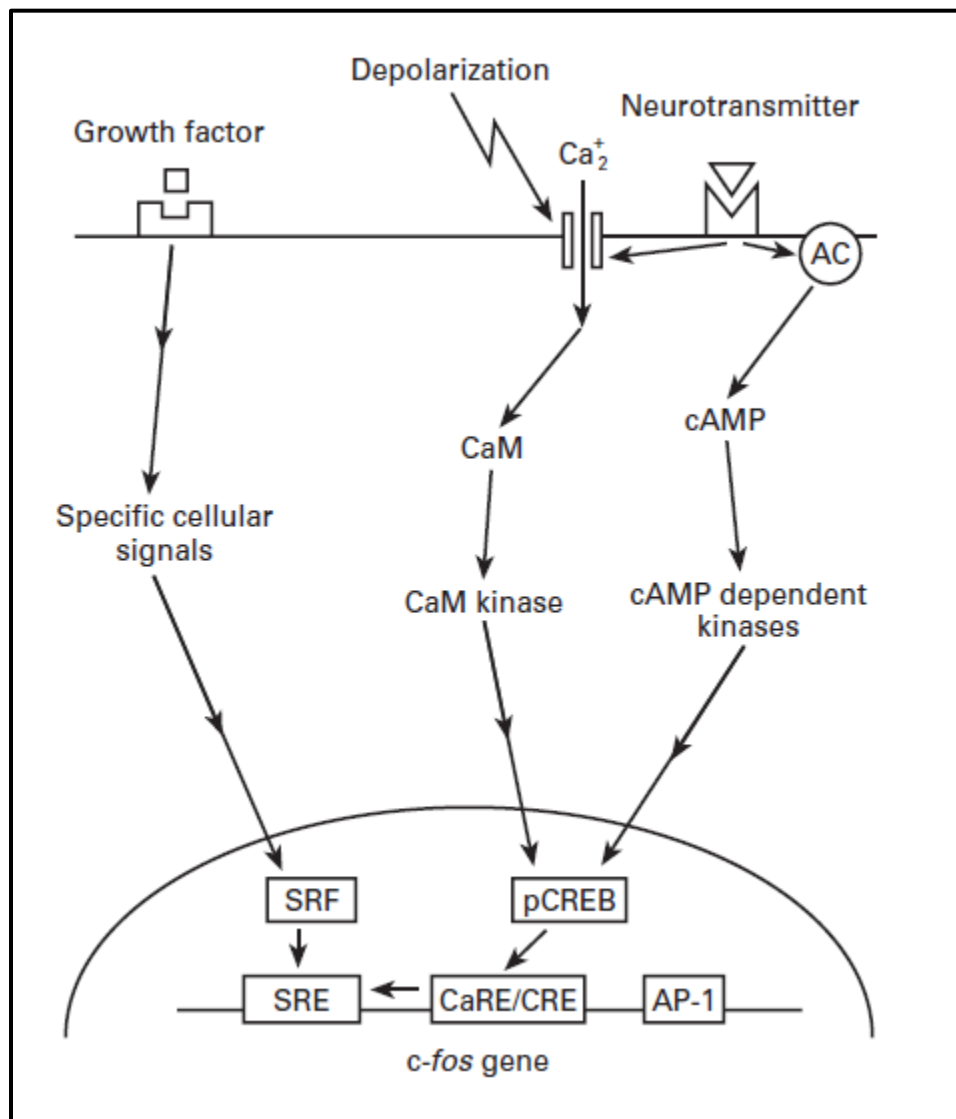
Figure 6.1 Illustration of the principal signal transduction pathways that evoke c-Fos in neurons. (AP-1: activating-protein 1; CaM: calcium binding protein calmodulin; CaRE/CRE: calcum response element/cAMP response element; SRF: serum response factor; SRE: serum response element; Hoffman and Lyo, 2002).

6.2 A subpopulation of cholinergic terminals within the PnC co-release glutamate and/or GABA

Inhibitory cholinergic neurons in the PPTg/LDTg have been proposed to be major participants in PPI (Fendt et al., 2001) as they reportedly project to the PnC and potentially innervate PnC giant neurons (Mitani et al., 1988). However, while cholinergic release is important for PPI, it is not the sole neurotransmitter responsible for mediating this circuit (Leitner et al., 1981; Semba et al., 1990; Fendt et al., 1994; Fendt, 1999; Li and Yeomans, 2000), and Wang and Morales's (2009) finding that the PPTg/LDTg contain distinct populations of cholinergic, glutamatergic, and GABAergic neurons led to our hypothesis that cholinergic terminals within the PnC co-localize with glutamatergic and/or GABAergic markers.

As predicted, our results show that a proportion of cholinergic terminals within the PnC co-express glutamate or GABA markers, including a very small number that co-localizes with both markers (Figures 5.9-5.11), which is a novel finding for midbrain cholinergic neurons. The number of single or dual labeled cholinergic terminals in close contact with either the soma or proximal dendrites of PnC giant neurons was also analyzed. Our findings demonstrate cholinergic terminals co-expressing either GABA or glutamate markers contacting the neuronal soma of PnC giant neurons; however, proximal dendrites were innervated only by cholinergic terminals expressing GABAergic markers but not by double cholinergic and glutamatergic marked terminals (Figure 5.14). This observed apposition of dual-labeled terminals with the PnC giant neurons shows an increase in the likelihood of synapses occurring at this location, nonetheless assurance cannot be determined using our methodology (see section 6.4).

Our study supports the increasing view that neurons release more than one neurotransmitter which can implicate modes of signaling (Hnasko and Edwards, 2012). A proportion of cholinergic neurons in the retina have been shown to co-release GABA (Duarte et al., 1999) and both the basal forebrain (Allen et al., 2006) and the striatum (Guzman et al., 2011) contain populations of glutamate-releasing cholinergic neurons. The possible reasons for the physiological role of co-release is poorly understood, although since both released transmitters can activate postsynaptic receptors, the potential for differential or synergistic regulation of signaling and behaviour is suggested (Guzman et al., 2011; Hnasko and Edwards, 2012). For

instance, the differential release of GABA and acetylcholine (ACh) in Starburst retinal amacrine cells contributes to direction-selective motion sensing; GABA is proposed to encode direction selectivity and ACh motion sensitivity (Demb, 2007). More so, as demonstrated by Allen and colleagues (2006), the release of one neurotransmitter (ACh) in basal forebrain cholinergic neurons, exerts a negative-feedback inhibition on its co-released partner (glutamate). Furthermore, both glutamate and ACh transmitters, co-released from midbrain interpeduncular nuclei, work together to activate postsynaptic neurons via distinct transmission pathways (Ren et al., 2011).

Another physiological role for the co-release of neurotransmitters can be to regulate filling of one transmitter through vesicular uptake of the other, by influencing the H^+ electrochemical driving force (Hnasko and Edwards, 2012). Therefore, the release of one neurotransmitter may help drive the gradient allowing for the uptake and subsequent release of the other transmitter, which perhaps plays a more functional role in synaptic transmission.

Interestingly, we also observed the co-localization of two functionally opposing neurotransmitters, glutamate and GABA (Figures 5.9C and 5.10C). Consistent with this finding, Gutiérrez et al. (2000) describe the co-release of GABA from glutamatergic neurons of granule cells onto pyramidal neurons in the hippocampal dentate gyrus. They report that the GABAergic transmission may serve a homeostatic role by restraining the excitability responsible for epilepsy. In contrast, the co-release of glutamate and GABA transmitters from the medial nucleus of the trapezoid body are both excitatory and regulate sound localization in the auditory system during early development (Gillespie et al., 2005).

Our data thus provides evidence for the combined roles that acetylcholine, glutamate and GABA may have in the mediation of PPI. Since inhibitory GABAergic projections from the substantia nigra reticulata (SNR) are known to partially mediate PPI (Koch et al., 2000), inhibitory GABAergic release from cholinergic terminals in the PnC may play a similar role, thus resulting in the rapid and long-lasting inhibition characteristic of PPI. Additionally, functionally opposing excitatory glutamatergic release may play a role in regulating the extent of inhibition by cholinergic terminals projecting from the PPTg/LDTg to the PnC, although glutamate can also be inhibitory, since Schmid and colleagues (2010) found that PnC giant neurons express inhibitory metabotropic glutamate receptors.

6.3 BK channels implicated in habituation are localized on auditory glutamatergic afferents

Previous research with *Aplysia* (Castellucci et al., 1970), *Drosophila* (Engel and Wu, 1998), *Caenorhabditis elegans* (Unpublished data, personal communication, Catharine Rankin), and *Slo1* homozygous knock-out mice (Typlt et al., 2013) suggests that short-term habituation is mediated via a presynaptic mechanism involving synaptic depression and a reduction of neurotransmitter release. More importantly, these studies proposed the BK channel to be a key player in this process. Thus, one of the aims of this work was to show the expressing of BK channels on PnC glutamatergic terminals using dual labeling immunofluorescence, in order to further validate this theory. Our results indicate that more than 85% of the glutamatergic terminals found within the PnC co-localize with BK channel markers (Figures 5.15A and 5.16A), which is a strong support for the implication of BK channels in habituation. Electron microscopy techniques in the hippocampus (Hu et al., 2001; Sailer et al., 2006) also confirm our hypothesis that BK channels are important modulators of membrane excitability at the presynaptic level (Robitaille et al., 1993; Xu and Slaughter, 2005). Interestingly, we also observed the co-expression of BK channel markers on a subpopulation of GABAergic (Figures 5.15B and 5.16B) and cholinergic (Figures 5.15C and 5.16C) terminals within the PnC, although whether or not they may be involved in habituation needs to be further investigated. Most likely however, these terminals do not play a role in modulating habituation since BK channels preferentially regulate excitatory neurotransmitter release over inhibitory and only minimally control GABA release (Martire et al., 2010). Finally, sparse immunolocalization of BK channels was also noted at the post-synaptic site which is consistent with findings in retinal amacrine cells (Grimes et al., 2009) and hippocampal pyramidal neurons (Sailer et al., 2006).

The number of glutamatergic, GABAergic, or cholinergic terminals, single-labeled or co-labeled with BK channel markers, in close contact with either the soma or proximal dendrites of PnC giant neurons was also analyzed. Our imaging demonstrates contact between the neuronal soma and both single and dual-labeled glutamatergic, cholinergic, and GABAergic terminals; contact between the proximal dendrites of PnC giant neurons and labeled terminals mimicked that seen at the soma (Figure 5.19). Electron microscopy of labeled axons and terminals from the CRN to PnC giant neurons (Nodal and López, 2003) confirmed some of the features we

observed using confocal fluorescence microscopy, with a few interesting differences. They noted that axosomatic contact was rare and only established via an en passant bouton, while the majority of synaptic contacts were axodendritic in manner. Our observed juxtaposition of single/dual-labeled terminals with PnC giant neurons at the microscopic level shows a higher number of axosomatic contacts than in the study conducted by Nodal and López (2003), nonetheless our methodology alone cannot guarantee certainty (see section 6.4).

6.4 Technical considerations

As with any scientific study, there are a few limitations that need to be acknowledged. As alluded to in previous sections, while this work does provide evidence for functional synaptic connections between the synaptic terminals labeled and our PnC giant neurons of interest, it does not actually prove that functional synapses are formed. Z-series images acquired at 0.60 μm intervals with the SP5 TCS II Confocal Microscope allowed observation of terminals within a 2 μm distance from the neuronal soma or dendrite to be defined as juxtaposed. Actual synaptic activity however would need to be determined using electron microscopy (Nodal and López, 2003; Sailer et al., 2006), antibodies against selective pre-synaptic (Synapsin I) or post-synaptic (PSD 95) markers (Sailer et al., 2006), and/or electrophysiological methods in functional studies. Additionally, the apposition of single/dual labeled terminals on the soma or proximal dendrites of PnC giant neurons is biased by the fact that FG does not label the entire cell. Due to this incomplete retrograde filling, entire dendritic trees were not visualized, thus only terminals located at the most proximal parts of the dendrites were considered juxtaposed terminals (Nodal and López, 2003). The same consideration can be applied to NeuN which limits the extent of axonal/dendritic labeling. Finally, while the Image Pro Premier software was useful in determining percent colocalization, only two channels at a time could be analyzed. Therefore, in a triple labeling immunofluorescence of CHT1, GAD67, and VGLUT1, combinations of two channels were selected to measure colocalization. This may have led to a possible overestimation of the number of double-labeled terminals in each case as well as an underestimation of the number of triple-labeled terminals since those had to be counted manually. Nevertheless, our imaging techniques were sufficient for our purposes in providing

strong evidence for the occurrence of colocalization, and to give a rough estimate of the amount of co-localization. Further tests need to be done to verify quantities.

6.5 Significance of the study

Firstly, this study is significant because it uses an alternate method, imaging, to validate our current understanding of the acoustic startle response and its modulations. Startle is mediated by a hypothetical pathway that is constantly refined as new techniques and experiments come to light. It is therefore interesting to see our immunohistochemistry and histology results build upon previous theory established by behavioural and electrophysiological studies, as well as bring to light novel findings such as the discovery that a subpopulation of midbrain cholinergic neurons co-release glutamate and/or GABA. Secondly, it is important to look at the big picture and study the acoustic startle response and its modulations for its obvious clinical relevance. Deficits in habituation and/or prepulse inhibition result in information overload received by the brain which is characteristic of many neurological disorders, including fragile X syndrome (Frankland et al., 2004), schizophrenia (Braff et al., 1978; Geyer and Braff, 1982), autism spectrum disorders (Perry et al., 2007), Alzheimer's disease, Tourette's syndrome, and Huntington's chorea (Putzki, 2008). Therefore, a better understanding of the cellular and molecular mechanisms involved in habituation and prepulse inhibition will help to determine potential drug targets and, further down the line, aid in finding a treatment for these neurological disorders.

6.6 Concluding remarks

In conclusion, this study aimed to use histology and immunohistochemistry in order to understand the synaptic organization of the primary ASR pathway and its modulatory afferents. The work presented here showed that giant neurons within the PnC form the sensorimotor interface of the oligosynaptic ASR pathway and play a key role in mediating the startle response because they project to the cervical spine and express pCREB when activated by a startle stimulus. Using dual and triple labeling immunofluorescence, we additionally

demonstrated that a subpopulation of cholinergic terminals within the PnC co-express glutamate and/or GABA synaptic markers, implying that a combination of transmitters may be involved in the attenuation of startle during PPI. Finally, markers for BK channels were employed to show the co-localization of these channels to glutamatergic presynaptic afferents, which greatly supports the theory that BK channels are essential for the synaptic depression and reduced neurotransmitter release that underlies habituation. Thus, taken together, the results of this study allow for greater insight into the synaptic inputs modulating startle and provide a better understanding of the neurotransmitters involved, which will help in determining effects that multiple drugs may have on sensorimotor gating mechanisms.

7 References

AAT Bioquest, Inc. [WWW Document] (2014) . URL http://www.aatbio.com/

Allen, T.G.J., Abogadie, F.C., & Brown, D.A. (2006) Simultaneous release of glutamate and acetylcholine from single magnocellular "cholinergic" basal forebrain neurons. *J. Neurosci.*, **26**, 1588–1595.

Antonucci, F., Alpár, A., Kacza, J., Caleo, M., Verderio, C., Giani, A., Martens, H., Chaudhry, F.A., Allegra, M., Grosche, J., Michalski, D., Erck, C., Hoffmann, A., Harkany, T., Matteoli, M., & Härtig, W. (2012) Cracking down on inhibition: selective removal of GABAergic interneurons from hippocampal networks. *J. Neurosci.*, **32**, 1989–2001.

Baird, D.H., Koto, M., & Wyman, R.J. (1993) Dendritic reduction in Passover, a Drosophila mutant with a defective giant fiber neuronal pathway. *J. Neurobiol.*, **24**, 971–984.

Benito, E. & Barco, A. (2010) CREB's control of intrinsic and synaptic plasticity: implications for CREB-dependent memory models. *Trends Neurosci.*, **33**, 230–240.

Billups, B. (2005) Colocalization of vesicular glutamate transporters in the rat superior olivary complex. *Neurosci. Lett.*, **382**, 66–70.

Borszcz, G.S., Cranney, J., & Leaton, R.N. (1989) Influence of long-term sensitization on long-term habituation of the acoustic startle response in rats: central gray lesions, preexposure, and extinction. *J. Exp. Psychol. Anim. Behav. Process.*, **15**, 54–64.

Bosch, D. & Schmid, S. (2006) Activation of muscarinic cholinergic receptors inhibits giant neurones in the caudal pontine reticular nucleus. *Eur. J. Neurosci.*, **24**, 1967–1975.

Bosch, D. & Schmid, S. (2008) Cholinergic mechanism underlying prepulse inhibition of the startle response in rats. *Neuroscience*, **155**, 326–335.

Braff, D., Stone, C., Callaway, E., Geyer, M., Glick, I., & Bali, L. (1978) Prestimulus effects on human startle reflex in normals and schizophrenics. *Psychophysiology*, **15**, 339–343.

Buckland, G., Buckland, J., Jamieson, C., & Ison, J.R. (1969) Inhibition of startle response to acoustic stimulation produced by visual prestimulation. *J. Comp. Physiol. Psychol.*, **67**, 493–496.

Bull, N. (1951) *The Attitude Theory of Emotion*. Nervous and Mental Disease Monographs.

Carlezon, W.A., Duman, R.S., & Nestler, E.J. (2005) The many faces of CREB. *Trends Neurosci.*, **28**, 436–445.

Castellucci, V., Pinsker, H., Kupfermann, I., & Kandel, E.R. (1970) Neuronal mechanisms of habituation and dishabituation of the gill-withdrawal reflex in Aplysia. *Science*, **167**, 1745–1748.

Charpier, S., Behrends, J.C., Triller, A., Faber, D.S., & Korn, H. (1995) "Latent" inhibitory connections become functional during activity-dependent plasticity. *Proc. Natl. Acad. Sci. U. S. A.*, **92**, 117–120.

Chevalier, G., Thierry, A.M., Shibazaki, T., & Féger, J. (1981) Evidence for a GABAergic inhibitory nigrotectal pathway in the rat. *Neurosci. Lett.*, **21**, 67–70.

Christoffersen, G.R. (1997) Habituation: events in the history of its characterization and linkage to synaptic depression. A new proposed kinetic criterion for its identification. *Prog. Neurobiol.*, **53**, 45–66.

Cirelli, C. & Tononi, G. (2000) On the functional significance of c-fos induction during the sleep-waking cycle. *Sleep*, **23**, 453–469.

Cui, J., Yang, H., & Lee, U.S. (2009) Molecular mechanisms of BK channel activation. *Cell. Mol. Life Sci.*, **66**, 852–875.

Currie, S. & Carlsen, R.C. (1985) A rapid startle response in larval lampreys. *Brain Res.*, **358**, 367–371.

Davis, M. (1974) Signal-to-noise ratio as a predictor of startle amplitude and habituation in the rat. *J. Comp. Physiol. Psychol.*, **86**, 812–825.

Davis, M. & File, S.E. (1984) Intrinsic and extrinsic mechanisms of habituation and sensitization: Implications for the design and analysis of experiments. In *Habituation, Sensitization, and Behavior,* pp. 287-323. Eds. H.V. S. Peeke and L. Petrinovich. Academic Press, New York.

Davis, M., Gendelman, D.S., Tischler, M.D., & Gendelman, P.M. (1982a) A primary acoustic startle circuit: lesion and stimulation studies. *J. Neurosci.*, **2**, 791–805.

Davis, M., Parisi, T., Gendelman, D.S., Tischler, M., & Kehne, J.H. (1982b) Habituation and sensitization of startle reflexes elicited electrically from the brainstem. *Science*, **218**, 688–690.

Demb, J.B. (2007) Cellular mechanisms for direction selectivity in the retina. *Neuron*, **55**, 179–186.

Desmedt, J.E. (1962) Auditory-Evoked Potentials from Cochlea to Cortex as Influenced by Activation of the Efferent Olivo-Cochlear Bundle. *J. Acoust. Soc. Am.*, **34**, 1478.

Dragunow, M. & Faull, R. (1989) The use of c-fos as a metabolic marker in neuronal pathway tracing. *J. Neurosci. Methods*, **29**, 261–265.

Dragunow, M. & Robertson, H.A. (1987) Generalized seizures induce c-fos protein(s) in mammalian neurons. *Neurosci. Lett.*, **82**, 157–161.

Duarte, C.B., Santos, P.F., & Carvalho, A.P. (1999) Corelease of two functionally opposite neurotransmitters by retinal amacrine cells: experimental evidence and functional significance. *J. Neurosci. Res.*, **58**, 475–479.

Ebert, U. & Koch, M. (1992) Glutamate receptors mediate acoustic input to the reticular brain stem. *Neuroreport*, **3**, 429–432.

Ekman, P., Friesen, W. V, & Simons, R.C. (1985) Is the startle reaction an emotion? *J. Pers. Soc. Psychol.*, **49**, 1416–1426.

Engel, J.E. & Wu, C.F. (1998) Genetic dissection of functional contributions of specific potassium channel subunits in habituation of an escape circuit in Drosophila. *J. Neurosci.*, **18**, 2254–2267.

Esclapez, M., Tillakaratne, N.J., Kaufman, D.L., Tobin, A.J., & Houser, C.R. (1994) Comparative localization of two forms of glutamic acid decarboxylase and their mRNAs in rat brain supports the concept of functional differences between the forms. *J. Neurosci.*, **14**, 1834–1855.

Farley, J. & Rudy, B. (1988) Multiple types of voltage-dependent Ca2+-activated K+ channels of large conductance in rat brain synaptosomal membranes. *Biophys. J.*, **53**, 919–934.

Fendt, M. (1999) Enhancement of prepulse inhibition after blockade of GABA activity within the superior colliculus. *Brain Res.*, **833**, 81–85.

Fendt, M., Koch, M., & Schnitzler, H.U. (1994a) Lesions of the central gray block the sensitization of the acoustic startle response in rats. *Brain Res.*, **661**, 163–173.

Fendt, M., Koch, M., & Schnitzler, H.U. (1994b) Sensorimotor gating deficit after lesions of the superior colliculus. *Neuroreport*, **5**, 1725–1728.

Fendt, M., Li, L., & Yeomans, J.S. (2001) Brain stem circuits mediating prepulse inhibition of the startle reflex. *Psychopharmacology (Berl).*, **156**, 216–224.

Fleshler, M. (1965) Adequate acoustic stimulus for startle reaction in the rat. *J. Comp. Physiol. Psychol.*, **60**, 200–207.

Fluorescence SpectraViewer. [WWW Document] (2014). URL http://www.lifetechnologies.com/

Forbes, A. & Sherrington, C.S. (1914) Acoustic reflexes in the decerebrate rat. *Amer. J. Psych.*, **35**, 367–76

Fox, J.E. (1979) Habituation and prestimulus inhibition of the auditory startle reflex in decerebrate rats. *Physiol. Behav.*, **23**, 291–297.

Frankland, P.W., Wang, Y., Rosner, B., Shimizu, T., Balleine, B.W., Dykens, E.M., Ornitz, E.M., & Silva, A.J. (2004) Sensorimotor gating abnormalities in young males with fragile X syndrome and Fmr1-knockout mice. *Mol. Psychiatry*, **9**, 417–425.

French, A.P., Mills, S., Swarup, R., Bennett, M.J., & Pridmore, T.P. (2008) Colocalization of fluorescent markers in confocal microscope images of plant cells. *Nat. Protoc.*, **3**, 619–628.

Geyer, M.A. & Braff, D.L. (1982) Habituation of the Blink reflex in normals and schizophrenic patients. *Psychophysiology*, **19**, 1–6.

Gho, M. & Ganetzky, B. (1992) Analysis of repolarization of presynaptic motor terminals in Drosophila larvae using potassium-channel-blocking drugs and mutations. *J. Exp. Biol.*, **170**, 93–111.

Gillespie, D.C., Kim, G., & Kandler, K. (2005) Inhibitory synapses in the developing auditory system are glutamatergic. *Nat. Neurosci.*, **8**, 332–338.

Gomeza, J., Zhang, L., Kostenis, E., Felder, C.C., Bymaster, F.P., Brodkin, J., Shannon, H., Xia, B., Duttaroy, A., Deng, C.X., & Wess, J. (2001) Generation and pharmacological analysis of M2 and M4 muscarinic receptor knockout mice. *Life Sci.*, **68**, 2457–2466.

Graham, F.K. (1975) Presidential Address, 1974. The more or less startling effects of weak prestimulation. *Psychophysiology*, **12**, 238–248.

Greenberg, M.E., Ziff, E.B., & Greene, L.A. (1986) Stimulation of neuronal acetylcholine receptors induces rapid gene transcription. *Science*, **234**, 80–83.

Grimes, W.N., Li, W., Chávez, A.E., & Diamond, J.S. (2009) BK channels modulate pre- and postsynaptic signaling at reciprocal synapses in retina. *Nat. Neurosci.*, **12**, 585–592.

Grofova, I. & Keane, S. (1991) Descending brainstem projections of the pedunculopontine tegmental nucleus in the rat. *Anat. Embryol. (Berl).*, **184**, 275–290.

Groves, P., & Thompson, R. (1970). Habituation: a dual-process theory. *Psychol. Rev*., **77**, 419-450.

Guo, W., Crossey, E.L., Zhang, L., Zucca, S., George, O.L., Valenzuela, C.F., & Zhao, X. (2011) Alcohol exposure decreases CREB binding protein expression and histone acetylation in the developing cerebellum. *PLoS One*, **6**, e19351.

Gutiérrez, R. (2000) Seizures induce simultaneous GABAergic and glutamatergic transmission in the dentate gyrus-CA3 system. *J. Neurophysiol.*, **84**, 3088–3090.

Guzman, M.S., De Jaeger, X., Raulic, S., Souza, I.A., Li, A.X., Schmid, S., Menon, R.S., Gainetdinov, R.R., Caron, M.G., Bartha, R., Prado, V.F., & Prado, M.A.M. (2011) Elimination of the vesicular acetylcholine transporter in the striatum reveals regulation of behaviour by cholinergic-glutamatergic co-transmission. *PLoS Biol.*, **9**, e1001194.

Hnasko, T.S. & Edwards, R.H. (2012) Neurotransmitter corelease: mechanism and physiological role. *Annu. Rev. Physiol.*, **74**, 225–243.

Hoffman, G.E. & Lyo, D. (2002) Anatomical markers of activity in neuroendocrine systems: are we all "fos-ed out"? *J. Neuroendocrinol.*, **14**, 259–268.

Hoffman, H.S. & Fleshler, M. (1963) Startle reaction: modification by background acoustic stimulation. *Science*, **141**, 928–930.

Hoffman, H.S. & Searle, J.L. (1965) Acoustic variables in the modification of startle reaction in the rat. *J. Comp. Physiol. Psychol.*, **60**, 53–58.

Holmstrand, E.C. & Sesack, S.R. (2011) Projections from the rat pedunculopontine and laterodorsal tegmental nuclei to the anterior thalamus and ventral tegmental area arise from largely separate populations of neurons. *Brain Struct. Funct.*, **216**, 331–345.

Hu, H., Shao, L.R., Chavoshy, S., Gu, N., Trieb, M., Behrens, R., Laake, P., Pongs, O., Knaus, H.G., Ottersen, O.P., & Storm, J.F. (2001) Presynaptic Ca2+-activated K+ channels in glutamatergic hippocampal terminals and their role in spike repolarization and regulation of transmitter release. *J. Neurosci.*, **21**, 9585–9597.

Illing, R.-B., Michler, S.A., Kraus, K.S., & Laszig, R. (2002) Transcription factor modulation and expression in the rat auditory brainstem following electrical intracochlear stimulation. *Exp. Neurol.*, **175**, 226–244.

Inoue, R., Kitamura, K., & Kuriyama, H. (1985) Two Ca-dependent K-channels classified by the application of tetraethylammonium distribute to smooth muscle membranes of the rabbit portal vein. *Pflugers Arch.*, **405**, 173–179.

Ison, J., & Hammond, G. (1971). Modification of the startle reflex in the rat by changes in the auditory and visual environments. *J. Comp Physiol Psychol.,* **75**, 435-452.

Jones, B.E. (1990) Immunohistochemical study of choline acetyltransferase-immunoreactive processes and cells innervating the pontomedullary reticular formation in the rat. *J. Comp. Neurol.*, **295**, 485–514.

Jordan, W.P., Strasser, H.C., & McHale, L. (2000) Contextual control of long-term habituation in rats. *J. Exp. Psychol. Anim. Behav. Process.*, **26**, 323–339.

Katz, E., Ferro, P.A., Cherksey, B.D., Sugimori, M., Llinás, R., & Uchitel, O.D. (1995) Effects of Ca2+ channel blockers on transmitter release and presynaptic currents at the frog neuromuscular junction. *J. Physiol.*, **486 (Pt 3**, 695–706.

Kaufman, D.L., Houser, C.R., & Tobin, A.J. (1991) Two forms of the gamma-aminobutyric acid synthetic enzyme glutamate decarboxylase have distinct intraneuronal distributions and cofactor interactions. *J. Neurochem.*, **56**, 720–723.

Koch, M. (1999) The neurobiology of startle. *Prog. Neurobiol.*, **59**, 107–128.

Koch, M., Fendt, M., & Kretschmer, B.D. (2000) Role of the substantia nigra pars reticulata in sensorimotor gating, measured by prepulse inhibition of startle in rats. *Behav. Brain Res.*, **117**, 153–162.

Koch, M., Kungel, M., & Herbert, H. (1993) Cholinergic neurons in the pedunculopontine tegmental nucleus are involved in the mediation of prepulse inhibition of the acoustic startle response in the rat. *Exp. brain Res.*, **97**, 71–82.

Koch, M., Lingenhöhl, K., & Pilz, P.K. (1992) Loss of the acoustic startle response following neurotoxic lesions of the caudal pontine reticular formation: possible role of giant neurons. *Neuroscience*, **49**, 617–625.

Koch, M. & Schnitzler, H.U. (1997) The acoustic startle response in rats--circuits mediating evocation, inhibition and potentiation. *Behav. Brain Res.*, **89**, 35–49.

Kolston, J., Osen, K.K., Hackney, C.M., Ottersen, O.P., & Storm-Mathisen, J. (1992) An atlas of glycine- and GABA-like immunoreactivity and colocalization in the cochlear nuclear complex of the guinea pig. *Anat. Embryol. (Berl).*, **186**, 443–465.

Kolta, A., Westberg, K.G., & Lund, J.P. (2000) Identification of brainstem interneurons projecting to the trigeminal motor nucleus and adjacent structures in the rabbit. *J. Chem. Neuroanat.*, **19**, 175–195.

Krase, W., Koch, M., & Schnitzler, H.U. (1993) Glutamate antagonists in the reticular formation reduce the acoustic startle response. *Neuroreport*, **4**, 13–16.

Landis, C. & Hunt, W. (1939) *The Startle Pattern.* Oxford: Farrar and Rinehart.

Lärkfors, L., Lindsay, R.M., & Alderson, R.F. (1996) Characterization of the responses of Purkinje cells to neurotrophin treatment. *J. Neurochem.*, **66**, 1362–1373.

Larrauri, J. & Schmajuk, N. (2006) Prepulse inhibition mechanisms and cognitive processes: a review and model. *EXS*, **98**, 245–278.

Latorre, R. & Miller, C. (1983) Conduction and selectivity in potassium channels. *J. Membr. Biol.*, **71**, 11–30.

Leaton, R. & Supple, W. (1986) Cerebellar vermis: essential for long-term habituation of the acoustic startle response. *Science (80-.).*, **232**, 513–515.

Leaton, R.N., Cassella, J. V, & Borszcz, G.S. (1985) Short-term and long-term habituation of the acoustic startle response in chronic decerebrate rats. *Behav. Neurosci.*, **99**, 901–912.

Leaton, R.N. & Supple, W.F. (1991) Medial cerebellum and long-term habituation of acoustic startle in rats. *Behav. Neurosci.*, **105**, 804–816.

Lee, Y., López, D.E., Meloni, E.G., & Davis, M. (1996) A primary acoustic startle pathway: obligatory role of cochlear root neurons and the nucleus reticularis pontis caudalis. *J. Neurosci.*, **16**, 3775–3789.

Leitner, D.S. & Cohen, M.E. (1985) Role of the inferior colliculus in the inhibition of acoustic startle in the rat. *Physiol. Behav.*, **34**, 65–70.

Leitner, D.S., Powers, A.S., Stitt, C.L., & Hoffman, H.S. (1981) Midbrain reticular formation involvement in the inhibition of acoustic startle. *Physiol. Behav.*, **26**, 259–268.

Li, L., Du, Y., Li, N., Wu, X., & Wu, Y. (2009) Top-down modulation of prepulse inhibition of the startle reflex in humans and rats. *Neurosci. Biobehav. Rev.*, **33**, 1157–1167.

Li, L. & Yeomans, J.S. (2000) Using intracranial electrical stimulation to study the timing of prepulse inhibition of the startle reflex. *Brain Res. Brain Res. Protoc.*, **5**, 67–74.

Lingenhöhl, K. & Friauf, E. (1994) Giant neurons in the rat reticular formation: a sensorimotor interface in the elementary acoustic startle circuit? *J. Neurosci.*, **14**, 1176–1194.

Liu, Q., Chen, B., Ge, Q., & Wang, Z.-W. (2007) Presynaptic Ca2+/calmodulin-dependent protein kinase II modulates neurotransmitter release by activating BK channels at Caenorhabditis elegans neuromuscular junction. *J. Neurosci.*, **27**, 10404–10413.

Loeb, M. (1964) Psychophysical correlates of intratympanic reflex action. *Psychol. Bull.*, **61**, 140–152.

Lonze, B.E. & Ginty, D.D. (2002) Function and regulation of CREB family transcription factors in the nervous system. *Neuron*, **35**, 605–623.

Lopiano, L., de'Sperati, C., & Montarolo, P.G. (1990) Long-term habituation of the acoustic startle response: role of the cerebellar vermis. *Neuroscience*, **35**, 79–84.

Malakhova, O.E. & Davenport, P.W. (2001) c-Fos expression in the central nervous system elicited by phrenic nerve stimulation. *J. Appl. Physiol.*, **90**, 1291–1298.

Maloney, K.J., Mainville, L., & Jones, B.E. (2000) c-Fos expression in GABAergic, serotonergic, and other neurons of the pontomedullary reticular formation and raphe after paradoxical sleep deprivation and recovery. *J. Neurosci.*, **20**, 4669–4679.

Martin, G. F., Holstege, G. and Mehler, W. R. (1990) Reticular formation of the pons and medulla. In *Human Nervous System*, pp. 203-220. Ed. G. Paxinos. Academic Press, San Diego, CA.

Martire, M., Barrese, V., D'Amico, M., Iannotti, F.A., Pizzarelli, R., Samengo, I., Viggiano, D., Ruth, P., Cherubini, E., & Taglialatela, M. (2010) Pre-synaptic BK channels selectively control glutamate versus GABA release from cortical and hippocampal nerve terminals. *J. Neurochem.*, **115**, 411–422.

Marty, A. (1981) Ca-dependent K channels with large unitary conductance in chromaffin cell membranes. *Nature*, **291**, 497–500.

McCue, M.P. & Guinan, J.J. (1997) Sound-evoked activity in primary afferent neurons of a mammalian vestibular system. *Am. J. Otol.*, **18**, 355–360.

Meredith, M.A., Wallace, M.T., & Stein, B.E. (1992) Visual, auditory and somatosensory convergence in output neurons of the cat superior colliculus: multisensory properties of the tecto-reticulo-spinal projection. *Exp. Brain Res.*, **88**, 181–186.

Miserendino, M.J.D., Boulis, N.M., Spiera, R.F., (1990) Role of excitatory amino acids in the neural circuit mediating the acoustic startle reflex. *Soc Neurosci Abstr* **16**, 1185.

Mitani, A., Ito, K., Hallanger, A.E., Wainer, B.H., Kataoka, K., & McCarley, R.W. (1988) Cholinergic projections from the laterodorsal and pedunculopontine tegmental nuclei to the pontine gigantocellular tegmental field in the cat. *Brain Res.*, **451**, 397–402.

Mongeluzi, D.L., Hoppe, T.A., & Frost, W.N. (1998a) Prepulse inhibition of the Tritonia escape swim. *J. Neurosci.*, **18**, 8467–8472.

Mongeluzi, D.L., Tian, L.M., & Frost, W.N. (1998b) Prepulse inhibition of siphon bending and inking in the marine mollusc, *Aplysia californica. Soc. Neurosci. Abstr.* **24**, 702.

Mori, S. (1995) [Control mechanisms of locomotor movements from a viewpoint of behavioral control]. *Nihon Shinkei Seishin Yakurigaku Zasshi*, **15**, 281–287.

Nodal, F.R. & López, D.E. (2003) Direct input from cochlear root neurons to pontine reticulospinal neurons in albino rat. *J. Comp. Neurol.*, **460**, 80–93.

Ornitz, E.M. & Guthrie, D. (1989) Long-term habituation and sensitization of the acoustic startle response in the normal adult human. *Psychophysiology*, **26**, 166–173.

Pallotta, B.S., Magleby, K.L., & Barrett, J.N. (1981) Single channel recordings of Ca2+-activated K+ currents in rat muscle cell culture. *Nature*, **293**, 471–474.

Palmer, A.A. & Printz, M.P. (1999) Strain differences in Fos expression following airpuff startle in Spontaneously Hypertensive and Wistar Kyoto rats. *Neuroscience*, **89**, 965–978.

Paxinos, G. & Watson, C. (2004) *The Rat Brain in Stereotaxic Coordinates - The New Coronal Set (Google eBook)*. Academic Press.

Perry, W., Minassian, A., Lopez, B., Maron, L., & Lincoln, A. (2007) Sensorimotor gating deficits in adults with autism. *Biol. Psychiatry*, **61**, 482–486.

Pérez-Cadahía, B., Drobic, B., & Davie, J.R. (2011) Activation and function of immediate-early genes in the nervous system. *Biochem. Cell Biol.*, **89**, 61–73.

Pfeiffer, W. (1962) The fright reaction of fish. *Biol. Rev. Camb. Philos. Soc.*, **37**, 495–511.

Pilz, P.K., Caeser, M., & Ostwald, J. (1988) Comparative threshold studies of the acoustic pinna, jaw and startle reflex in the rat. *Physiol. Behav.*, **43**, 411–415.

Pilz, P.K. & Schnitzler, H.U. (1996) Habituation and sensitization of the acoustic startle response in rats: amplitude, threshold, and latency measures. *Neurobiol. Learn. Mem.*, **66**, 67–79.

Pilz, P.K.D., Arnold, S.W., Rischawy, A.T., & Plappert, C.F. (2013) Longterm-habituation of the startle response in mice is stimulus modality, but not context specific. *Front. Integr. Neurosci.*, **7**, 103.

Pinckney, L.A. (1976) Inhibition of the startle reflex in the rat by prior tactile stimulation. *Anim. Learn. Behav.*, **4**, 467–472.

Prosser, L. & Hunter, W. (1936) The extinction of startle responses and spinal reflexes in the white rat. *Am. J. Physiol. -- Leg. Content*, **117**, 609 – 618.

Putzki, N., Graf, K., Stude, P., Diener, H.-C., & Maschke, M. (2008) Habituation of the auditory startle response in cervical dystonia and Parkinson's disease. *Eur. Neurol.*, **59**, 172–178.

Pyott, S.J., Meredith, A.L., Fodor, A.A., Vázquez, A.E., Yamoah, E.N., & Aldrich, R.W. (2007) Cochlear function in mice lacking the BK channel alpha, beta1, or beta4 subunits. *J. Biol. Chem.*, **282**, 3312–3324.

Raffaelli, G., Saviane, C., Mohajerani, M.H., Pedarzani, P., & Cherubini, E. (2004) BK potassium channels control transmitter release at CA3-CA3 synapses in the rat hippocampus. *J. Physiol.*, **557**, 147–157.

Rankin, C.H., Abrams, T., Barry, R.J., Bhatnagar, S., Clayton, D.F., Colombo, J., Coppola, G., Geyer, M.A., Glanzman, D.L., Marsland, S., McSweeney, F.K., Wilson, D.A., Wu, C.-F., & Thompson, R.F. (2009) Habituation revisited: an updated and revised description of the behavioral characteristics of habituation. *Neurobiol. Learn. Mem.*, **92**, 135–138.

Rankin, C.H., Beck, C.D., & Chiba, C.M. (1990) Caenorhabditis elegans: a new model system for the study of learning and memory. *Behav. Brain Res.*, **37**, 89–92.

Redgrave, P., Mitchell, I.J., & Dean, P. (1987) Descending projections from the superior colliculus in rat: a study using orthograde transport of wheatgerm-agglutinin conjugated horseradish peroxidase. *Exp. brain Res.*, **68**, 147–167.

Reisch, A., Illing, R.-B., & Laszig, R. (2007) Immediate early gene expression invoked by electrical intracochlear stimulation in some but not all types of neurons in the rat auditory brainstem. *Exp. Neurol.*, **208**, 193–206.

Ren, J., Qin, C., Hu, F., Tan, J., Qiu, L., Zhao, S., Feng, G., & Luo, M. (2011) Habenula "cholinergic" neurons co-release glutamate and acetylcholine and activate postsynaptic neurons via distinct transmission modes. *Neuron*, **69**, 445–452.

Robitaille, R., Garcia, M.L., Kaczorowski, G.J., & Charlton, M.P. (1993) Functional colocalization of calcium and calcium-gated potassium channels in control of transmitter release. *Neuron*, **11**, 645–655.

Rundén-Pran, E., Haug, F.M., Storm, J.F., & Ottersen, O.P. (2002) BK channel activity determines the extent of cell degeneration after oxygen and glucose deprivation: a study in organotypical hippocampal slice cultures. *Neuroscience*, **112**, 277–288.

Russell, I.J. (1974) Central and peripheral inhibition of lateral line input during the startle response in goldfish. *Brain Res.*, **80**, 517–522.

Rüttiger, L., Sausbier, M., Zimmermann, U., Winter, H., Braig, C., Engel, J., Knirsch, M., Arntz, C., Langer, P., Hirt, B., Müller, M., Köpschall, I., Pfister, M., Münkner, S., Rohbock, K., Pfaff, I., Rüsch, A., Ruth, P., & Knipper, M. (2004) Deletion of the Ca2+-activated potassium (BK) alpha-subunit but not the BKbeta1-subunit leads to progressive hearing loss. *Proc. Natl. Acad. Sci. U. S. A.*, **101**, 12922–12927.

Sailer, C.A., Kaufmann, W.A., Kogler, M., Chen, L., Sausbier, U., Ottersen, O.P., Ruth, P., Shipston, M.J., & Knaus, H.-G. (2006) Immunolocalization of BK channels in hippocampal pyramidal neurons. *Eur. J. Neurosci.*, **24**, 442–454.

Sausbier, U., Sausbier, M., Sailer, C.A., Arntz, C., Knaus, H.-G., Neuhuber, W., & Ruth, P. (2006) Ca2+ -activated K+ channels of the BK-type in the mouse brain. *Histochem. Cell Biol.*, **125**, 725–741.

Schmid, S., Brown, T., Simons-Weidenmaier, N., Weber, M., & Fendt, M. (2010) Group III metabotropic glutamate receptors inhibit startle-mediating giant neurons in the caudal pontine

reticular nucleus but do not mediate synaptic depression/short-term habituation of startle. *J. Neurosci.*, **30**, 10422–10430.

Semba, K., Reiner, P.B., & Fibiger, H.C. (1990) Single cholinergic mesopontine tegmental neurons project to both the pontine reticular formation and the thalamus in the rat. *Neuroscience*, **38**, 643–654.

Semba, K. & Fibiger, H.C. (1992) Afferent connections of the laterodorsal and the pedunculopontine tegmental nuclei in the rat: a retro- and antero-grade transport and immunohistochemical study. *J. Comp. Neurol.*, **323**, 387–410.

Simons-Weidenmaier, N.S., Weber, M., Plappert, C.F., Pilz, P.K.D., & Schmid, S. (2006) Synaptic depression and short-term habituation are located in the sensory part of the mammalian startle pathway. *BMC Neurosci.*, **7**, 38.

Spann, B.M. & Grofova, I. (1992) Cholinergic and non-cholinergic neurons in the rat pedunculopontine tegmental nucleus. *Anat. Embryol. (Berl).*, **186**, 215–227.

Steininger, T.L., Rye, D.B., & Wainer, B.H. (1992) Afferent projections to the cholinergic pedunculopontine tegmental nucleus and adjacent midbrain extrapyramidal area in the albino rat. I. Retrograde tracing studies. *J. Comp. Neurol.*, **321**, 515–543.

Swerdlow, N.R. & Geyer, M.A. (1993) Clozapine and haloperidol in an animal model of sensorimotor gating deficits in schizophrenia. *Pharmacol. Biochem. Behav.*, **44**, 741–744.

Swerdlow, N.R., Karban, B., Ploum, Y., Sharp, R., Geyer, M.A., & Eastvold, A. (2001) Tactile prepuff inhibition of startle in children with Tourette's syndrome: in search of an "fMRI-friendly" startle paradigm. *Biol. Psychiatry*, **50**, 578–585.

Tian, J. Bin & Bishop, G.A. (2002) Stimulus-dependent activation of c-Fos in neurons and glia in the rat cerebellum. *J. Chem. Neuroanat.*, **23**, 157–170.

Thompson, R.F. & Spencer, W.A. (1966) Habituation: a model phenomenon for the study of neuronal substrates of behavior. *Psychol. Rev.*, **73**, 16–43.

Typlt, M., Mirkowski, M., Azzopardi, E., Ruth, P., Pilz, P.K.D., & Schmid, S. (2013) Habituation of reflexive and motivated behavior in mice with deficient BK channel function. *Front. Integr. Neurosci.*, **7**, 79.

Valsamis, B. & Schmid, S. (2011) Habituation and prepulse inhibition of acoustic startle in rodents. *J. Vis. Exp.*, e3446.

Vornov, J.J. & Sutin, J. (1983) Brainstem projections to the normal and noradrenergically hyperinnervated trigeminal motor nucleus. *J. Comp. Neurol.*, **214**, 198–208.

Wang, H.-L. & Morales, M. (2009) Pedunculopontine and laterodorsal tegmental nuclei contain distinct populations of cholinergic, glutamatergic and GABAergic neurons in the rat. *Eur. J. Neurosci.*, **29**, 340–358.

Wang, Z.-W. (2008) Regulation of synaptic transmission by presynaptic CaMKII and BK channels. *Mol. Neurobiol.*, **38**, 153–166.

Weber, M., Schmitt, A., Wischmeyer, E., & Döring, F. (2008) Excitability of pontine startle processing neurones is regulated by the two-pore-domain K+ channel TASK-3 coupled to 5-HT2C receptors. *Eur. J. Neurosci.*, **28**, 931–940.

Weber, M., Schnitzler, H.-U., & Schmid, S. (2002) Synaptic plasticity in the acoustic startle pathway: the neuronal basis for short-term habituation? *Eur. J. Neurosci.*, **16**, 1325–1332.

Wicks, S.R., Roehrig, C.J., & Rankin, C.H. (1996) A dynamic network simulation of the nematode tap withdrawal circuit: predictions concerning synaptic function using behavioral criteria. *J. Neurosci.*, **16**, 4017–4031.

Wu, M.F., Jenden, D.J., Fairchild, M.D., & Siegel, J.M. (1993) Cholinergic mechanisms in startle and prepulse inhibition: effects of the false cholinergic precursor N-aminodeanol. *Behav. Neurosci.*, **107**, 306–316.

Wu, M.F., Suzuki, S.S., & Siegel, J.M. (1988) Anatomical distribution and response patterns of reticular neurons active in relation to acoustic startle. *Brain Res.*, **457**, 399–406.

Xu, J.W. & Slaughter, M.M. (2005) Large-conductance calcium-activated potassium channels facilitate transmitter release in salamander rod synapse. *J. Neurosci.*, **25**, 7660–7668.

Yao, W. & Godfrey, D.A. (1992) Quantitative evidence that cochlear root neurons are not cholinergic. *Soc. Neurosci. Abstr.,* **18**, 1036

Yeomans, J.S., Bosch, D., Alves, N., Daros, A., Ure, R.J., & Schmid, S. (2010) GABA receptors and prepulse inhibition of acoustic startle in mice and rats. *Eur. J. Neurosci.*, **31**, 2053–2061.

Yeomans, J.S. & Frankland, P.W. (1996) The acoustic startle reflex: neurons and connections. *Brain Res. Brain Res. Rev.*, **21**, 301–314.

Yeomans, J.S., Li, L., Scott, B.W., & Frankland, P.W. (2002) Tactile, acoustic and vestibular systems sum to elicit the startle reflex. *Neurosci. Biobehav. Rev.*, **26**, 1–11.

Curriculum Vitae

Name:	Mahabba Smoka

Post-secondary Education and Degrees:

Western University
London, Ontario, Canada
2008-2012 BMSc. Honors Specialization

Honours and Awards:

Natural Sciences and Engineering Research Council of Canada (NSERC) Scholarship
2013-2014

Western Graduate Research Scholarship (WGRS)
2012-2014

Anatomy and Cell Biology (ACB) Graduate Entrance Scholarship
2012-2013

Related Work Experience:

Teaching Assistant – Human Systemic Anatomy 3319
Western University
2012-2014

Research Assistant – Dr. Edith Arany
Lawson Health Research Institute
Summer 2012

Publications:

Smoka M., Rajakumar N., deOliveira C., and Schmid S. (2013) *Synaptic architecture of the acoustic startle response pathway.*

Published abstract for Southern Ontario Neuroscience Association (2014), London Health Research Day (2014), and the 20th Annual Murray Barr Day (2013)

Smoka M., Rajakumar N., deOliveira C., and Schmid S. (2013) *Mapping the acoustic startle pathway: giant startle neurons in the caudal pontine reticular nucleus.*

Published abstract for Southern Ontario Neuroscience Association (2013), London Health Research Day (2013), and Western Research Forum (2013)